Geoscience Frontiers 8 (2017) 1187–1232

HOSTED BY

Contents lists available at ScienceDirect

China University of Geosciences (Beijing)

Geoscience Frontiers

journal homepage: www.elsevier.com/locate/gsf

Focus Paper

Deformation correlations, stress field switches and evolution of an orogenic intersection: The Pan-African Kaoko-Damara orogenic junction, Namibia

Ben Goscombe [a,*], David A. Foster [b], David Gray [c], Ben Wade [d], Antonios Marsellos [e], Jason Titus [b]

[a] Integrated Terrane Analysis Research (ITAR), 18 Cambridge Rd, Aldgate, 5154, SA, Australia
[b] Department of Geological Sciences, University of Florida, Gainesville, FL, 32611, USA
[c] School of Earth Sciences, University of Tasmania, Hobart, TAS, Australia
[d] Adelaide Microscopy, University of Adelaide, Adelaide, 5005, SA, Australia
[e] Hofstra University, Hempstead, NY, USA

ARTICLE INFO

Article history:
Received 13 February 2017
Received in revised form
12 April 2017
Accepted 10 May 2017
Available online 30 May 2017
Handling Editor: M. Santosh

Keywords:
Damara Orogen
Stress fields
Orogeny
Assembly of Gondwana
Event geochronology
Deformation correlations

ABSTRACT

Age calibrated deformation histories established by detailed mapping and dating of key magmatic time markers are correlated across all tectono-metamorphic provinces in the Damara Orogenic System. Correlations across structural belts result in an internally consistent deformation framework with evidence of stress field rotations with similar timing, and switches between different deformation events. Horizontal principle compressive stress rotated clockwise ~180° in total during Kaoko Belt evolution, and ~135° during Damara Belt evolution. At most stages, stress field variation is progressive and can be attributed to events within the Damara Orogenic System, caused by changes in relative trajectories of the interacting Rio De La Plata, Congo, and Kalahari Cratons. Kaokoan orogenesis occurred earliest and evolved from collision and obduction at ~590 Ma, involving E–W directed shortening, progressing through different transpressional states with ~45° rotation of the stress field to strike-slip shear under NW–SE shortening at ~550–530 Ma. Damaran orogenesis evolved from collision at ~555–550 Ma with NW–SE directed shortening in common with the Kaoko Belt, and subsequently evolved through ~90° rotation of the stress field to NE–SW shortening at ~512–508 Ma. Both Kaoko and Damara orogenic fronts were operating at the same time, with all three cratons being coaxially convergent during the 550–530 Ma period; Rio De La Plata directed SE against the Congo Craton margin, and both together over-riding the Kalahari Craton margin also towards the SE. Progressive stress field rotation was punctuated by rapid and significant switches at ~530–525 Ma, ~508 Ma and ~505 Ma. These three events included: (1) Culmination of main phase orogenesis in the Damara Belt, coinciding with maximum burial and peak metamorphism at 530–525 Ma. This occurred at the same time as termination of transpression and initiation of transtensional reactivation of shear zones in the Kaoko Belt. Principle compressive stress switched from NW–SE to NNW–SSE shortening in both Kaoko and Damara Belts at this time. This marks the start of Congo-Kalahari stress field overwhelming the waning Rio De La Plata-Congo stress field, and from this time forward contraction across the Damara Belt generated the stress field governing subsequent low-strain events in the Kaoko Belt. (2) A sudden switch to E–W directed shortening at ~508 Ma is interpreted as a far-field effect imposed on the Damara Orogenic System, most plausibly from arc obduction along the orogenic margin of Gondwana (Ross-Delamerian Orogen). (3) This imposed stress

* Corresponding author.
E-mail address: ben.goscombe@gmail.com (B. Goscombe).
URL: http://www.terraneanalysis.com.au
Peer-review under responsibility of China University of Geosciences (Beijing).

http://dx.doi.org/10.1016/j.gsf.2017.05.001

field established a N–S extension direction exploited by decompression melts, switch to vertical shortening, and triggered gravitational collapse and extension of the thermally weakened hot orogen core at ~505 Ma, producing an extensional metamorphic core complex across the Central Zone.

1. Introduction

Intersections between ancient and modern orogenic belts are key locations for deciphering the accretion of supercontinents, processes of structural interference, and causes of orogenic curvature associated with highly oblique stress regimes and ridged indenters. The Damara Orogenic System is an orogenic triple junction at the core of Gondwana, made of the Kaoko, Damara and Gariep Belts (Fig. 1). Consequently, the tectonic evolution of this region is crucial to understanding the assembly of Gondwana and crustal response to different orogenic episodes. Damara and Kaoko Belts of interest in this contribution, together preserve a history from 650 to 470 Ma with a range of deformational styles, including those associated with: subduction and accretionary complexes, magmatic arcs, obduction, transpression, high-angle fold-thrust belts, high-grade gneissic terranes, transtension, extensional metamorphic core complexes and low-grade low-strain belts.

The Damara Belt is a classic example of a deeply eroded and well-exposed high-angle collisional orogen with boundary conditions still intact (i.e. Gray et al., 2006). Whereas, the Kaoko Belt is a classic example of a deeply eroded and well-exposed transpressional orogen with boundaries and tectonic context preserved (i.e. Goscombe and Gray, 2008). The Ugab Zone junction between the two is also well exposed, with crucial time relationships from punctuated granite intrusion events; thus preserving a comprehensive record of orogenic events in common with the two belts, linking them and informing understanding of both. As a result, the Damara Orogenic System preserves a rich record of the complex deformation history resulting from relative movements between the Rio De La Plata, Congo and Kalahari Cratons; an unsurpassed natural laboratory for documenting the tectono-metamorphic response to supercontinent assembly.

This research tracks relative movements of the cratons bounding the Damara Orogenic System by following a three-fold approach: (1) Establish time calibrated deformation frameworks for each the four distinct tectono-metamorphic provinces in the orogenic system: transpressional Kaoko Belt, and within the Damara Belt, highly variable northern margin, high-grade orogen core, and southern orogenic margin. (2) Constrain probable

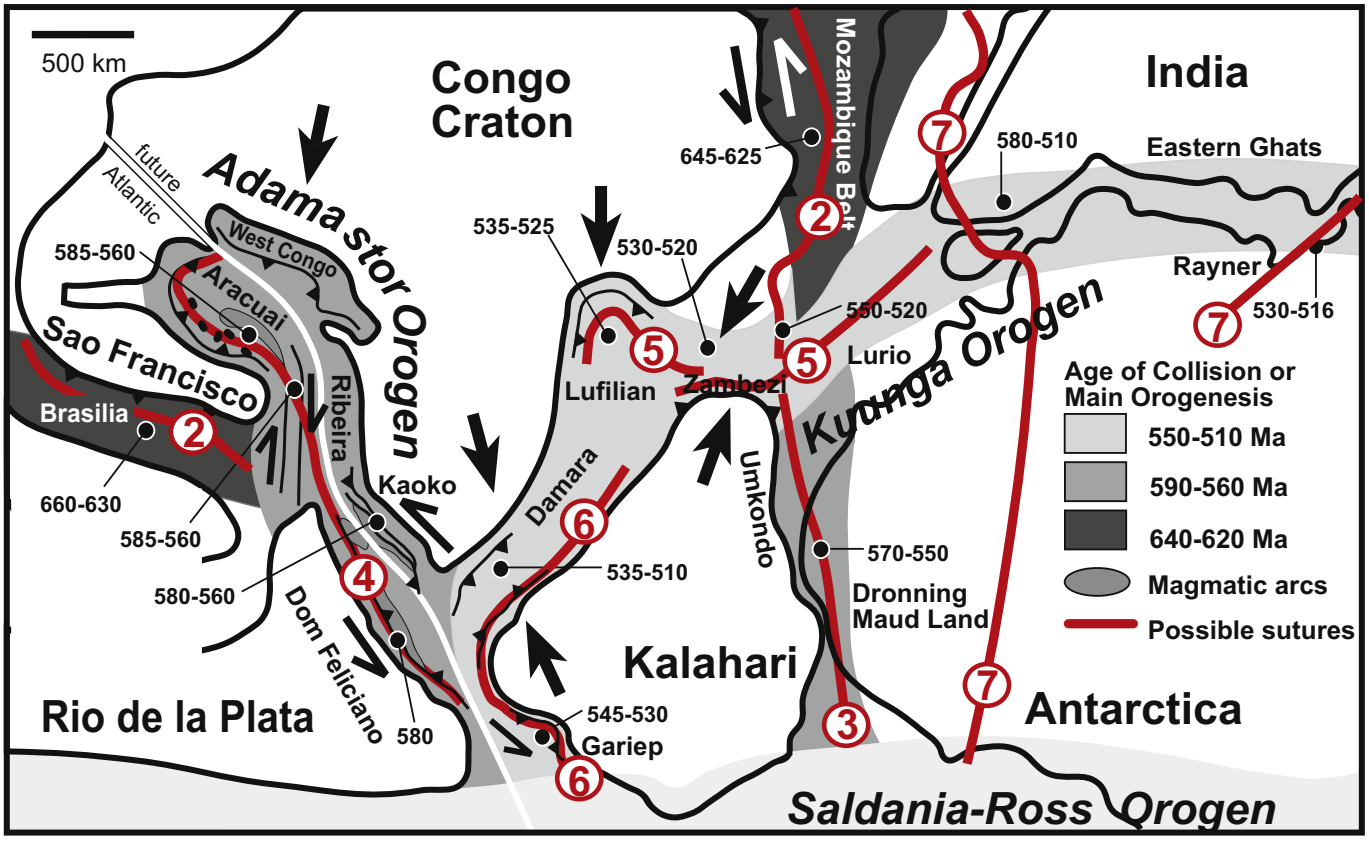

Figure 1. Schematic map of Gondwana with the Damara Belt located for context. The approximate age range of main phase orogenesis in the different metamorphic belts is summarized from the literature. Location of sutures involved in amalgamation of Gondwana is indicated (red lines), with the relative timing of suture closure numbered within circles. Suture 2: ~640 Ma collision of Azania in the North Mozambique Belt and Brasilia Belt between Rio De La Plata/Amazonia and Sao Fransico Cratons. Suture 3: ~585–565 Ma collision of Kalahari Craton and Antarctica. Suture 4: ~590–550 Ma collision of South Amerian and African components at the Kaoko, Dom Feliciano, Ribeira, Aracuai Belts. Suture 5: ~575–550 Ma collision of Congo and Kalahari Cratons within the Lufilian-Zambezi-Sth Malawi-Lurio Belts of the central Kuunga Orogen. Suture 6: ~555–530 Ma collision of Congo and Kalahari Cratons within the Gariep-Damara Belts of the west Kuunga Orogen and collisions in the east Kuunga Orogen. Suture 7: Collision of east and west Gondwana.

principle compressive stress direction during each deformation episode, following the approach previously established to unravel the evolution of the East Yilgarn Craton (Blewett and Czarnota, 2007a,b; Blewett et al., 2010; Czarnota et al., 2010). (3) Correlate deformations between these provinces on the basis of stress fields in common and absolute age constraints, resulting in an internally consistent model for evolving stress fields in central Gondwana between 590 Ma and 500 Ma.

To achieve these aims has required extensive field mapping in all parts of the system over 23 years. A small portion of this work has been published (Goscombe et al., 2003a,b, 2004, 2005a,b; Gray et al., 2006, 2008; Goscombe and Gray, 2007, 2008; Passchier et al., 2007; Foster et al., 2009), and detailed descriptions and comprehensive databases are available in Goscombe et al. (2017b). Absolute age calibration of the relative deformation frameworks has been undertaken by: (1) U-Pb dating of zircon in magmatic bodies with mapped relationships to deformation structures. (2) U-Pb dating of monazite in peak metamorphic parageneses correlated with deformation structures (Goscombe et al., 2017a). (3) An extensive literature review of metamorphic and magmatic age determinations for areas where the analyses contain sufficient field relationships to correlate to deformation features (Appendix 1). Deformation frameworks are strongly informed by integration with research that documents metamorphic response and thus orogen architecture, in all parts of the Damara Orogenic System (Goscombe et al., 2003b, 2004, 2005a, 2017a). The resultant internally consistent deformation framework, covering two mutually interacting orogenic systems, allows evolution of tectonic-scale stress fields to be documented beyond the local belt or province. Accurately pinning down rapid and dramatic stress switches has wider implications for the assembly of Gondwana and intra-plate orogenesis in the assembled supercontinent.

2. Large-scale architecture of the Damara orogenic system

Damara Orogenic System is a triple junction orogen that played a central role in the assembly of Gondwana through two orogenic periods (Fig. 2): Kaokoan Phase (590–535 Ma) and Damaran Phase (555–505 Ma). Three constituent belts (Gariep, Kaoko and Damara) experienced different histories governed by contrasting tectonic setting, convergence obliquity and lithosphere thickness etc.; resulting in distinct deformational style, metamorphic response and crustal architecture. N-trending Gariep Belt involved sinistral obduction of oceanic thrust sheets onto the Kalahari Craton (Frimmel and Frank, 1998), and is not considered further in this paper.

The NNW-trending Kaoko Belt involved obduction of the Coastal Terrane magmatic arc onto the Congo Craton and is contiguous with the Ugab Zone at the orogenic triple junction (Fig. 3; Goscombe and Gray, 2007). Coastal Terrane formed at the leading edge of attenuated Congo Craton margin, with deep-sea turbidites and slope sequences deposited in a backarc setting within the internal parts of the Kaoko Belt (Goscombe and Gray, 2008). Subduction outboard of the Coastal Terrane was terminated by collision of the Rio De La Plata Craton resulting in obduction of the arc along low-angle west-dipping decollements. Subsequent sinistral transpressional orogenesis at this margin was governed by thick Congo Craton lithosphere in the foreland, producing strong kinematic partitioning, steepening of crustal-scale shear zones and paired metamorphic response. Internal high-grade parts of the orogen have steep orogenic grain with lenticular shear lenses transected by crustal-scale oblique-slip shear zones. External parts of the belt are inverted Barrovian series, foreland vergent fold, thrust and basement-cored nappes with higher angles of transport. Decollements in the Kaoko Belt dip away from the Congo Craton, which is in a lower-plate setting (Fig. 4).

The ENE-trending Damara Belt involved closure of the Khomas ocean basin and high-angle collision of the Congo and Kalahari Cratons producing an asymmetric, bi-vergent orogen (Coward, 1981; Miller, 1983; Porada et al., 1983; Gray et al., 2008). Decollements in the Damara Belt dip away from the Kalahari Craton, which was thrust beneath attenuated Congo Craton in an upper-plate setting (Fig. 4; Gray et al., 2008). Damara Belt shows pronounced kinematic and thermal regime zonation:

(1) Southern orogenic margin consists of an intensely transposed schist belt in the Southern Zone and marginal fold-thrust belt with basement-cored nappes in the Southern Margin Zone (Fig. 4; Porada and Wittig, 1983). Uis-Pass Suture between these zones is the site of closure of a deep ocean basin and contains dismembered serpentinite (Kasch, 1983; Barnes, 1983; Killick, 2000). Upper-plate Southern Zone is a thick homoclinal accretionary wedge of deep-sea turbidites with Congo Craton provenance (Kukla and Stanistreet, 1991; Gray et al., 2008; Foster et al., 2015), devoid of basement and containing inter-thrust oceanic lithosphere (Killick, 2000). Southern Margin Zone has intensely sheared sequences with Kalahari Craton provenance deposited on a rifted passive margin abutting thick crustal lithosphere in the cratonic foreland (Ritter et al., 2003). The majority of collisional strain was partitioned into the southern margin, and transport was south-directed throughout. Deep burial produced inverted Barrovian series metamorphic response, overprinted by metamorphic discontinuities (MD) that accommodated extensional telescoping of the margin during exhumation (Goscombe et al., 2017a).

(2) Northern margin is complex, with dramatic along-orogen variation in deformation and metamorphic response (Goscombe et al., 2004). Central northern margin abuts thick crustal lithosphere in the Congo Craton foreland, resulting in a steep fold-thrust belt with complex fold interference (Fig. 4; Gray et al., 2008; Lehmann et al., 2015). In the east, a thick turbidite sequence deposited in a rift within the attenuated passive margin (Porada, 1979, 1983) was deeply buried to Barrovian metamorphic conditions and inverted late in the orogenic history (Goscombe et al., 2017a). In contrast, further west the Ugab Zone at the Kaoko-Damara junction is a thin 1.7 km sequence of turbidites (Swart, 1992) floored by thin lithosphere, similar to turbidites in the central Kaoko Belt. Consequently, the SW Congo Craton margin is ringed by disconnected deep-sea turbiditic basins indicating extreme attenuation of the passive margin in the Neoproterozoic. In the absence of exposed basement in the Ugab Zone, it is unknown if lithospheric attenuation at the triple junction progressed to seafloor formation in a Red Sea type setting. Kaokoan transpression inverted the Ugab turbidite basin resulting in bi-vergent flower-structure geometry with chevrons verging both east onto the Congo Craton and west onto Kaoko Belt terranes outboard of the Ogden Mylonite Zone (Fig. 4; Coward, 1983; Porada et al., 1983; Gray et al., 2006). This geometry is a primary feature that requires two basal decollements dipping east and west towards the central Ugab Zone where structures are steepest and probably rooting into a sinistral transcurrent structure at depth. Absence of exposed basement and high shortening strains in the Ugab Zone also imply decollements between turbidite sequences and basement substrate (Gray et al., 2006), consistent with flat lying bedding parallel fabrics and boudinage at earliest stages in the deformation history. Bi-vergent flower geometry is consistent with closure of a back arc

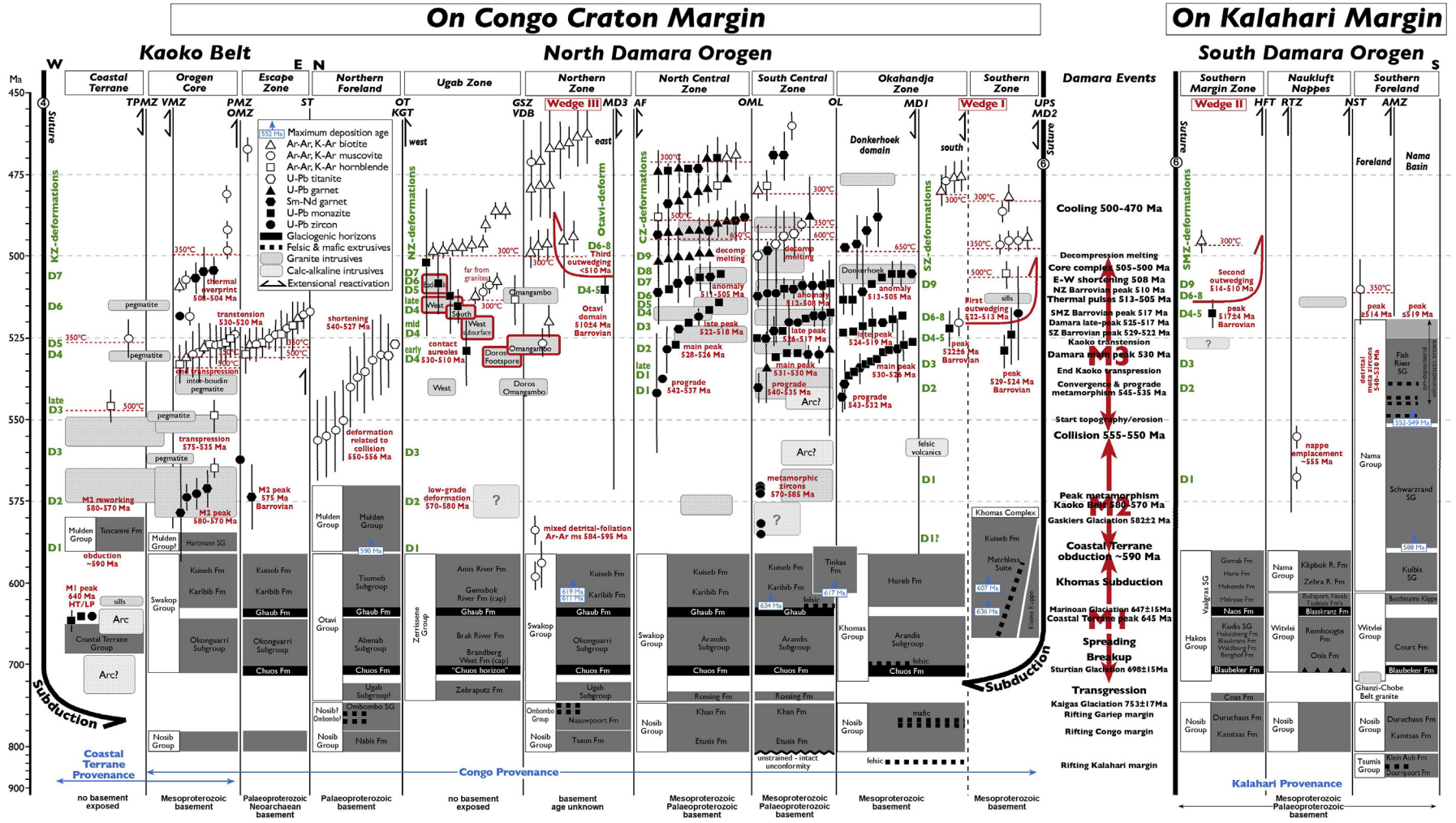

Figure 2. Time-space diagram outlining the stratigraphy in different zones of the Damara Belt. Modified after Hoffmann (1989) with latest corrections to stratigraphy from Halverson et al. (2002) and Hoffmann et al. (2004), recent geochronology of felsic extrusives (e.g. Hoffman et al., 1996). Older published stratigraphy for the internal parts of the Kaoko Belt (i.e. Guj, 1970; Henry et al., 1992; Prave, 1996; Stanistreet and Charlesworth, 2001) are inconsistent with recently mapped geology such as the recognition of two diamictites, and have been modified (Goscombe et al., 2005b; Goscombe and Gray, 2007, 2008). Otherwise in other provices no changes have been made and the most recent and accepted stratigraphy is presented (Hoffmann, 1989, 1994, 1997; Swart, 1992; Hoffman et al., 1996; Halverson et al., 2002; Hoffmann et al., 2004). All available metamorphic and cooling age determinations sourced from literature and this project are indicated (Appendices 1 and 2). Only robust U-Pb monazite, zircon, garnet and titanite metamorphic ages, Lu-Hf and Sm-Nd garnet metamorphic ages and Ar-Ar hornblende, muscovite and biotite cooling ages have been compiled. The age range for different episodes of granitoid crystallization is indicated by grey cross-hatching.

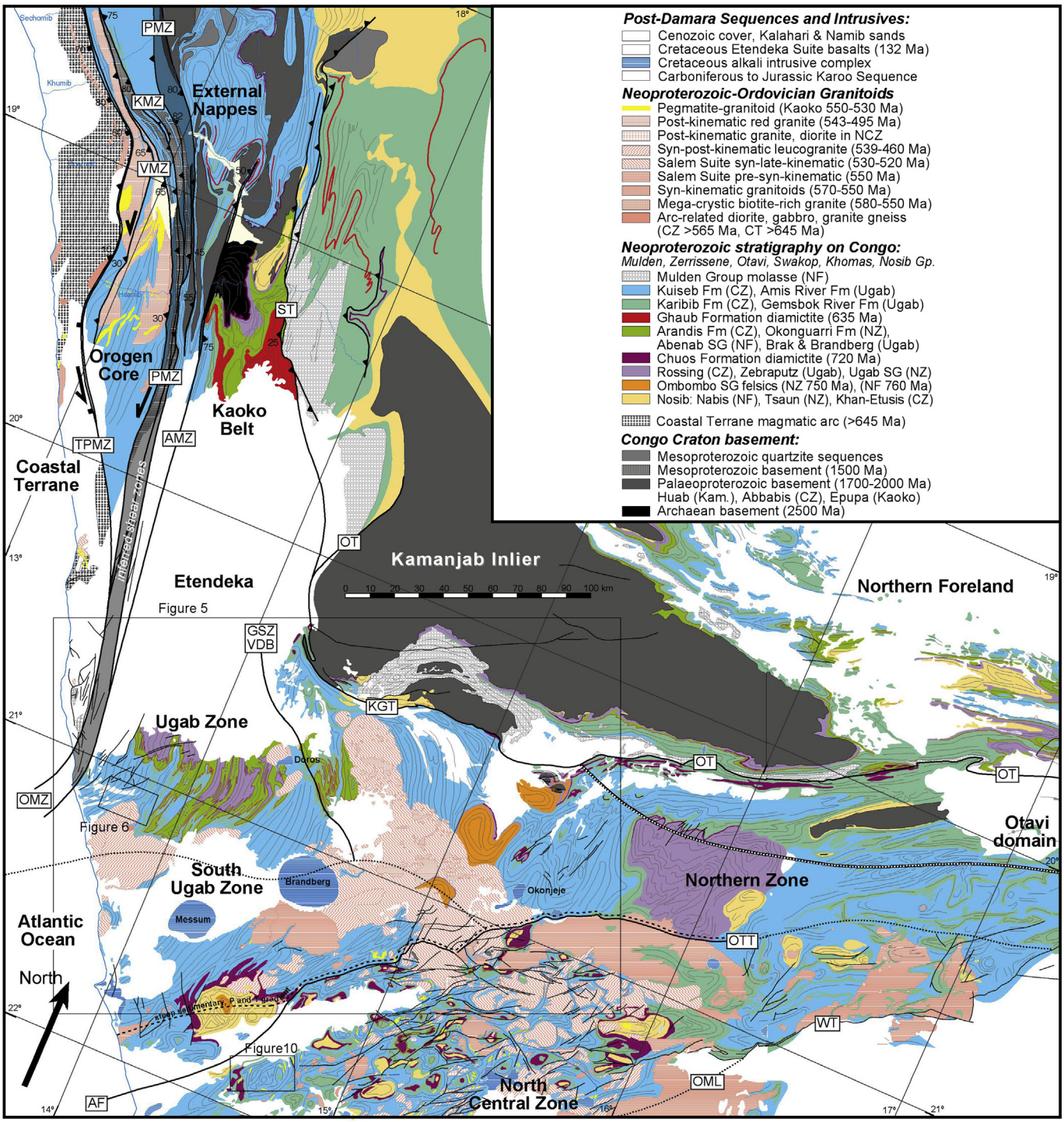

Figure 3. Geological map of the Damara Belt – Kaoko Belt junction, compiled primarily from the published 1:500,000 geological map of Namibia for the Damara Belt component (Miller and Grote, 1988), and published mapping of the Kaoko Belt (Guj, 1970; Goscombe et al., 2003a, 2005a,b; Goscombe and Gray, 2007, 2008). Tectono-metamorphic zone labels are as currently accepted in the literature except for the South Ugab Zone, North Central Zone and Okahandja Zone, which have been modified in response to new metamorphic data (Goscombe et al., 2017a). Most zones are demarcated by crustal-scale shear zones, thrusts or faults, which are indicated by abbreviations: Crustal-scale shear zone abbreviations: ST – Sesfontain Thrust, PMZ – Purros Mylonite Zone, KMZ – Khumib Mylonite Zone, VMZ – Village Mylonite Zone, AMZ – Ahub Mylonite Zone, HMZ – Hartmann Mylonite Zone, TPMZ – Three Palms Mylonite Zone, OT – Outjo Thrust, AF – Autseib Fault, GSZ/VDB – Goantagab Shear Zone (Vrede-Doros-Brandberg line), KGT – Khorixas-Gaseneirob Thrust, OMZ – Ogden Mylonite Zone, WT – Waterberg Thrust, OTT – Otjorongo Thrust, OML – Omaruru Lineament.

basin setting, and inconsistent with transport out of an ocean basin onto a cratonic margin, such as in the Gariep Belt (Gray et al., 2006; Goscombe and Gray, 2008). Damaran Phase events in the Ugab Zone produced complex low-strain fold and fabric interference (Passchier et al., 2002, 2007, 2016; Goscombe et al., 2004), at low-grade metamorphic conditions, and punctuated by diachronous contact metamorphism associated with granite plutonism (Goscombe et al., 2017a).

(3) Central Zone in the orogen core has relatively thin Damaran strata deposited on highly attenuated basement of the former Congo Craton passive margin (Fig. 4). Deformation was moderate

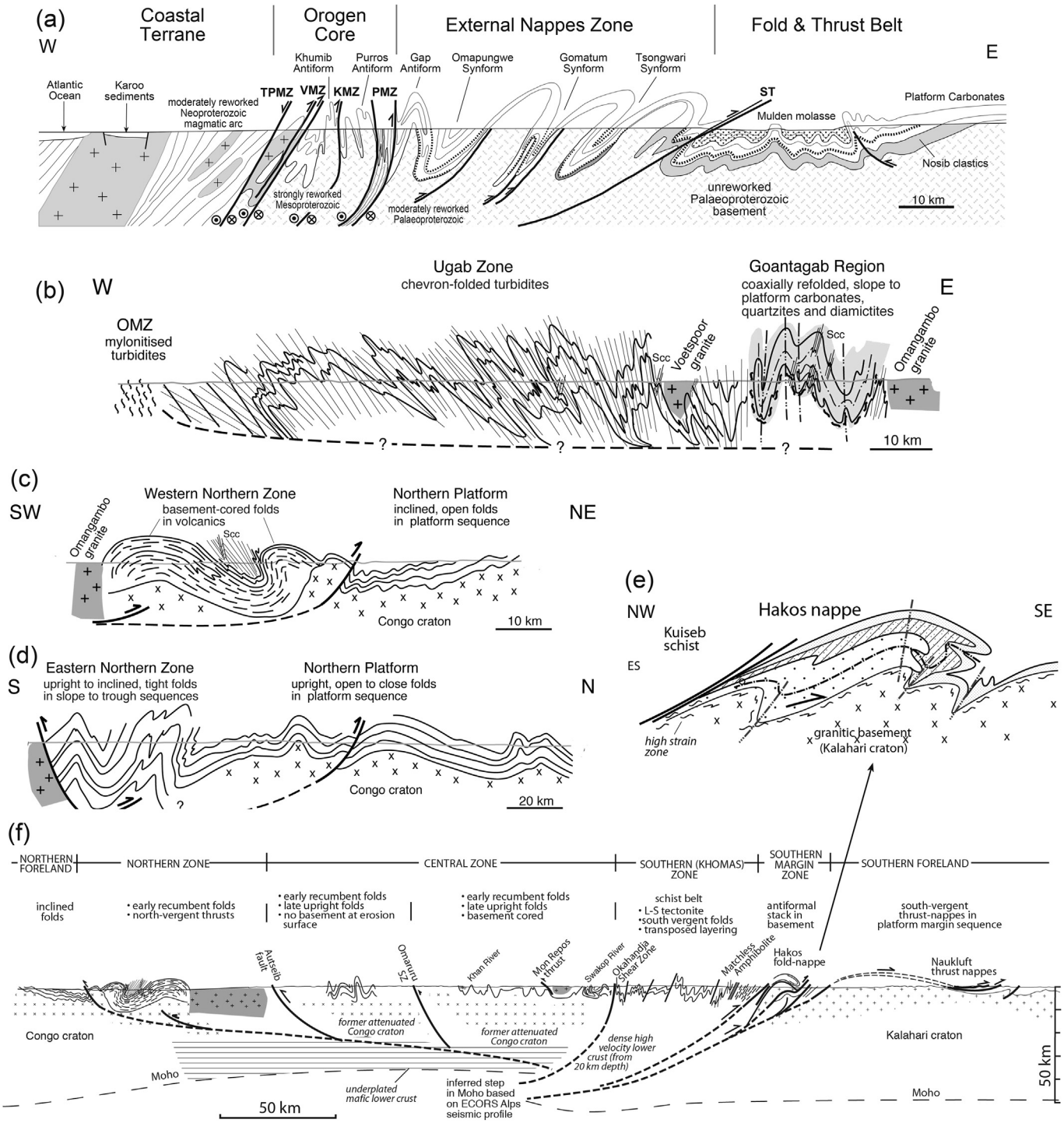

Figure 4. Simplified structural profiles across the (a) Kaoko (from Goscombe et al., 2003a), (b) Ugab Zone, (c) west Northern Zone (from Goscombe et al., 2004), (d) east Northern Zone (from Goscombe et al., 2004), (e) Hakos Nappe in the Southern Margin Zone, and (f) Damara Belt (from Gray et al., 2007, 2008).

strain N–S shortening with upright to inclined folds and later cross-folds producing dome and basin interference (Longridge et al., 2011, 2014). Metamorphic response was long-lived medium-P granulite conditions (Masberg, 2000; Goscombe et al., 2017a; Longridge et al., 2017) and associated with large volumes of syn-kinematic granite originating from mid- to lower-crustal melting (McDermott et al., 2000; Jung et al., 2001). The Okahandja Zone is steep dipping, tightly folded upper stratigraphy, metamorphosed to medium-P amphibolite facies, and over-printed by post-kinematic Donkerhoek leucogranite batholith. This zone is the leading edge of attenuated Congo Craton and is transitional in character between the high-grade orogen core and Barrovian southern margin.

3. Methodology

Deformation histories are established for each of the four tectono-metamorphic provinces making up the Damara Orogenic System on the basis of field relationships, over-printing criteria and

radiometric age data (Fig. 2; Table 1; Appendix 3). These extend and refine the partial structural frameworks already published (Goscombe et al., 2003a, 2004, 2005a,b, 2007; Gray et al., 2006, 2008; Passchier et al., 2007; Goscombe and Gray, 2008; Foster et al., 2009). The scope of this project is such that complete structural, mapping and observational datasets cannot be published here, nevertheless comprehensive datasets are available in Goscombe et al. (2017b) and relevant subsets are available as electronic Appendices 1–4. Four modes of approach were taken:

Relative Structural Frameworks: Detailed mapping of key regions with clear structural and magmatic over-printing criteria and representative of a province; was undertaken using high-resolution satellite imagery (Fig. 3). Over-printing relationships between deformation structures, fabrics, mineral growth and intrusives, were made at map-scale, in outcrop and in thin section (Goscombe et al., 2017a). Key mapping areas were supplemented with field observations and semi-continuous structural profiles across all parts of the system. These results are integrated with over-printing relationships available in literature and published mapping. A large variety of deformation structures have been exploited to determine tectonic vergence and shear sense (Lister and Snoke, 1984; Simpson, 1984; Passchier and Simpson, 1986; Goscombe and Trouw, 1998; Passchier, 2001; Goscombe and Passchier, 2003; Passchier and Trouw, 2005). Bulk strain, strain regime and foliation intensity are estimated by the simplified semi-quantitative methods outlined in Goscombe and Gray (2008), and dataset presented in Appendix 4.

Stress Field Interpretations: Principle compressive stress, or shortening direction, is estimated for each deformation period on the basis of geometry of developed structures, such as folds, linear and planar fabrics, boudins trains, tension gashes and magmatic intrusions, as outlined by Blewett and Czarnota (2007a,b) and Blewett et al. (2010). Relatively low-strain deformation environments with upright structures, such as the Central and Ugab Zones have coaxial strain regimes near pure shear, and principle compressive stress is approximately orthogonal to fold axial planes, cleavages and schistosity. All other deformation environments have varying degrees of non-coaxial strain and principle compressive stress direction is limited to the quadrant bound by principle slip plane (C-plane), the plane orthogonal to this, and within the plane

Table 1
Simplified time-space table of deformation correlations across the four distinct tectono-metamorphic provinces of the Damara Orogenic System. Summary ranges of age determinations from intrusives (grey), metamorphic parageneses (red) and cooling ages are presented as pinning-points to constrain probable age range for deformation events (yellow). Consequently, deformation age ranges are interpretive, based on correlations and over-printing criteria with respect to directly dated magmatic events and metamorphic parageneses. Underlined – Age determination undertaken for this project: Metamorphic parageneses dated by LA-ICPMS U-Pb monazite; Igneous bodies dated by MC-ICPMS U-Pb zircon. All other age ranges collated from age determinations in literature. * – Approximate trend of principle compressive stress (σ_1), with arrow indicating transport direction of the upper-plate, based primarily on Kaoko Belt and west Ugab Zone. Deformation events are labelled by province: Dkz – Coastal Terrane and Kaoko Belt north of the Etendeka Plateau. Dnz – Ugab Zone and west Northern Zone. Dcz – South Ugab Zone, Central Zone and north and central Okahandja Zone. Dsz – south Okahandja, Southern and Southern Margin Zones, Southern Foreland.

σ1*	KAOKO BELT			NORTHERN MARGIN			OROGEN CORE			BARROVIAN MARGINS		
	Coastal Terrane Only:											
	661-655		Calc-alkaline arc granitoids									
	650-640		M1-peak metamorphism									
	638-620		Granite sills									
				<598-584		Ar-Ar ms, defm/detrital [NZ]						
to 090°	~590	Obduction of Coastal Terrane								≥580-555?	D1sz?	Bedding foliation, qtz-veins [SZ]
to 090°	~590-580	D1kz	Flat-lying early foliation	~590-580	D1nz	E-W stretching lineation [UZ]						
to 120°	~580-570	D2kz	Main L-S fabric	~580-570	D2nz	Chevron folds, main foliation	585-570		Metamorphic zircons	588-545		Schwarzrand SG deposition
	579-571		M2-peak metamorphism	~580-570		M2-peak main foliation	580		End of deposition on Congo	580		End deposition on Kalahari
	580-562		Syn-kinematic granite	~573-562		Granite	580-570		Pre-kinematic granite	580-555	D1sz	Bedding foliation, qtz-veins [SMZ]
to 120°	~570-550	D3kz	Progressive transpression	~570-550	D3nz	NE-SW sinistral folds	568-556		I-type granitoids			
to ~140°		Collision Congo-Kalahari Cratons		556-550		K-Ar defm age [Foreland]				555		Nappe Ar-Ar ms [Naukluft]
	559-549		Late-kinematic granite				555-534	D1cz	Prograde, melt, gneissic fabric		D2sz	Axial planar main foliation
to 140°	~550-540	late-D3kz	Strike-slip sinistral shear zones				546-534		S-type syn-kinematic granite	552-519		Fish River SG deposition
to 140°	539±6		Final late-kinematic melt	~540		West, Doros, Omangambo	543-534		M3a-prograde metamorphism	540-530		Detrital metamorphic zircons
				540		K-Ar phyllite age [Foreland]	539-536		Anatectic Red granites			
				535-530		K-Ar phyllite age [Foreland]	≥530	late-D1cz	Intrafolial isoclines		D3sz	Main folds, nappes
to 160°	>531	D4kz	End ductile shearzones	~530	early-D4nz	NNW-SSE shortening folds	~530-516	D2cz	Peak metamorphic events, melt			
	531-530		Post-kinematic pegmatite	534-528	M3#1	Doros, Footspore Granites	531-530		M3b-peak#1 [main peak SCZ]			
				530-527		Mineralization [Foreland]	530.0±2.7		Syn-peak leucogranite sill [SCZ]			
				527-526		Omangambo Granite	528±7		Aplite-granite sills [NCZ]			
							528-519		M3b-peak#1 [NCZ, OZ]			
to 160°?	~533-525	D5kz	Transtension reactivation				≤530-521	D3cz	N over S folds, foliation, melt	~529-522	D4-5sz	Peak mineral growth [SZ-OZ]
	533-525		Rapid cooling exhumation				525-523		M3b-peak#2 [SCZ]	529-524	1st cycle	M3-peak [SZ]
to 160°				~522	mid-D4nz	NNW-SSE shortening	518.4±1.9		M3b-peak#2 [main peak NCZ]	522		M3-peak [Sth OZ]
				521-519	M3#2	South Ugab Granite	525		A-type syn-kinematic granite	~522-513	D6-8sz	Initiate exhumation [SZ-OZ]
	524-507		Regional cooling Ar-Ar	520		Cooling Ar-Ar [west NZ]	521-520		Syn-kinematic grey granite		1st cycle	
							~518-516	D4cz	NNW over SSE tight folds			
							520-517		M3b-peak#3 [SCZ]			
							517.4±1.3		Late-kinematic pegmatite [NCZ]			
to 180°	<525	D6kz	N-S shortening folds	~516, >512	late-D4nz	N-S shortening	~518-516	D5cz	Tight folds, S over N, foliation	~517	D4-5sz	Peak mineral growth [SMZ-SF]
							516-513	early-D6cz	Magmatism, oblate shortening	<519	2nd cycle	M3-peak [Nama]
	515		Post-kinematic N-S pegmatite	516±3	M3#3	West Ugab Granite	516.3±1.3		Alkali-feldspar pegmatite [NCZ]	517±4		M3-peak [SMZ]
							516-514		M3b-peak#3 [NCZ]	≥514-510		M3-peak [SF]
							516-513		Post-peak S-type granite	~517-513	D6-8sz	Initiate exhumation [SMZ]
							513-508	late-D6cz	Thermal anomaly, extension			
							515-505		M3c-late thermal pulse [CZ]	514±6	2nd cycle	Post-kinematic granite [SF]
				513-511	M3#4	Omangambo, Baddocks Bay	512-507		Late-kinematic granite [CZ]	513±17		Post-kinematic granite [SZ]
							511-508		Extensional granite veins [SCZ]			
to 225°				<512	D5nz	NE-SW shortening, warps						
to 225°				<512	D6nz	NE-SW shortening, kinks					D9sz	NE-SW shortening, kinks
				512-508		Distal cooling Ar-Ar ms				510		350°C cooling Ar-Ar ms, [SF]
			Otavi Domain	510±4	D4-5	M3-peak metamorphism						
				<510	D6-8	Initiate exhumation [Otavi]						
to 270°				512-508	D7nz	E over W shortening folds	~508	D7cz	E over W upright folds, domes			
to 270°				~512-508	D8nz	Brittle E-W thrusting						
	508		Post-kinematic ESE pegmatite	508		Strathmore Granite	508-504		Donkerhoek granite			
vertical σ1	~508-505	D7kz	N-S extension				~505	D8cz	Flattening folds, N-S extension	505		500°C cooling Ar-Ar hbl
	507-505		M3c-late thermal pulse									
							502±9		Decompression melting			
vertical σ1							~500	D9cz	Core complex, N-S extension			
	498-481		Late-cooling Ar-Ar ms,bt	499-486		Cooling Ar-Ar ms,bt	500-470		Cooling 700 to 500 °C	496-486		350°C cooling Ar-Ar ms
							488-460		Cooling 500 to 300 °C	495-482		300°C cooling Ar-Ar bt

Table 2
Summary of new U-Pb zircon and monazite age data generated in this project to constrain the age range of deformation events. Metamorphic parageneses have been dated using LA-ICPMS U-Pb analysis of monazite (Ben Wade, University of Adelaide). Granitic intrusives have been dated using MC-ICPMS U-Pb analysis of zircon (David Foster, University of Florida). Crystallization age indicates the crystallization of an igneous rock and is interpreted to approximate the time of intrusion. Sample details and methodologies used to generate these data are presented in text and Appendix 2.

Location	Sample	Stratigraphic unit	Rock-type	Method	*n*	Age (Ma)	Interpretation
Ugab Zone							
Ogden Mylonite Zone	BG9-298 (DF9-39)	Neoarchaean basement	Sheared orthogneiss	Pb^{207}/Pb^{206} LA-MC-ICPMS upper intercept (zrn)	[15]	2606.3 ± 7.7	Crystallization age
Ogden Mylonite Zone	BG9-297 (DF9-38)	Palaeoproterozoic basement	Sheared orthogneiss	Pb^{207}/Pb^{206} LA-MC-ICPMS upper intercept (zrn)	[25]	1861.8 ± 5.4	Crystallization age
Doros granite	U305	Pan-African granitoid	Granodiorite	Pb^{206}/U^{238} LA-MC-ICPMS concordant (zrn)	[1]	522 ± 14	Crystallization age
West Ugab granite	BG14-368	Damara Sequence	Aureole crd-and-metapelite	Pb^{207}/Pb^{206} LA-ICPMS weighted mean (mnz)	[17]	529 ± 11	Contact metamorphism
West Ugab granite	BG13-214	Damara Sequence	Aureole metapelite	Pb^{206}/U^{238} LA-ICPMS weighted mean (mnz)		~510–520	Contact metamorphism, spread
West Ugab granite	98, 296, 259, 255a	Pan-African granitoid	Grey granite, phase #2	Pb^{206}/U^{238} LA-MC-ICPMS weighted mean (zrn)	[21]	515.7 ± 3.1	Crystallization age, pooled samples
West Ugab granite	BG13-98	Pan-African granitoid	Grey granite, phase #2	Pb^{206}/U^{238} LA-MC-ICPMS weighted mean (zrn)	[5]	515 ± 7	Crystallization age
West Ugab granite	BG9-296 (DF9-37)	Pan-African granitoid	Grey granite, phase #2	Pb^{206}/U^{238} LA-MC-ICPMS weighted mean (zrn)	[10]	511.9 ± 5.2	Crystallization age
West Ugab granite	BG13-98, BG9-296	Pan-African granitoid	Grey granite, phase #2	Pb^{206}/U^{238} LA-MC-ICPMS weighted mean (zrn)	[15]	514.6 ± 3.4	Crystallization age, pooled samples
South Ugab granite subsurface	BG13-99,239	Pan-African granitoid	Aplite #3, pegmatite #4	Pb^{206}/U^{238} LA-MC-ICPMS weighted mean (zrn)	[7]	520.9 ± 6.9	Crystallization age, pooled samples
South Ugab granite subsurface	BG13-99	Pan-African granitoid	Aplite dyke, phase #3	Pb^{206}/U^{238} LA-MC-ICPMS weighted mean (zrn)	[5]	519.3 ± 3.3	Crystallization age
South Ugab granite subsurface	BG13-239	Pan-African granitoid	Pegmatite dyke, phase #4	Pb^{206}/U^{238} LA-MC-ICPMS weighted mean (zrn)	[3]	521 ± 24	Crystallization age
South Ugab granite subsurface	BG14-475b	Damara Sequence	Aureole crd-metapelite	Pb^{207}/Pb^{206} LA-ICPMS weighted mean (mnz)	[17]	502 ± 24	Contact metamorphism
South Ugab granite	U255a, U259	Pan-African granitoid	Hornblende granite	Pb^{206}/U^{238} LA-MC-ICPMS weighted mean (zrn)	[5]	519 ± 11	Crystallization age, pooled samples
South Ugab granite	U259	Pan-African granitoid	Megacrystic granite	Pb^{206}/U^{238} LA-MC-ICPMS concordant (zrn)	[1]	~517	Crystallization age
South Ugab granite	U255a	Pan-African granitoid	Hornblende granite	Pb^{206}/U^{238} LA-MC-ICPMS weighted mean (zrn)	[4]	515 ± 5	Crystallization age
Badocks Bay granite	BG14-537	Damara Sequence	Aureole metapelite	Pb^{207}/Pb^{206} LA-ICPMS weighted mean (mnz)	[16]	512 ± 12	Contact metamorphism
Badocks Bay granite	BG14-569	Pan-African granitoid	Granite	Pb^{206}/U^{238} LA-MC-ICPMS weighted mean (zrn)		~507	Crystallization age, inaccurate
Strathmore region	BG14-494b	Damara Sequence	Aureole metapelite	Pb^{207}/Pb^{206} LA-ICPMS weighted mean (mnz)	[20]	508 ± 9	Contact/reional metamorphism
Northern Zone							
Otavi domain	BG6-94A	Damara Sequence	BARROVIAN metapelite	Pb^{207}/Pb^{206} LA-ICPMS lower intercept (mnz)	[19]	510 ± 4	Regional Barrovian metamorphism
West Northern Zone	DF9-26 (BG9-277)	Damara Sequence	L Kuiseb Fm. metasediment	Pb^{206}/U^{238} LA-MC-ICPMS 1.81 −10.1% discordance (zrn)	[6]	611 ± 10	Maximum deposition age
West Northern Zone	DF9-30 (BG9-283)	Damara Sequence	U Kuiseb Fm. metasediment	Pb^{206}/U^{238} LA-MC-ICPMS 3% discordance (zrn)	[1]	619 ± 8	Maximum deposition age
Central Zone							
Lower Omaruru River	BG16-11	Damara Sequence	Metapelite granulite melt	Pb^{206}/U^{238} LA-MC-ICPMS weighted mean (zrn)	[21]	518.4 ± 1.9	Peak granulite metamorphism
Lower Omaruru River	BG14-599	Damara Sequence	Metapelite granulite	Pb^{207}/Pb^{206} LA-ICPMS weighted mean (mnz)	[20]	507 ± 4	Secondary metamorphic anomaly
Lower Omaruru River	BG16-12a	Pan-African granitoid	Syn-peak garnet aplite sill	Pb^{206}/U^{238} LA-MC-ICPMS weighted mean (zrn)	[10]	528.1 ± 6.9	Crystallization age
Lower Omaruru River	BG16-12b	Pan-African granitoid	Late-kinematic bt-pegmatite	Pb^{206}/U^{238} LA-MC-ICPMS weighted mean (zrn)	[41]	517.4 ± 1.9	Crystallization age
Lower Omaruru River	BG16-10a	Pan-African granitoid	Alkali-feldspar pegmatite	Pb^{206}/U^{238} LA-MC-ICPMS weighted mean (zrn)	[54]	516.3 ± 1.3	Crystallization age
Middle Khan River	BG16-5	Pan-African granitoid	Syn-peak leucogranite sill	Pb^{206}/U^{238} LA-MC-ICPMS weighted mean (zrn)	[35]	530.0 ± 2.7	Crystallization age
Middle Khan River	DF9-43	Proterozoic basement	Basement granite orthogneiss	Pb^{206}/U^{238} LA-MC-ICPMS weighted mean (zrn)	[38]	1027.9 ± 2.2	Magmatic age
Middle Khan River	DF9-43	Proterozoic basement	Basement granite orthogneiss	Pb^{206}/U^{238} LA-MC-ICPMS -1.0% discordance (zrn)	[1]	~520 ± 25	~Metamorphic age
Middle Khan River	DF9-44	Damara Sequence	Nosib Group metasediment	Pb^{206}/U^{238} LA-MC-ICPMS -0.30% discordance (zrn)	[1]	~542 ± 9	~Metamorphic age
South Central Zone	CZ53b	Damara Sequence	Tinkas Fm. metasediment	Pb^{206}/U^{238} LA-MC-ICPMS 2.30% discordance (zrn)	[1]	617 ± 22	Maximum deposition age
South Central Zone	CZ53b	Damara Sequence	Tinkas Fm. metasediment	Pb^{206}/U^{238} LA-MC-ICPMS 7.1% discordance (zrn)	[1]	582 ± 25	Maximum metamorphic age
South Central Zone	CZ35	Damara Sequence	Karibib Gp. metasediment	Pb^{206}/U^{238} LA-MC-ICPMS 4.5–8.3% discordance (zrn)	[3]	634 ± 10	Maximum deposition age

Table 2 (*continued*)

Location	Sample	Stratigraphic unit	Rock-type	Method	*n*	Age (Ma)	Interpretation
South Central Zone	CZ35	Damara Sequence	Metasediment	Pb^{206}/U^{238} LA-MC-ICPMS 10% discordance (zrn)	[1]	585 ± 12	Maximum metamorphic age
Southern Zones							
South Okahandja Zone	BG9-345a	Damara Sequence	Barrovian metapelite	Pb^{207}/Pb^{206} LA-ICPMS lower intercept (mnz)	[15]	522 ± 6	Peak Barrovian metamorphism
Nth Southern Zone	SZ13	Damara Sequence	Barrovian metapsammite	Pb^{206}/U^{238} LA-MC-ICPMS 0.24% discordance (zrn)	[1]	607 ± 22	Maximum deposition age
Nth Southern Zone	SZ41a	Damara Sequence	Barrovian metapelite	Pb^{207}/Pb^{206} LA-ICPMS intercept (mnz)	[16]	529 ± 5	Peak Barrovian metamorphism
Nth Southern Zone	SZ40	Damara Sequence	Barrovian metapelite	Pb^{206}/U^{238} LA-MC-ICPMS 3.3% discordant (zrn)	[1]	517 ± 8	~Peak Barrovian metamorphism
Nth Southern Zone	SZ40	Damara Sequence	Barrovian metapelite	Pb^{206}/U^{238} LA-MC-ICPMS 3.7% discordant (zrn)	[1]	636 ± 9	Maximum deposition age
Nth Southern Zone	SZ44a	Damara Sequence	Barrovian metapelite	Pb^{207}/Pb^{206} LA-ICPMS intercept (mnz)	[16]	524 ± 9	Peak Barrovian metamorphism
Nth Southern Zone	BG09-322	Pan-African Granitoid	Post-main foliation granite sill	Pb^{206}/U^{238} LA-MC-ICPMS (zrn)	[2]	~513 ± 17	Crystallization age
Nth Southern Margin	SMZ1	Damara Sequence	Barrovian metapelite	Pb^{207}/Pb^{206} LA-ICPMS weighted mean (mnz)	[26]	517 ± 4	Peak Barrovian metamorphism

containing the stretch direction. By using a variety of coeval structures from a region, shortening direction is progressively narrowed. This approximation is reliable in high-strain environments approaching simple shear and where stretching directions are well developed, such as the southern orogenic margin and Kaoko Belt. Intermediate-strain deformation environments with inclined structures, may have strain regimes far from pure and simple shear end-members and limiting principle compressive stress direction more ambiguous.

Time Calibrated Frameworks: Absolute age range for deformation events is constrained by over-printing relationships and bracketing with respect to metamorphic parageneses or magmatic intrusions of known age (Table 1). To establish absolute time markers, a select number of samples with key relationships have been dated (Table 2), with sample descriptions, full analytical details and results contained in Appendix 2. Key granitoid intrusions with mapped relationships to deformation events, have been dated using LA-MC-ICP-MS U-Pb analysis of zircon following the method described by Foster et al. (2015). Peak metamorphic parageneses representative of each tectono-metamorphic zone, have been dated using LA-ICP-MS U-Pb analysis of monazite following the method of Payne et al. (2008). In addition, a comprehensive database of metamorphic and magmatic age determinations for the Damara Orogenic System has been compiled from literature, and used to limit deformation age ranges where possible (Appendix 1). Specific arguments constraining probable deformation ages are discussed along with the relevant structures and over-printing relationships described in Section 4.

Orogen Wide Correlations: We attempted to correlate between time calibrated deformation frameworks for each of the four provinces (Table 1; Appendix 3), and produce an internally consistent deformation framework for the entire orogenic system. Correlations are based on stress fields in common and absolute age constraints. The resulting integrated framework is internally consistent; stress fields are mutually reinforcing between the different provinces and age limits overlap within analytical errors (Appendix 3). This deformation framework is consistent with the metamorphic history established in parallel (Goscombe et al., 2003b, 2004, 2005a, 2017a), and together result in a comprehensive internally consistent tectono-metamorphic model for the Damara Orogenic System. The high degree of internal consistency and accuracy validates the model framework. This model confidently documents 1st-order evolution of the stress field for the orogenic system as a whole, independent of 3rd-order ad hoc variables such as developed structures, deformation style, strain state, rock units, metamorphic grade, etc., in the different parts of the system.

4. Integrated structural histories

4.1. Kaoko Belt

4.1.1. Overview

Kaoko Belt is a classic transpressional orogen, formed during oblique collision between the Congo and Rio De La Plata Cratons (Coward, 1983; Porada, 1989; Prave, 1996; Trompette, 1997). Kaokoan Phase orogenesis evolved from; W over E obduction of the Coastal Terrane onto the Congo Craton margin at ~590 Ma, main phase transpressional orogenesis and syn-kinematic granitoids at 580–560 Ma, progressive sinistral transpression partitioned between wrench and shortening deformation, and finally strain localization in strike-slip shear zones after ~550 Ma (Seth et al., 1998; Goscombe et al., 2003a, 2005a,b; Konopásek et al., 2005). Transpressional orogenesis was terminated at ~530–525 Ma by stress switch to NNW–SSE shortening in response to Damaran Phase orogenesis, resulting in transtensional reactivation of shear zones, pegmatites and rapid exhumation (Goscombe et al., 2005b; Foster et al., 2009). Ongoing N–S shortening produced E–W buckling of shear zones and structural grain and N–S trending pegmatites of ~515 Ma age (Goscombe et al., 2005b). Final imprint was a stress switch that imposed E–W shortening across the belt, resulting in N–S extension, pegmatites and thermal pulse at ~508–505 Ma (Fig. 2).

Kaoko Belt has steep bivergent flower and half-flower geometry controlled by a network of arcuate crustal-scale shear zones (Fig. 4; Dürr and Dingeldey 1996; Goscombe et al., 2003a, 2005a). Shear zones are predominantly steep west dipping to listrically inclined at depth, with decreasing dips in the south of the belt (Guj, 1970; Dingeldey et al., 1994; Stanistreet and Charlesworth, 2001; Goscombe et al., 2003a; Konopásek et al., 2005). The structural architecture was controlled by two predominant shear zones with contrasting slip trajectories (Fig. 3). At highest structural levels, Three Palms Mylonite Zone (TPMZ) was an oblique-slip sinistral-normal shear zone that transported the Coastal Terrane downwards and to the south with respect to the core of the belt. Purros Mylonite Zone (PMZ) is an oblique-slip sinistral-reverse shear zone that accommodated upward and SSE-directed transport of the orogen core. Orogen architecture resulted from progressive

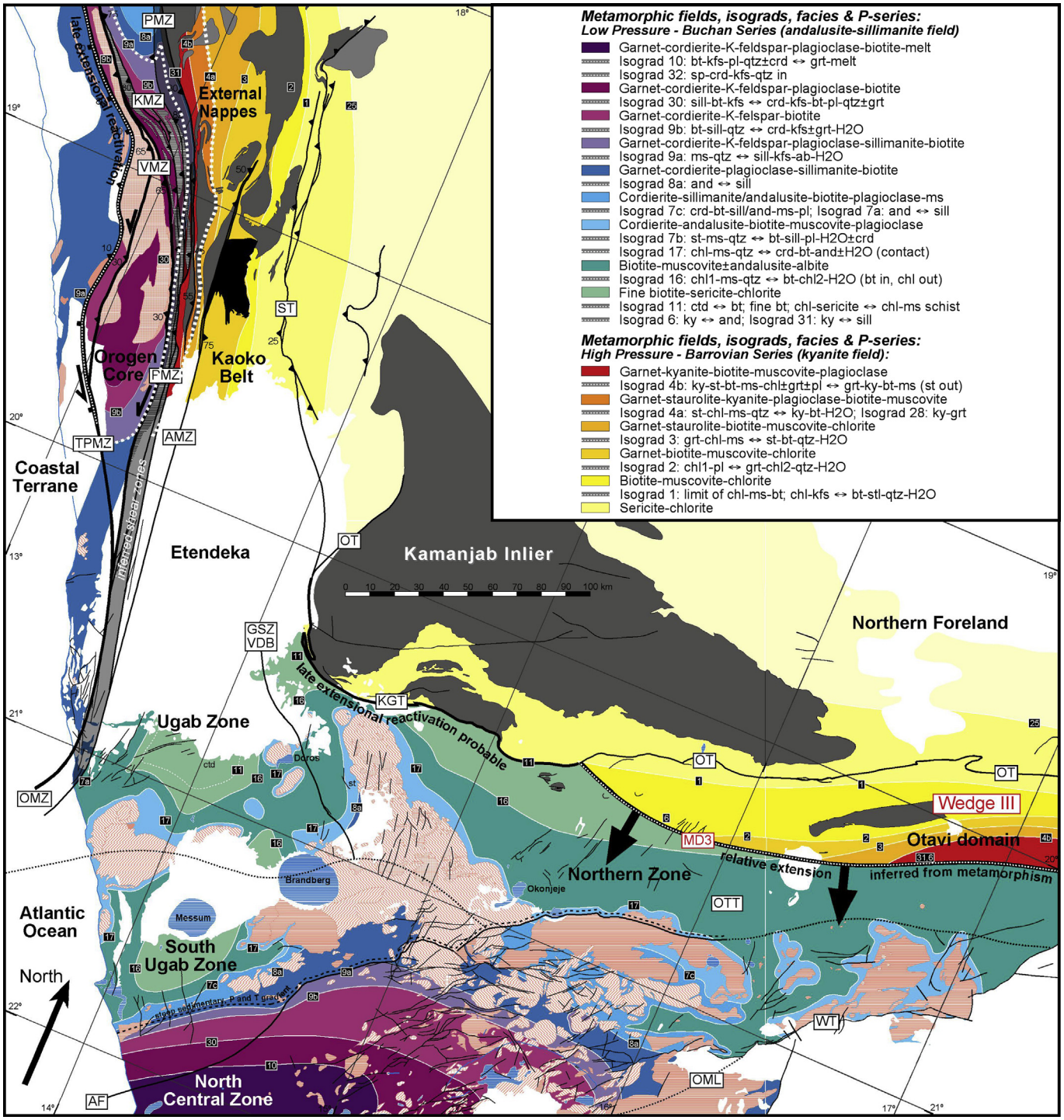

Figure 5. Metamorphic map of the Damara Belt – Kaoko Belt junction. Metamorphic fields and isograds have been compiled from a number of published sources (e.g. Hartmann et al., 1983; Kasch, 1983; Miller, 1983; Goscombe et al., 2003b, 2004, 2005a, 2017a), and modified after new metamorphic mapping, petrology and quantitative PT determinations, particularly in the Ugab and Northern Zones (Goscombe et al., 2004, 2017a). Crustal-scale shear zone abbreviations are as listed in Fig. 3. MD3 – metamorphic discontinuity is inferred from metamorphic field gradients (Goscombe et al., 2017a).

rotation of shear zones into steeper orientations due to shortening across the orogen, while continuing to localise transcurrent shear (Goscombe et al., 2003a; Konopásek et al., 2005). Kinematic partitioning, deformation style and metamorphic response are controlled by these crustal-scale shear zones; dividing the belt into distinct tectono-metamorphic zones (Goscombe et al., 2005a):

(1) **Eastern Foreland** has sub-greenschist facies Damara Sequence platform carbonates unconformably overlying unreworked Palaeoproterozoic Congo Craton. Deformation involved E–W directed coaxial shortening of the carbonates giving km-scale upright, open to close cylindrical folds, box folds, ramp anticlines and steep discontinuous thrusts (Guj, 1970; Coward,

1983; Hoffman et al., 1994, 1998). Overlying, phyllonitic, Mulden Group molasse developed progressively shallower dipping folds and crenulations, ending with a discontinuous network of west-inclined dip-slip thrusts, such as the Sesfontein Thrust (ST) at the western margin (Guj, 1970).

(2) **External Nappe Zone** has strongly deformed slope and deep-water facies Damara Sequence, with large-scale east-directed over-folds and nappes, cored by variably reworked Archaean-Palaeoproterozoic basement (Guj, 1970; Dingeldey et al., 1994; Dürr and Dingeldey, 1996; Stanistreet and Charlesworth, 2001; Goscombe et al., 2003a). Structures tighten and steepen towards, and root into the steep medial Purros Mylonite Zone at the western margin. External Nappe Zone is also characterized by inverted greenschist to upper-amphibolite facies Barrovian series metamorphism (Dingeldey, 1997; Goscombe et al., 2003b, 2005a; Will et al., 2004).

(3) **Orogen Core** is mostly high-grade, deep-water Damara Sequence intruded by syn-kinematic S-type granitoids of 580–562 and 559–549 Ma age, and dissected into lenticular panels by a network of crustal-scale shear zones (Seth et al., 1998; Franz et al., 1999; Goscombe et al., 2003a,b, 2005a; Kröner et al., 2004; Konopásek et al., 2005). Three distinct domains are recognised. Hartmann domain in the north is almost devoid of exposed basement, metamorphosed to upper-amphibolite grade, with syn- to post-kinematic pegmatite sills. Khumib domain is shallow crustal level, lower amphibolite facies sequence of turbidites with upright chevron folding similar to Zerrissene Group in the Ugab Zone (Goscombe et al., 2005a). Hoarusib domain in the south consists of isoclinally folded high-grade Damaran Sequence meta-greywackes with Mesoproterozoic basement cores and lenticular syn-kinematic granitoids (Fig. 5; Seth et al., 1998; Franz et al., 1999; Kröner et al., 2004; Goscombe et al., 2005b).

(4) **Coastal Terrane** has provenance distinct from the rest of the Kaoko Belt and consists of juvenile meta-arkose Neoproterozoic sequences (>650 Ma), intruded by 661–655 and 638–620 Ma arc-related, I-type intrusives (Seth et al., 1998; Kröner et al., 2004; Goscombe et al., 2005b; Goscombe and Gray, 2007). These were metamorphosed to high-T/moderate-P conditions of 725 °C and 6.9 kbar typical of arc-settings, between 650 and 640 Ma (Franz et al., 1999). Different lithostratigraphy, provenance, magmatism and thermal regime indicate the Coastal Terrane was a continental margin arc at the leading edge of attenuated passive margin or back arc (Goscombe et al., 2003b, 2005a,b; Goscombe and Gray, 2007, 2008). Coastal Terrane was obducted along the Three Palms Mylonite Zone during its early history, and variably reworked and down graded at shallow crustal levels during progressive transpression.

4.1.2. Main phase transpressional fabrics (D1kz-D2kz)

4.1.2.1. Early flat-lying L-S fabrics. Earliest formed structures are sub-horizontal to shallow west-dipping L-S mylonitic fabrics (D1kz) preserved within dm- to m-scale, low-strain shear lenses enveloped by steeper main phase foliations, and localized to the footwall below the Three Palms Mylonite Zone (Goscombe et al., 2005a; Konopásek et al., 2005; Goscombe and Gray, 2008). Stretching lineations are developed at high-angles to the grain of the belt, in common with early flat-lying L-S fabrics in the Ugab Zone (Section 4.2.2.1). These relict fabrics are interpreted to have formed at earliest stages of orogenesis during initial collision and obduction of the Coastal Terrane (Konopásek et al., 2005; Goscombe and Gray, 2008). Collision and obduction must have post-dated the youngest magmatic arc events in the Coastal Terrane (<620 Ma), and pre-dated transpression (>580 Ma), indicating a probable collisional age of ~590 Ma (Goscombe et al., 2005b; Goscombe and Gray, 2008).

4.1.2.2. Main phase S-L fabrics at ~570–580 Ma. Main phase transpressional orogenesis produced an intense penetrative bedding-parallel S-L fabric (D2kz) associated with colinear small-scale isoclinal folds (Dürr and Dingeldey, 1996; Goscombe et al., 2003a; Konopásek et al., 2005). Deformation was associated with a high wrench component and resulted in almost complete recrystallization of the matrix producing peak metamorphic parageneses. At low grades, main foliation is schistose alignment of micas and quartz-feldspar aggregate ribbons. Foliated gneiss and grain-refinement foliations developed at higher grades, either as penetrative foliations and shearbands within the polygonal granoblastic matrix, or mylonite to ultra-mylonite in high-strain zones. Stretching lineations are defined by quartz and feldspar sub-grain ribbons and aligned micas, sillimanite and amphibole. Stretching lineations are regionally pervasive, and range from sub-horizontal to shallow NNW-plunging in the Orogen Core through smooth arcuate traces to shallow WNW-plunges in the External Nappe Zone (Guj, 1970; Dürr and Dingeldey, 1996; Goscombe et al., 2003a). Shear sense is consistently sinistral with oblique-reverse transports dominating in all parts of the belt, except for oblique-normal in the shallow crustal Khumib domain, north Coastal Terrane and Three Palms Mylonite Zone (Goscombe et al., 2005a). Boudinage is common and formed in association with the enveloping main phase foliation with extension direction parallel to the stretching lineation (Goscombe et al., 2003a).

Main foliation was progressively recycled during ongoing transpression and folding and is continuous into crustal-scale mylonite to ultramylonite shear zones initiated early in the deformation history. Foliation intensity and semi-quantitative strain gauges indicate high strains throughout the belt, though strongly partitioned and extremely high in major shear zones (Goscombe and Gray, 2008). Foliation intensity is lowest in the Foreland and eastern External Nappe Zone where basement infolds are not pervasively reworked. Strain contrast between basement and cover decreases westward and in the Orogen Core is insignificant, both partitioned similar strains, developed identical deformational structures and are nearly indistinguishable. Strain ratios average 8 in the External Nappe Zone, 12 in the Orogen Core and 40 in the crustal-scale shear zones. Transpressional reworking was lowest in the Coastal Terrane, with strain ratios averaging 3 and grading to 8 and 75% grain refinement in the basal zone adjacent to the Three Palms Mylonite Zone (Goscombe and Gray, 2008). Orogen Core as a whole experienced a minimum of ~123–182 km sinistral lateral movement, estimated by integrating shear strains from panels and shear zones.

Peak metamorphic parageneses in the main foliation have been dated directly at 589–571 Ma using Sm-Nd garnet and U-Pb zircon (Goscombe et al., 2003b, 2005b), and overlap in age with oldest syn-kinematic granites ranging 580–562 Ma (Seth et al., 1998). Peak metamorphic conditions vary substantially between different panels (Goscombe et al., 2003b, 2005a, 2017a). Barrovian metamorphics in the External Nappe Zone range from 534 °C in the east to 689 °C in the west, at constant pressures of 8.5–8.6 kbar, indicating an increase in thermal regime from 18 °C/km to 23 °C/km towards the core of the belt (Fig. 5). Orogen Core is characterized by granulites with thermal regimes ranging 28–34 °C/km and peak conditions averaging 769 °C/8.0 kbar, 843 °C/8.1 kbar and 785 °C/6.7 kbar in different panels. In contrast the turbiditic Khumib domain at higher structural levels, has peak conditions averaging 597 °C/5.2 kbar and similar thermal regimes of 33 °C/km. All regions experienced clockwise P-T paths: External Nappe Zone following

steep trajectories and isothermal decompression reflecting advection dominated metamorphism, and Orogen Core experienced low ΔP/ΔT clockwise paths with isobaric cooling, indicating long residence times and less topographic development (Goscombe et al., 2005a).

4.1.3. Progressive transpression: shortening structures (D3kz)

With progressive transpression, deformation was strongly partitioned between wrench-dominated shear zones and significant E–W shortening component in intervening lenticular panels and external nappes. Strain regime was plain strain to simple shear in shear zones and deformed conglomerate clasts show plane to flattening strains dominate in inter-shear zone panels and nappes (Goscombe et al., 2003a; Goscombe and Gray, 2008). Map-scale, shallow NNW- and SSE-plunging, tight to isoclinal nappes and inclined asymmetric folds with W over E vergence dominate the structure of the Kaoko Belt. These folded the penetrative main phase foliation and lineation, and indicate progressive deformation and partitioning of greater shortening component during transpression. Fold inclination varies systematically across the belt defining the half-flower architecture, from steep isoclinal folds in the Orogen Core, to progressively shallower east-vergent nappes across the External Nappe Zone (Stanistreet and Charlesworth, 2001; Goscombe et al., 2003a). Main phase foliations and lineations were transposed, recycled and refolded by these folds with only minor development of axial planar fabrics. At lowest-grades axial planar crenulation cleavages are developed in the External Nappe Zone. Low-grade turbidites of the Khumib domain developed upright tight to open chevron folds with W over E vergence and axial planar foliations ranging from crenulations, aligned muscovite and sinistral shearbands. The Hoarusib domain experienced high strain coaxial shortening as well as wrenching, producing upright tight to isoclinal folds with axial planar spaced biotite schistosity, migmatitic segregations and pegmatite veins. Folds are colinear with main phase stretching lineations and range from cylindrical to curvilinear to sheath folds. The Hartmann domain developed open to tight asymmetric E-vergent folds with axial planar crenulations. The Coastal Terrane developed small-scale E-vergent asymmetric folds with no axial planar foliation (Goscombe and Gray, 2007).

Second generation stretching lineations are developed in the External Nappe Zone and Khumib domain; defined by aligned hornblende and biotite laths plunging down-dip to the W–WNW at high angles to fold and nappe axes (Dürr and Dingeldey, 1996; Goscombe et al., 2003a). These mineral lineations are uncommon and contrast with the pervasive, mineral aggregate lineations in the main foliation. Both lineation directions overlap slightly, indicating progressive deformation from sub-horizontal wrench transport to higher angle oblique transport associated with folding and shortening (Goscombe and Passchier, 2003). Second generation boudin structures also formed under shortening regimes, with extension axes trending E–W and W over E shear sense, consistent with fold-nappe transport (Goscombe and Passchier, 2003). Latest formed shortening structures include progressive tightening of folds, late-stage crenulations and low-grade Sesfontein Thrust at the foreland margin.

4.1.4. Progressive transpression: crustal-scale shear zones (late-D3kz)

Greater strain was progressively partitioned into crustal-scale shear zones as the belt evolved. Late-kinematic granites and pegmatites of 559–549 Ma age, post-date the regional main foliation and are over-printed by crustal-scale shear zones, indicating transcurrent slip continued after 549 Ma (Goscombe et al., 2005a,b). Main phase foliations trace continuous arcs and smooth strain gradients into shear zones indicating early development out of the regional foliation pattern. Nowhere are shear zones folded, indicating shear zones localized strain and continued to operate after development of shortening structures such as fold-nappes. Progressive strain partitioning coeval with significant shortening, resulted in steepening of the shear zones and exploitation as root zones for large-scale fold-nappes, such as Ahub Mylonite Zone (AMZ) root to a “Penninic”-style Neoarchaean nappe (Goscombe and Gray, 2008).

Purros Mylonite Zone is laterally continuous for at least 620 km from Angola to Ogden Mylonite Zone (OMZ) at the west margin of the Ugab Zone (Corner, 2000, 2004; Passchier et al., 2002; Goscombe et al., 2003a, 2004). Mylonitized orthogneiss with crystallization ages of 2606 ± 8 and 1862 ± 5 Ma in the Ogden Mylonite Zone (Table 2), correlate in age with basement orthogneiss in the central Kaoko Belt (Seth et al., 1998), and confirm these shear zones are linked (Corner, 2000, 2004; Passchier et al., 2002; Goscombe et al., 2003a, 2004). Evidence for reworked Congo Craton basement within the Ogden Mylonite Zone, as well as the inboard setting of the Purros-Ogden system, indicates that collision and obduction of the Coastal Terrane occurred further west, along the Three Palms Mylonite Zone, and not at the Ogden Mylonite Zone as published recently (Passchier et al., 2016).

The width of the Purros-Ogden zone varies from 1 to 5 km, consisting of intense schistosity in the north, and mylonite elsewhere with anastomosing 50–100 m wide ultra-mylonite zones. Geometry varies systematically from dipping 70°–90° west in the north, to 30°–50° west in the south Kaoko Belt, indicating listric form at depth. Ogden Mylonite Zone is sub-vertical and dips both east and west due to younger Damaran Phase cross-folding. Mineral aggregate stretching lineations plunge shallowly north and are colinear with small-scale isoclinal folds, sheath folds and boudin extension directions (Goscombe and Passchier, 2003). Stretched clasts, boudins and C-S fabrics in the Purros Mylonite Zone, gauge strain ratios of 10–27, and sheath folds 27–80 (Goscombe and Gray, 2008). Bulk strain was lower in the Ogden Mylonite Zone with strain ratios of 10–14, and flattened concretions indicate oblate strain regimes (Appendix 4). Progressive shear in the Ogden Mylonite Zone refolded the mylonitic foliation at outcrop and map-scales, into NE–SW trending asymmetric sinistral-vergent folds. Metamorphic conditions in the Purros Mylonite Zone average 640 °C at 7.4 kbar, with decompression to 5.2 kbar recorded in mineral parageneses, whereas Ogden Mylonite Zone formed at shallower crustal levels of 479 °C and 4.7 kbar (Foster et al., 2009). In contrast to all other shear zones in the Kaoko Belt, the Purros and Ogden Mylonite Zones are almost devoid of late-stage brittle reactivation (Foster et al., 2009).

Kaoko Belt architecture is controlled by the long-lived Purros and Three Palms Mylonite Zones, which bracket an oblique network of arcuate Hartmann (HMZ), Khumib (KMZ) and Village (VMZ) Mylonite Zones. These linking shear zones are 20–300 m wide with mylonite to ultra-mylonite fabrics, horizontal mineral aggregate stretching lineations and shear sense consistently sinistral. Small-scale isoclinal folds are strongly non-cylindrical and sheath folds are common. Shear foliations formed at 690–700 °C and 4.4–4.6 kbar and are over-printed by mid-amphibolite to greenschist facies mylonites, semi-ductile deformation and brittle gouge and breccia, indicating sinistral transtensional reactivation into the brittle field in common with the Three Palms Mylonite Zone (Konopásek et al., 2005; Foster et al., 2009).

The Three Palms Mylonite Zone acted as the primary basal thrust that obducted Coastal Terrane onto Damara Sequences of the Orogen Core (Goscombe and Gray, 2007). Progressive sinistral reworking of the zone resulted in a 1–2 km wide mylonite zone, with 300 m wide ultramylonite on the western margin and decreasing strain intensity to protomylonite in the east. Hanging

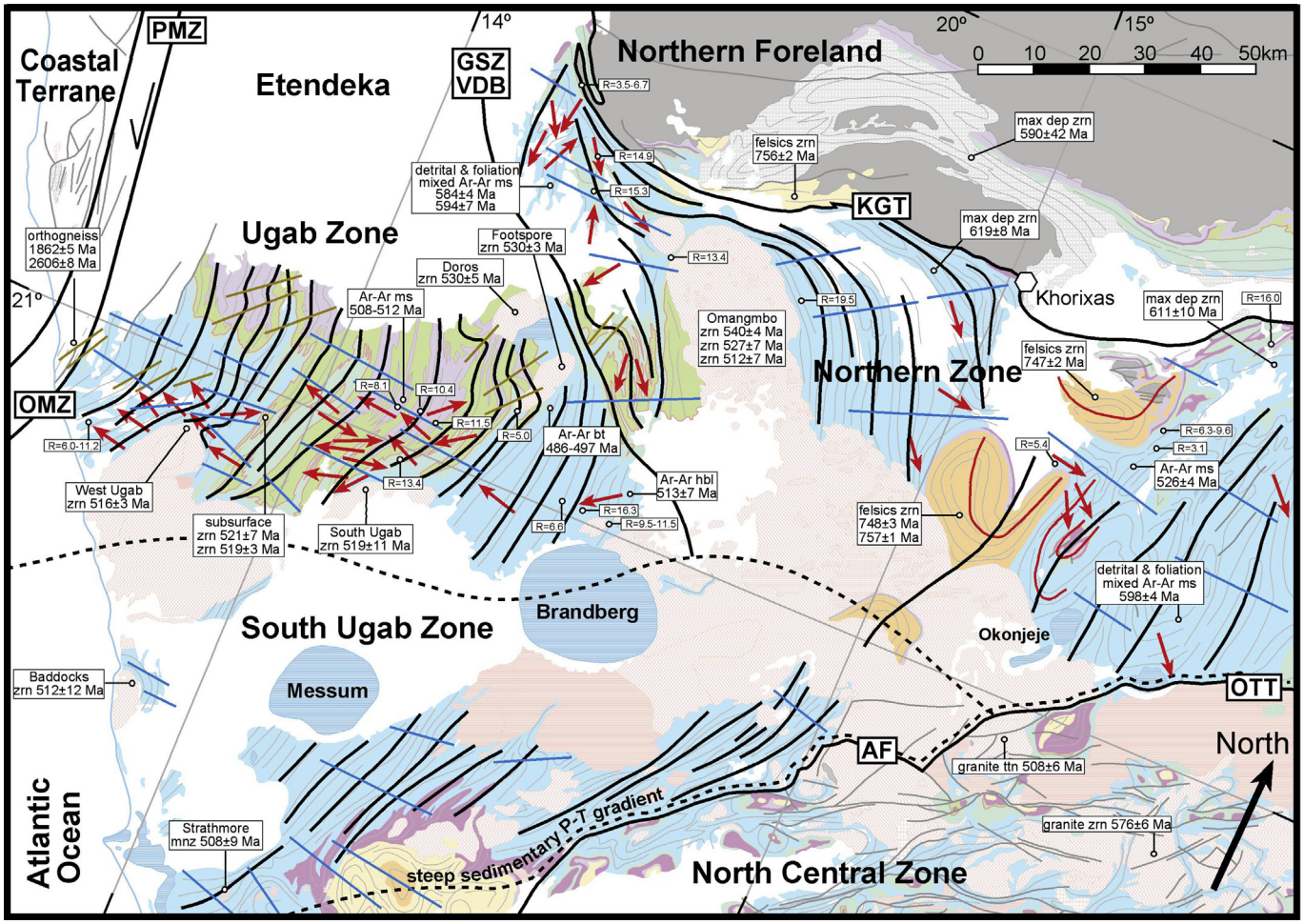

Figure 6. Simplified map of the Ugab Zone and western portion of the Northern Zone indicating the major chronostratigraphic rock units and regional and contact metamorphic isograds (Goscombe et al., 2004, 2017a). Geology based on Miller (1980), Miller and Grote (1988), Swart (1992) and Hoffman et al. (1994); see Fig. 3 for legend. Earliest formed D1nz stretching lineations and axial traces of probable pre-Kaokoan folds are indicated red. Early lineations in the west Ugab Zone have been rotated to near original orientations by unfolding D2nz effects. A select number of map-scale axial trace are indicated: main phase Kaokoan D2nz chevron folds (black), sinistral D3nz folds (gold), main phase Damaran upright open to close D4nz-D5nz folds (blue) and late-stage E–W shortening foliations and folds (green). Robust peak metamorphic U-Pb age determinations are annotated (Appendix 1). A select number of U-Pb magmatic age determinations (named plutons) and maximum deposition ages crucial to constraining the deformation and metamorphic history are also indicated (Appendix 1). A select number of semi-quantitative strain ratio determinations are indicated (Appendix 4). Crustal-scale shear zone abbreviations are as listed in Fig. 3.

wall Coastal Terrane is reworked by muscovite-biotite foliations and quartz-feldspar aggregate ribbons sub-parallel to the mylonite zone. Stretching lineations have shallow S- to SSE-plunges and shear sense is sinistral-normal, consistent with juxtaposition against deeper level Orogen Core (Goscombe et al., 2005a). Three Palms Mylonite Zone is retrogressive and associated with reworking and down-grading of older parageneses, at conditions averaging 557 °C at 4.5 kbar. Shearing evolved from ductile mylonite to semi-ductile shearbands, brittle-ductile deformation and finally brittle faults, pseudo-tachylite and fracturing. Post-kinematic 531–530 Ma pegmatite in the southern Coastal Terrane, are minimum age estimate for sinistral transpression in the Kaoko Belt (Goscombe et al., 2005a), and the switch to transtension, exhumation and brittle reactivation is dated by thermochronology at 533–525 Ma (Foster et al., 2009).

4.1.5. Damaran Phase over-printing events (D4kz–D7kz)

4.1.5.1. Transtensional reactivation of shear zones at ~533–525 Ma. Sinistral transpression in the Kaoko Belt was terminated when principle compressive stress rotated into acute angles with respect to the orogenic grain, inducing transtensional reactivation of shear zones (D5kz). Transtensional reactivation of Three Palms Mylonite Zone and linking shear zones, facilitated rapid exhumation of the Orogen Core, juxtaposing 4.5–5.2 kbar Coastal Terrane and Khumib domain against 6.7–8.1 kbar lower-plate rocks. Switch to transtension is constrained between 533 and 525 Ma by NNW–SSE trending post-kinematic pegmatites marking end of transpression (D4kz), syn-kinematic growth of muscovite in extensional structures, and rapid cooling and exhumation documented by thermochronology (Foster et al., 2009). This timing and stress field marks earliest Damaran over-print in the Kaoko Belt, and correlates with earliest Damaran over-print in Ugab Zone, where NNW–SSE shortening overlaps with intrusion of 534–526 Ma granite.

4.1.5.2. N–S shortening folds and pegmatites at ~515 Ma. Ongoing Damaran N–S shortening (D6kz) produced kinkbands and E–W trending mesoscopic to regional-scale (5–50 km wavelength) warps that buckled orogenic grain and the shear zones of the Kaoko Belt (Goscombe et al., 2003a). Transtensional shear zones are affected by this folding, so this phase is younger than ~525 Ma.

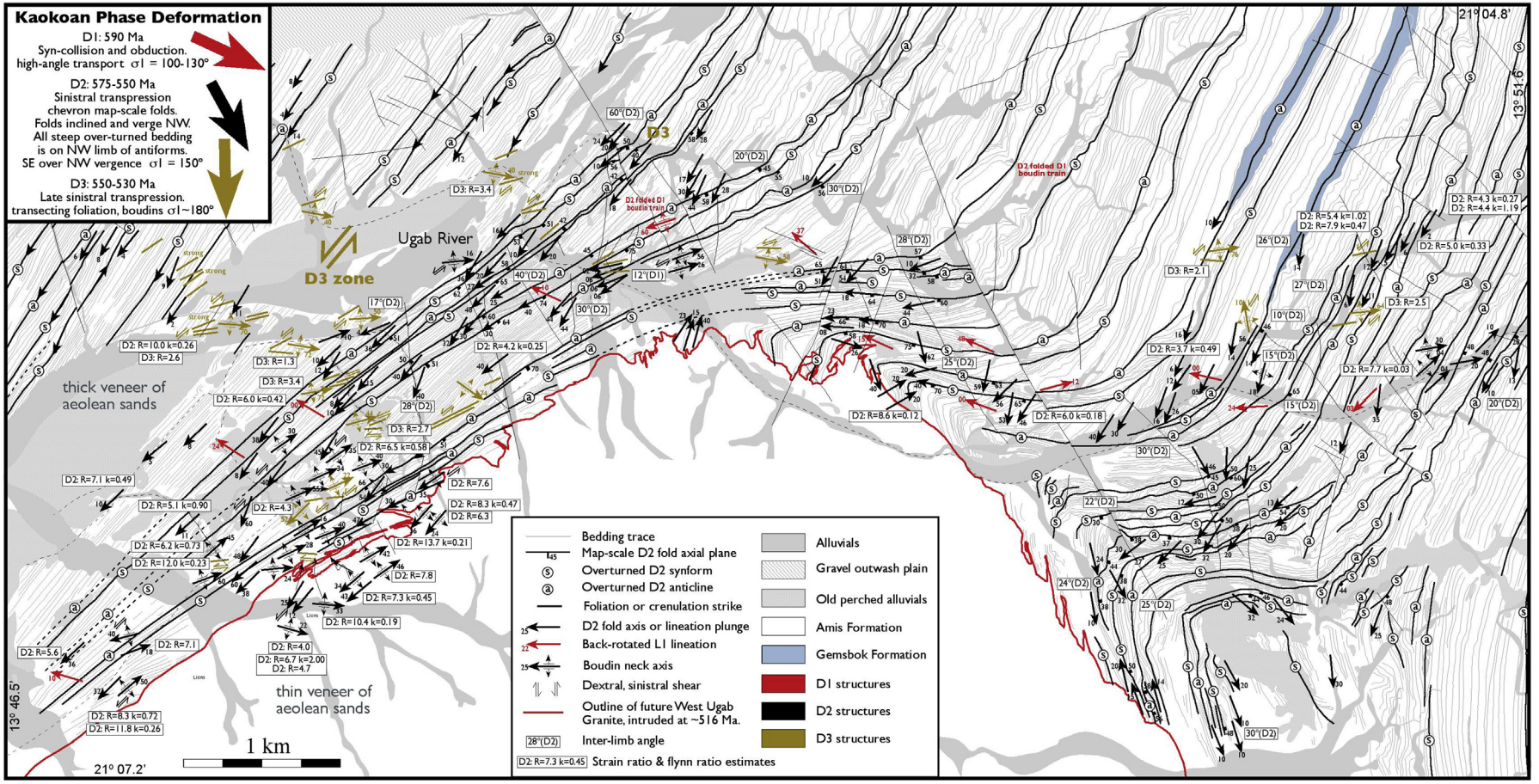

Figure 7. Detailed structural map of Kaokoan Phase structures in the region north of the West Ugab granite.

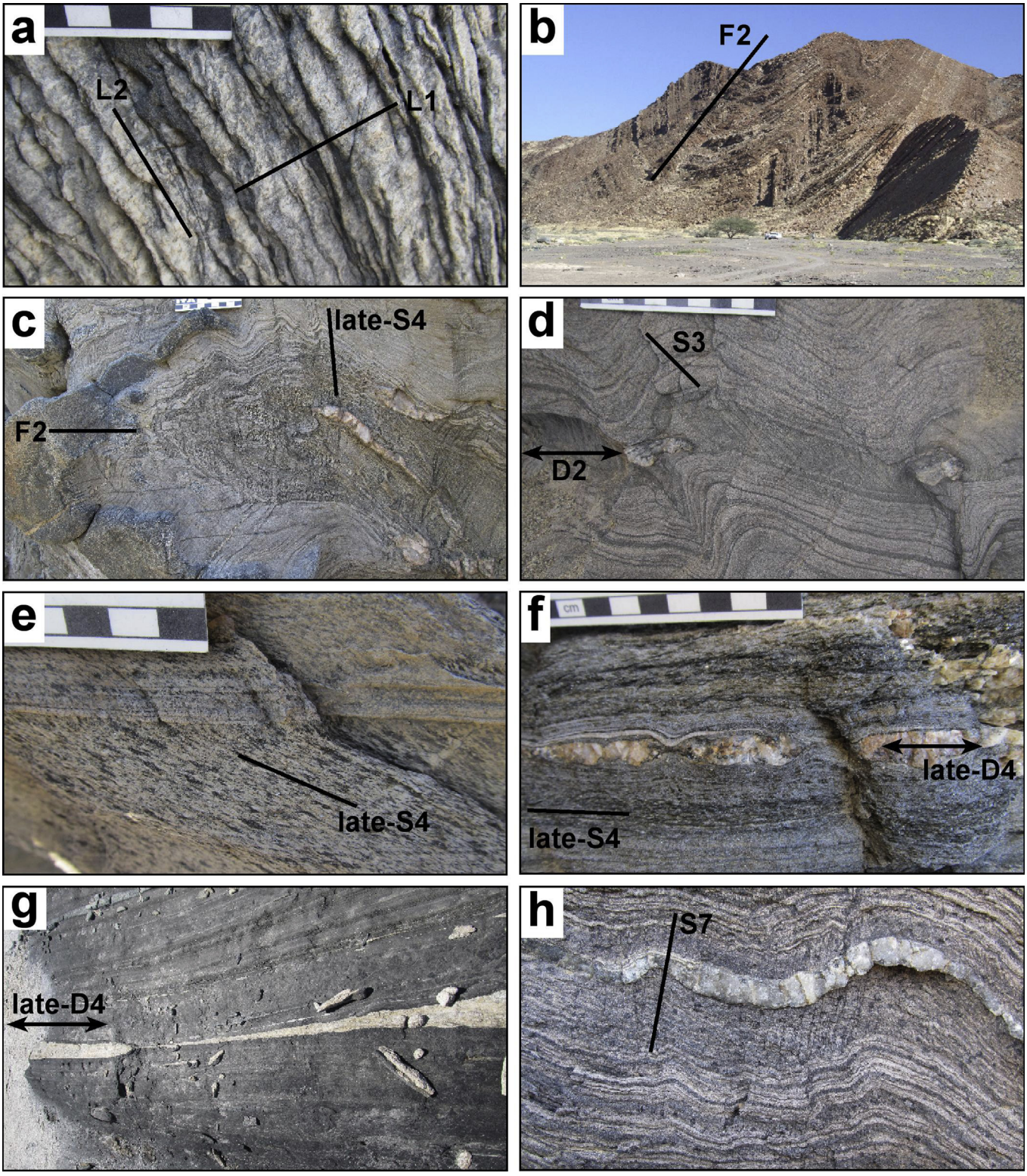

Figure 8. Representative deformation structures from the west Ugab Zone. (a) Earliest phase D1nz quartz aggregate stretching lineation in thin meta-chert bed, over-printed by D2nz Kaokoan main phase intersection mullions. (b) Inclined Kaokoan Phase D2nz tight map-scale chevron folds. (c) Kaokoan main phase D2nz folds transected by late-D4nz crenulations with axial planar biotite growth. (d) Kaokoan D2nz boudins train sinistral sheared by D3nz producing weak foliation parallel to the rotated inter-boudin plane. (e) Damaran Phase late-D4nz biotite foliation. (f) Late-D4nz boudinage and biotite foliation development in West Ugab granite contact aureole. (g) Strongly transposed D2nz and late-D4nz and extreme stretch of aplite dyke in West Ugab granite contact aureole. (h) Asymmetric D7nz folds with weak axial planar crenulation with biotite growth.

NNE–SSW trending post-kinematic pegmatite dykes in the southern Coastal Terrane give ~515 Ma age and are consistent with Damaran N–S shortening at this time (Goscombe et al., 2005b).

4.1.5.3. E–W shortening and pegmatites at ~508–505 Ma. The youngest event recognised in the Kaoko Belt (D7kz) is 508 Ma pegmatite dyke swarms and associated thermal anomalies at 507–505 Ma age (Goscombe et al., 2005b). Pegmatite dykes post-date both ductile and brittle fabrics in the Three Palms Mylonite Zone, and strike ESE–WNW to E–W indicating the local shortening direction.

4.2. Northern Margin: Ugab Zone and Northern Zone

4.2.1. Overview

The Ugab Zone and west Northern Zone cover the junction between the Kaoko and Damara Belts. These two zones experienced both Kaokoan and Damaran Phase deformations resulting in complex fold interference (Coward, 1983; Porada et al., 1983; Maloof, 2000; Passchier et al., 2002; Goscombe et al., 2004) and multiple metamorphic parageneses (Goscombe et al., 2004). Regional main foliations formed with map-scale chevron folding during Kaokoan transpression at ~570–580 Ma (Fig. 6; Coward, 1983; Maloof, 2000; Passchier et al., 2002; Goscombe et al., 2004; Lehmann et al., 2015). Ongoing transpression in the Kaoko Belt produced secondary sinistral-vergent structures in the Ugab Zone and Ogden Mylonite Zone (Freyer and Halbich, 1994; Maloof, 2000; Passchier et al., 2002; Goscombe et al., 2003a, 2004; Goscombe and Gray, 2008).

Damaran foliations of 556–550 and 540–530 Ma age, and 530–527 Ma mineralization are preserved in low-grade phyllites of the Northern Foreland (Clauer and Kroner, 1979; Kamona et al., 1999), correlating with collision, prograde and peak metamorphism episodes in the central Damara Belt (Fig. 2). Within the Ugab and west Northern Zones, Damaran orogenesis is punctuated by five granite-syenogranite episodes: ~540 Ma granitoids occur in the core of composite West Ugab, Doros and Omangambo plutons. 534–528 Ma Doros and Footspore granites and 527–526 Ma Omangambo granite plutons dominate the east Ugab Zone (Seth et al., 2000; Van de Flierdt et al., 2003; Lobo-Guerrero Sanz, 2005; Schmitt et al., 2012). Whereas west Ugab Zone contains sub-surface and South Ugab granite of 521–519 Ma age, West Ugab granite of 516 ± 3 Ma age and 513–508 Ma age determinations from Omangambo, Strathmore and Baddocks Bay granites (Table 2; Witts-Rio Tinto unpublished; Lehmann et al., 2015). These magmatic events bracket deformations and date ductile structures developed within contact aureoles, constraining Damaran deformation history in the triple junction.

Damaran structures formed at relatively low strains during high-angle contraction across the Damara Belt (Coward, 1981, 1983; Freyer and Halbich, 1994; Maloof, 2000; Passchier et al., 2002). Damaran strain increases eastward from moderate fold shortening in the Ugab Zone to north-vergent fold-thrust belt with multiple fold events and penetrative foliations within the Northern Zone (Coward, 1983; Miller, 1983; Gray et al., 2008; Lehmann et al., 2015). The northern boundary of the Northern Zone is a steep thrust complex against the Palaeoproterozoic Kamanjab Inlier, north of which low amplitude folding of the carbonate platform dominated (Hedberg, 1979). West Northern Zone has greenschist facies sequences and deformation history similar to the Ugab Zone (Porada et al., 1983; Goscombe et al., 2004; Lehmann et al., 2015). In contrast, east Northern Zone has a thicker succession of turbidites deposited in a rift basin (Porada, 1983; Porada and Wittig, 1983). These rocks were deeply buried during orogenesis and experienced Barrovian metamorphism of 637 °C/9.2 kbar at 510 ± 3 Ma, followed by isothermal decompression soon after (Goscombe et al., 2017a; Table 2). Exhumation of the east Northern Zone after 510 Ma, closely correlate in age with a stress switch to E–W shortening along the orogen, documented by E over W folding in the Central Zone and Ugab Zone between ~512 and 508 Ma.

4.2.2. Kaokoan events (D1nz–D3nz)

4.2.2.1. D1nz early flat-lying fabrics. Earliest fabrics (D1nz) in the Ugab Zone are mylonitic L-S fabrics with strong quartz-aggregate stretching lineations, developed in thin (<2 cm) laminated chert inter-beds and bedding-parallel quartz veins (Goscombe et al., 2004). Equivalent bedding-parallel foliation in metapelite is fine-grained sericite-chlorite ± biotite phyllonitic schistosity associated with small isoclinal folds. Unfolding later chevron effects, the early foliation dips shallowly west and stretching lineations plunge 16° towards 279°±16° on average (Fig. 7). Early bedding-parallel fabrics are not penetrative but restricted to discrete bedding surfaces and chert bands. These early fabrics occur throughout the deep-sea turbiditic basin of western and central Ugab Zone, to the west of the Goantagab Shear Zone or Vrede-Doros-Brandberg line (GSZ/VDB). Evidence for this earliest deformation is strong: (1) Mylonitic bedding-parallel fabrics are everywhere over-printed at low-angles by the main phase penetrative foliation associated with tight chevron folding (D2nz). (2) Early boudinage of bedding is evident as boudins trains folded by D2nz chevrons and thus constitute polyphase, non-congruent structures (Goscombe et al., 2004). (3) Mylonitic fabric is folded and transected by mullion development associated with D2nz chevron folds (Fig. 8a). Early flat-lying fabrics with E–W stretching direction are interpreted as bedding parallel shear during initial W over E obduction of the Coastal Terrane and Ugab Zone along shallow decollements, at ~590 Ma in common with the Kaoko Belt and before main phase transpressional deformation.

East of the Vrede-Doros-Brandberg line, passive margin carbonates are highly strained, preserve pre-Kaokoan isoclinal folds and L-S fabrics in what may constitute an early crustal-scale shear zone, the Goantagab Shear Zone (Goscombe et al., 2004; Passchier et al., 2011). Earliest stretching lineations are associated with small-scale intrafolial isoclinal folds with axial planar high-strain grain-shape fabrics in highly sheared and transposed carbonates (Goscombe et al., 2004; Passchier et al., 2011). These mylonitic fabrics are associated with high strain ratios ranging of 13.4–17.1, as gauged by boudinage, sheath folds and rotated quartz vein geometries (Appendix 4). Early low-plunge stretching lineations are also preserved in the west Northern Zone, and across both these regions early lineations consistently trend N–S to NNW–SSE (Goscombe et al., 2004; Passchier et al., 2016), which is orthogonal to early lineations developed in the west and central Ugab Zone (Fig. 6). Early bedding-parallel foliations in the Northern Zone, when unfolded, are interpreted to have original E–W traces (Lehmann et al., 2015). White mica from these foliations give Ar-Ar muscovite ages ranging 598–584 Ma that have been interpreted as deformation ages, and correlated with N–S shortening due to subduction and accretion in the Southern Zone at the leading edge of attenuated Congo Craton (Lehmann et al., 2015; Passchier et al., 2016). This interpretation is consistent with both timing of probable subduction at this margin, and N–S stretching direction early in the evolution of the east Ugab Zone (Passchier et al., 2016). However, Lehmann et al. (2015) indicated the samples contain detrital muscovite such that the 598–584 Ma apparent age is a mixture between detrital and metamorphic mica or the approximate age of the detrital mica. Detrital muscovite with an age of 598–584 Ma would be compatible with muscovite shed from the Coastal Terrane during initial obduction and first development of topography in the Kaoko Belt. Furthermore, interpretation of this age data as

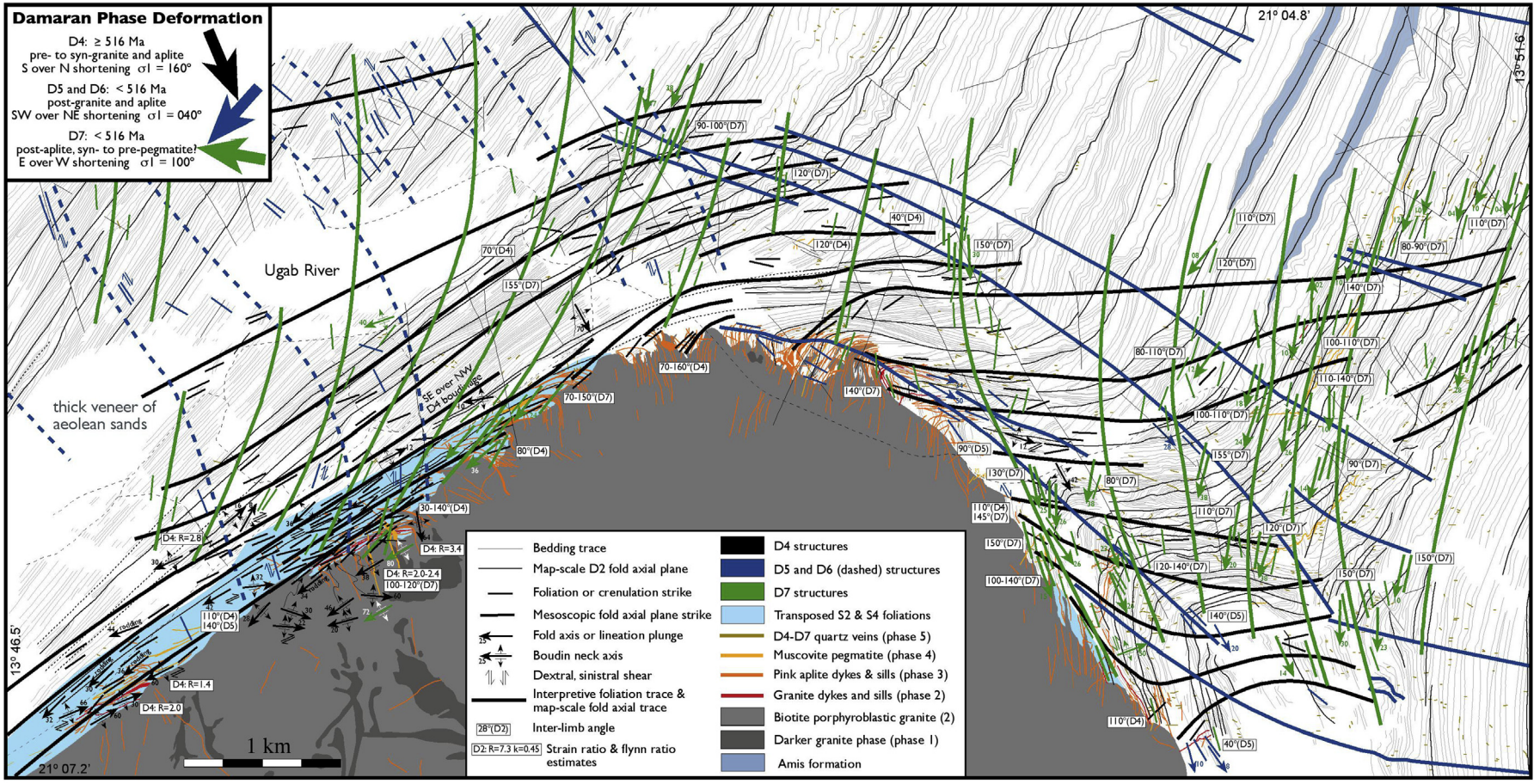

Figure 9. Detailed structural map of Damara Phase structures and contact metamorphic isograds, in the region north of the West Ugab granite.

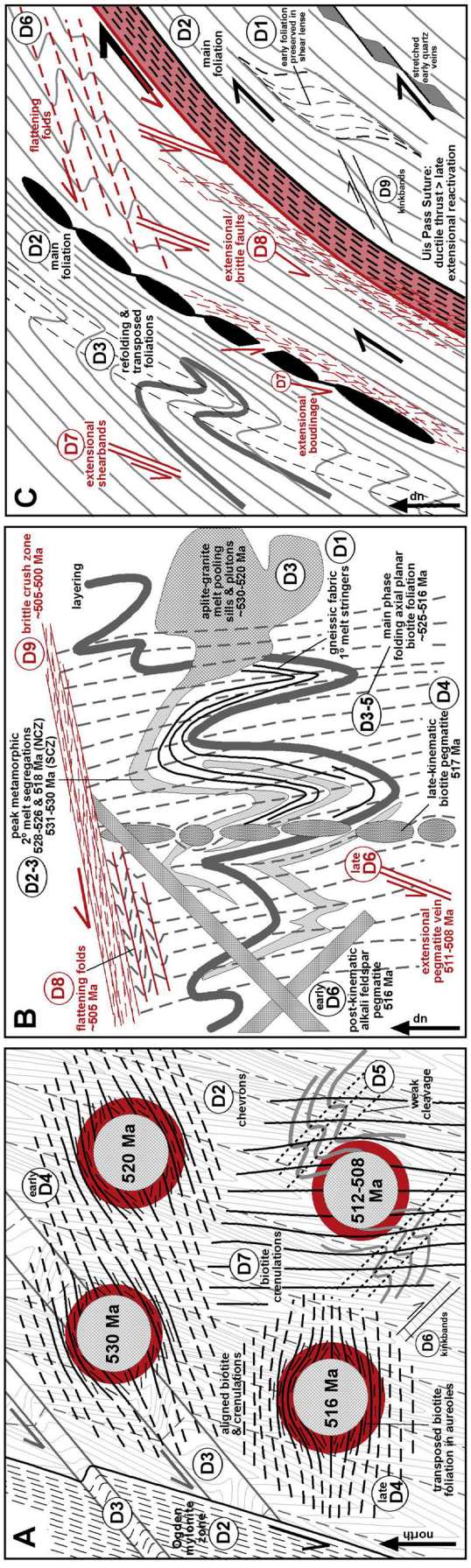

Figure 10. Diagrammatic summary of key over-printing relationships, timing and deformational styles in the key regions, (A) Ugab Zone (Figs. 6, 7 and 9), (B) Central Zone (Figs. 11 and 12) and (C) southern margin (Fig. 14). Relationships between deformation fabrics such as main phase foliations and fold axial planes (black and grey lines) and granite-pegmatite intrusions (cross-hatch and patterns) are represented diagrammatically. Contact aureoles in the Ugab Zone are indicated by red margins. Red structures and symbols in the Central Zone and southern margin indicate vertical flattening extensional structures.

entirely a deformational imprint, is inconsistent with deposition of Damara Sequences persisting to ~580 Ma (e.g. Hoffmann, 1989, 1994, 1997). Maximum deposition ages of ~590 Ma from Mulden Group molasse in the Northern Zone (Foster et al., 2015; Appendix 1) also indicate the deformation age interpretation is problematic, and are consistent with detrital material shed from the Coastal Terrane from ~590 Ma.

4.2.2.2. D2nz sinistral transpression chevron folding at ~570–580 Ma. Main phase foliation (D2nz) is penetrative quartz-sericite-chlorite ± biotite schistosity or cleavage with aligned mica growth, developed axial planar to tight chevron folds dominating the Ugab Zone (Fig. 8b). Kaokoan Phase regional metamorphism defined by this foliation, is biotite grade throughout, with biotite grainsize and modal proportion indicating slightly lower grades in the north and northeast and highest grades in the west (Fig. 5). At highest grades, main foliation in the west Ugab Zone is spaced to continuous biotite-muscovite schistosity (Fig. 8c). In the absence of pre-existing penetrative schistosity, main foliation is not developed as a crenulation, though crenulation cleavages associated with chevrons are evident at lower grades in central Ugab Zone. Main foliation is highly refracted between beds, with dissolution and biotite accumulation in psammites resulting in spaced schistosity and mm-scale lithons. Metasomatic epidote-quartz ± amphibole concretions develop in psammite beds with flat ellipsoid to pancake shapes aligned in the main foliation and nowhere folded, indicating formation during D2nz shortening. Flynn ratios range from 0.02 to 0.29 in the west Ugab Zone to 0.1–0.6 and 1.1–2.1 in the east, indicating oblate and plain strain regimes (Appendix 4). The long-axis of concretions typically sub-parallel quartz aggregate lineations and chevron fold axes, or occur at acute ~30° angles to the fold axes. Similarly, main phase boudinage of bedding-parallel quartz veins show along axis stretching direction. These indicators of oblique along-axis stretch are consistent with sinistral transpressive shear during chevron folding.

Main phase chevron folds are developed at map-scale with wavelengths ranging 0.1–6.0 km and mesoscopic folding being uncommon. Inter-limb angles average 41°±24° in the east and 24°±8° in the west, indicating highest strains in the west. Flattened concretions, S-C fabrics and boudinage strain gauges, however show similar strain ratios across the Ugab Zone; 3.3–10.6 in the west and 3.5–9.6 in the east (Appendix 4). Chevrons had sub-horizontal hinges with NNW to NNE trends, prior to later refolding (Fig. 6). Chevron folding was progressive, and secondary transecting-foliations developed at acute angles to the axial plane. Axial surfaces are bivergent and range from sub-vertical in the central Ugab Zone to dipping 10°–30° SE in the west, and dipping 40°–60° SW in the northeast (Fig. 6). Consequently, the Ugab Zone has bivergent flower structure with fold asymmetry and overturned limbs showing E-vergence in the east and W-vergence in the west. This bivergent geometry implies basal decollements that steepen towards the central Ugab Zone, as reflected by the sub-vertical axial surfaces, and explains the absence of exposed basement in the Ugab Zone. Penetrative main phase deformation occurred in a transpressional environment and is correlated with the pervasive deformation of the Kaoko Belt (Passchier et al., 2002; Goscombe et al., 2003a, 2004).

4.2.2.3. D3nz progressive sinistral transpression. Progressive sinistral transpressive shear produced secondary Kaokoan Phase folds, fabrics and boudinage structures (D3nz) that overprint main phase structures. Outcrop and map-scale tight to close upright folds with NE-trending axial trace, SW-plunges and fold asymmetry showing sinistral vergence (Fig. 8d), are common in the west and northeast Ugab Zone, Ogden Mylonite Zone and South Ugab Zone. Tight map-

scale folds in the east Ugab Zone are overprinted by the 530 Ma age Footspore granite (Passchier et al., 2007), indicating these structures formed prior to this time. Inter-limb angles range 70°–90°, indicating moderate strains. Map-scale folds are common in the west Northern Zone and responsible for fold interference patterns with coplanar main phase folds (Coward, 1983; Miller, 1983). Secondary folds have ramping geometries that transect main phase chevrons, and develop axial planar, spaced (1–5 mm) crenulation cleavage with alignment of biotite producing distinctive biotite seams. Main phase boudin trains are modified by sinistral-reverse ramp-folding and rotation of inter-boudin planes into acute angles with the enveloping surface and parallelism with transecting crenulation cleavages (Fig. 8d). A second generation of shearband boudinage also develops with inter-boudin plane parallel to crenulation cleavages and boudin axes at acute (~35°) angles to chevron folds. Inter-boudin plane rotation ranges 36°–40° in the west Ugab Zone, giving low strain ratios of 2.5–2.7, consistent with inter-limb angles of secondary folds. In the Ogden Mylonite Zone, inter-boudin planes experienced extreme rotation of 70°–74°, producing isoclinal flanking folds and re-boudinage of inter-boudin quartz veins, giving high strain ratio estimates of 9.5–14.2.

4.2.3. Peak Damaran events (D4nz)

Damaran over-print in the Ugab Zone occurred as punctuated deformation events with slightly different stress fields as convergence between the Congo and Kalahari Cratons evolved. Most of the Damaran stress field history is preserved by a series of evolving deformation structures in the west Ugab Zone (Fig. 9). Conveniently, the Ugab Zone as a whole experienced 5 distinct granite emplacement periods that bracket and date deformation events (Fig. 10). All occurred at elevated thermal conditions associated with granite plutons giving a long-lived diachronous and heterogeneous Damaran metamorphic cycle (Goscombe et al., 2017a). Even distant from granites, deformation structures invariably involved biotite growth and temperatures >450 °C across the whole Ugab and west Northern Zones. Highest-grade parageneses are developed in contact aureoles, which experienced tight anticlockwise P-T paths followed by isobaric cooling and peak conditions averaging 560 °C and 3.6 kbar, with each pluton representing a different aged thermal anomaly (Goscombe et al., 2004, 2017a). Deformation over this period evolved from NNW–SSE to N–S shortening, recorded by early-, mid- and late-D4nz structures with distinct field relationships and timing. Shortening strains were only moderate and heterogeneously partitioned, with most structuring closely associated with granite plutons that acted as heterogeneities in the stress field and perturbations in the thermal budget.

4.2.3.1. Early-D4nz NNW–SSE shortening at ~530 Ma. Footspore granite in the east Ugab Zone over-prints a map-scale sinistral-vergent fold typical of latest-stage Kaokoan deformation (Passchier et al., 2002; Goscombe et al., 2004), indicating subsequent deformations that impinged on this granite occurred during Damaran Phase. Main phase foliations in the east Ugab Zone are over-printed by steep ENE–WSW trending crenulation cleavages formed by NNW–SSE shortening (early-D4nz). Crenulations trace smooth curves towards the Footspore granite, and envelop the granite within the contact aureole where they are expressed as a steep continuous biotite-muscovite schistosity that transposed earlier Kaokoan fabrics. These relationships indicate NNW–SSE shortening overlaps in age with the Footspore granite thermal anomaly. Identical relationships are documented on the western margin of the Omangambo granite pluton of predominantly 527–526 Ma age (Appendix 1). Consequently, this earliest stage of Damaran shortening can be constrained to 530–526 Ma age. Early-D4nz deformation was strongly partitioned into contact aureoles, the higher temperatures being conducive to intense ductile deformation and formation of new contact metamorphic parageneses (Goscombe et al., 2004). High ductile strains are evident by; transposition recycling of foliations, isoclinally folded aplite dykes with axial planar schistosity and chocolate tablet boudinage is indicative of flattening strains.

4.2.3.2. Mid-D4nz NNW–SSE shortening at ~520 Ma. Sub-surface granites in the central and southwest Ugab Zone form contact aureole parageneses over broad regions distal from exposed granites (Fig. 9). Cordierites are particularly large (6–50 mm) in these aureoles, consistent with high thermal budget immediately above a granite body. Pegmatite, aplite and granite associated with a subsurface granite in west Ugab (Fig. 9), give U-Pb zircon age determinations of 521 ± 7 and 519 ± 3 Ma (Table 2). South Ugab granite is interpreted to be an exposed portion of this subsurface granite, and gives a similar U-Pb zircon age of 519 ± 11 Ma from pooled samples (Table 2). Foliation development and mineral growth relationships in this aureole differ from those developed near the 516 Ma West Ugab granites (Section 4.2.3.3). Cordierite and andalusite porphyroblasts and biotite and muscovite plates are typically random in orientation, indicating relatively low strains during granite emplacement. Porphyroblastic phases are over-printed by E–W tending biotite foliations formed in association with the West Ugab granite (late-D4nz), indicating N–S shortening was younger than 520 Ma. Similar to east Ugab Zone, oldest Damaran fabrics in the west Ugab Zone are biotite foliations with ENE–WSW trend (mid-D4nz; Fig. 9), that pre-date E–W foliations, indicating ages older than 516 Ma. Foliation geometries that can be correlated with mid-D4nz NNW–SSE shortening overlap in age with the 520 Ma age sub-surface granite. Spaced biotite foliations and aligned biotite plates with ENE–WSW trends are regionally developed independent of granite bodies and contact aureoles (Fig. 9). Whereas within the sub-surface granite aureoles, curviplanar biotite differentiation seams of 1–3 mm width are common, and formed by preferential biotite growth within crenulation cleavages. These foliations have a wide range of orientations and shallow dips, consistent with deflection above a granite pluton, indicating NNW–SSE shortening persisted to at least 520 Ma.

4.2.3.3. Late-D4nz N–S shortening at ~516 Ma. Emplacement of the West Ugab granite coincides with N–S directed shortening and the formation of E–W trending folds and foliations (Figs. 9 and 10). West Ugab granite samples give a pooled U-Pb zircon age of 516 ± 3 Ma (Table 2), accurately constraining late-D4nz N–S shortening. Late-D4nz folds in the west Ugab Zone are cylindrical to chevron folds, with inter-limb angles ranging 40°–120°, and where asymmetric show S over N vergence. A range of biotite foliations are developed axial planar to these folds; spaced biotite differentiation crenulation, spaced biotite schistosity, aligned biotite plates and flattened biotite aggregate spots (Fig. 8c, e). These foliations transect Kaokoan chevrons (Fig. 8f) and are well developed in both aureoles and distal from granites, indicating an elevated regional thermal regime throughout the west Ugab Zone. Distal from granites these biotite foliations trend E–W and have steep 70°–90° dips to the south. E–W foliations over-print cordierite porphyroblasts in the ~520 Ma sub-surface granite aureole, consistent with formation during emplacement of the younger West Ugab granite. Proximal to the West Ugab granite foliations are deflected due to ongoing N–S shortening across the pluton, resulting in trends ranging 050°–105° (Fig. 9). Within contact aureoles biotite and muscovite growth is coarse-grained and typically aligned micas to continuous schistosity. Kaokoan chevrons are refolded by map-scale late-D4nz folds into E–W trends within the high strain quadrant north of the West Ugab granite (Fig. 8); with axial planar

foliations transposed into parallelism with the late-D4nz biotite foliation. Aplite dykes and sills emanating from the granite, constitute a significant volume injected into the host rocks and limited to a concentric aureole of <1 km width. These had original preferential N–S strike, consistent with the late-D4nz stress field, and were folded into a bivergent fan by ongoing N–S shortening impinging on the pluton (Fig. 9).

West Ugab granite has moderate to steep margins dipping 35°–80° and thin contact aureole with porphyroblast and coarse mica growth restricted to <500 m from the granite margin (Fig. 9). N–S shortening coeval with granite emplacement produced alignment of contact metamorphic minerals and biotite-muscovite schistosity. Strain was highest on the SE-dipping western margin of the granite, where bedding, Kaokoan and D4nz foliations are all transposed into near-parallelism (Fig. 8f and g), and quartz aggregate and cordierite rodding lineations are developed. Asymmetric ramp folding with SSE over NNW vergence is common and consistent with being below the granite. Boudinage occurred in the transposed margin and ranges from weakly necked to strongly drawn. Bulk strain estimates from boudinage extension in Ugab Zone contact aureoles, give strain ratios as high as 6.6–19.4 (Appendix 4). Boudinaged granite, aplite and pegmatite dykes are enveloped by the transposed composite foliation, and pegmatite pools in neck zones indicating late-D4nz shortening overlaps with magmatism. Four geometries of late-D4nz boudinage are recognised. (1) S–SSE over N–NNW transport produced boudinage with shallow-plunging boudins necks and asymmetric boudins indicate dextral-reverse shear. (2) Boudinage with down-dip neck axes also formed by flattening across layering. (3) High-angle quartz veins were rotated during development of the transposed foliation, forming low-angle oblique boudin trains with flanking folds. (4) Kaokoan domino boudins were modified by flattening, reactivating the inter-boudin plane by shearband boudinage.

Elsewhere, late-D4nz folds in east Ugab Zone are upright, open to close with 35°–150° inter-limb angles, developed at scales from 0.1 m to 20 km wavelength and with E–W to ENE–WSW axial planar crenulation cleavages well-developed (Weber and Ahrendt, 1983; Freyer and Halbich, 1994; Maloof, 2000; Passchier et al., 2002, 2007; Goscombe et al., 2004). These are heterogeneously partitioned into 5–10 km wide zones closely associated with granites, indicating propagation from shortening across pre-existing granite bodies. East Ugab Zone granites range 530–526 Ma, indicating N–S shortening younger than 526 Ma, consistent with E–W crenulations over-printing earlier ductile schistosity in these contact aureoles. E–W trending late-D4nz folds with 50°–120° inter-limb angles and axial planar biotite are documented in the South Ugab Zone. These are crosscut by the Baddocks Bay granite with 512 ± 12 Ma U-Pb monazite age from the contact aureole, and Strathmore granite with 508 ± 9 Ma contact metamorphic monazite (Table 2). Consequently, late-D4nz shortening is older than ~512 Ma and over-lapping in age with the ca. 516 Ma West Ugab granite.

4.2.4. Post-peak shortening events (D5nz–D6nz)

A range of D5nz fold structures post-date both ~512 Ma and 516 Ma granites and forming at lower metamorphic grades and strain, with NNE–SSW to NE–SW shortening in common (Figs. 9 and 10). Map-scale open folds with sub-vertical axial surfaces trending NW–SE, propagate from the NE quadrant of the West Ugab granite where shortening strain was highest (Figs. 8 and 9). NW–SE trending folds in the central Ugab Zone are similarly interpreted to have propagated off sub-surface granites indicated by broad contact aureoles (Goscombe et al., 2004). On the east margin of the West Ugab granite, axial surfaces curve into NNW–SSE trends and tighter inter-limb angles of 50°–90°, due to shortening against the granite body (Fig. 9). South Ugab Zone asymmetric map-scale folds have axial surfaces trending 100°–120° and tight parasitic folds on the limb adjacent to the Baddocks Bay pluton, indicating shortening against the granite. These geometries indicate NE–SW shortening was imposed on pre-existing granite plutons at a late-stage in the deformation history. These late-stage folds are only developed at map-scale, typically with open inter-limb angles ranging 70°–150°, indicating low shortening strains. Weak axial planar crenulations develop without biotite growth, indicating shortening after cooling of the granite thermal anomaly below 450 °C. Asymmetric folds have SW over NE vergence, showing a change from S–SSE over N–NNW during earlier Damaran events.

Late-stage, mm- to cm-scale sub-vertical D6nz kinkbands are uncommon but widespread throughout the Ugab and west Northern Zones, particularly in relatively cool regions distant from granites such as west of Brandberg and central Ugab Zone. Two geometries are recognised; NE-trending sinistral kinkbands and NNW- to NW-trending dextral kinkbands. Map-scale and mesoscopic kinkbands are developed northwest of the West Ugab granite where the NE-trending structural grain is conducive to their development (Fig. 9). These have NW-trending axial surfaces and dextral vergence in common with D5nz folds and are simply more brittle expressions of the same NE–SW shortening.

4.2.5. Along orogen shortening events (D7nz-D8nz)

4.2.5.1. D7nz ductile E–W shortening at ~512–508 Ma. Youngest ductile deformation event documented in the northern margin are D7nz folds and crenulations associated with E–W shortening; particularly well developed in the west Ugab Zone (Figs. 9 and 10). Folds form at cm- to m-scales, have shallow north plunges and N–S trending axial surfaces are sub-vertical to steeply inclined east (Fig. 8h). Folds have inter-limb angles ranging 70°–155° (averaging 122°), and asymmetry invariably showing E over W vergence. D7nz folding is partitioned into broad zones, most of which are immediately adjacent to the West Ugab Granite and sub-surface granite, where shortening strain was greatest. Map-scale warps also developed, resulting in doubly plunging Kaokoan chevrons in E–W orientations conducive to along hinge shortening (Fig. 7). D7nz folds have weak, widely spaced (0.5–10 cm) axial planar crenulations with biotite growth, resulting in stripy biotite differentiation crenulations of ~1 mm width. Crenulation orientation varies little across the region; sub-vertical with dips >80° and strikes ranging 157°–214° (averaging 185°±15°), showing only minor deflection around the pre-existing West Ugab granite (Fig. 9). Narrow orientation range across a wide region accurately constrains sub-horizontal principle compressive stress trending 095°. Latest-stage muscovite-quartz ± K-feldspar hydrothermal veins are widespread, undeformed and trend E–W (averaging 094°), consistent with injection during D7nz.

D7nz crenulations transect D2nz, D4nz and D5nz folds with no deflection and clearly post-date all convergent Damaran events. D7nz folds and crenulations over-print all aplite and pegmatite generations and are nowhere folded. Any variation in strike is systematic at map-scale and due to shortening around a pre-existing granite pluton (Fig. 9). Sharing identical vergence and strike to main phase Kaokoan foliations, suggests D7nz crenulations may be obscured and hard to recognise elsewhere in the Ugab Zone. While these crenulations are clearly expressed in the west Ugab Zone because of domains with E–W trending structural grain; and without the young West Ugab granite, the late-stage timing of similar N–S foliations may go unrecognised elsewhere in the Ugab Zone. Youngest crenulation cleavage in northeast Ugab Zone has N–S trends and E over W vergence consistent with D7nz, but with much shallower dips of 30° to the east (Goscombe et al., 2004).

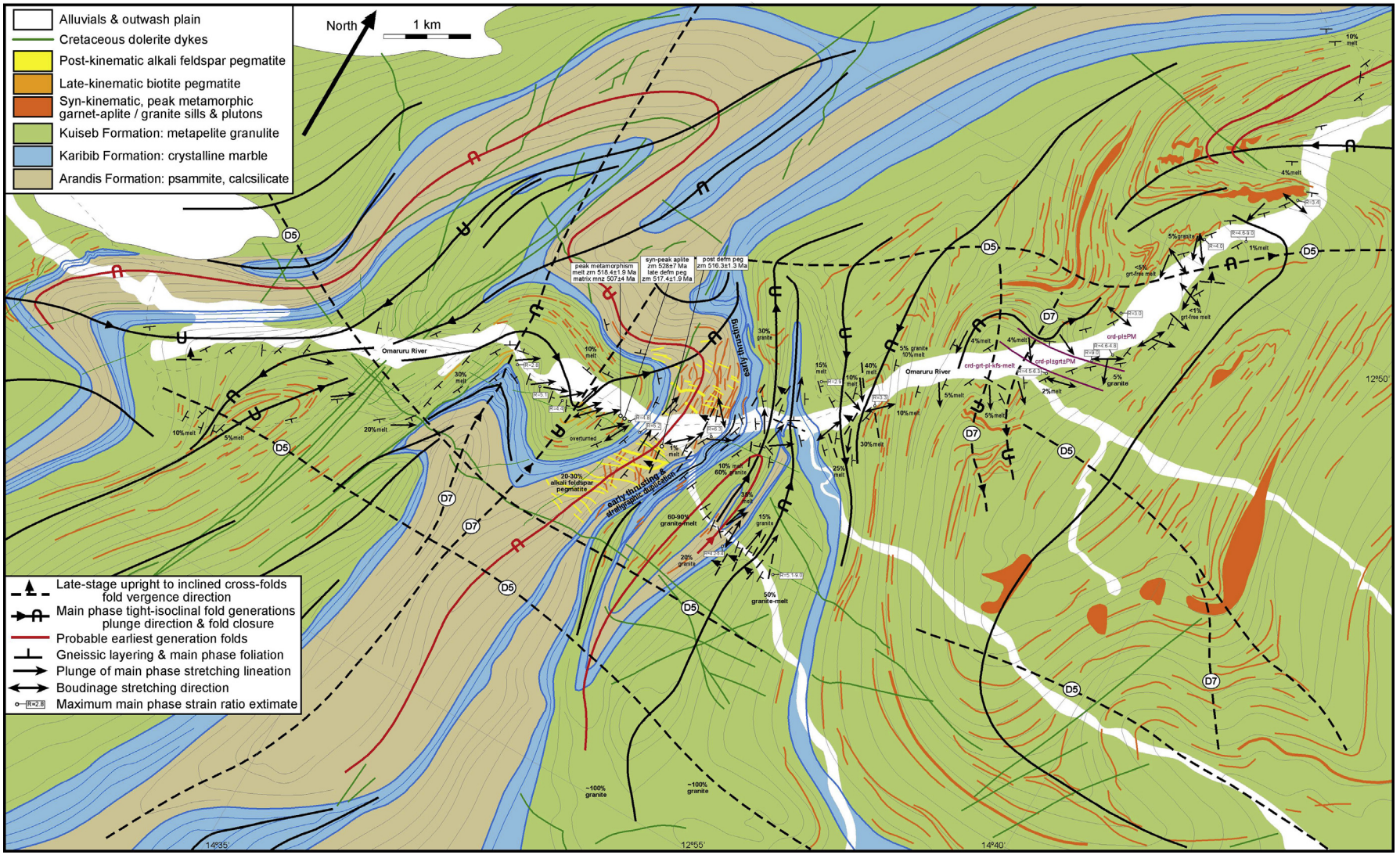

Figure 11. Structural and geological map of Damara Phase structures in lower Omaruru River map area. Earliest formed axial traces are indicated red. Undifferentiated main phase fold generations are indicated black, with late-stage cross folds (D5cz and D7cz) indicated by dashed lines. New U-Pb age determinations are annotated (Table 1). Maximum semi-quantitative strain ratio determinations are indicated (Appendix 4).

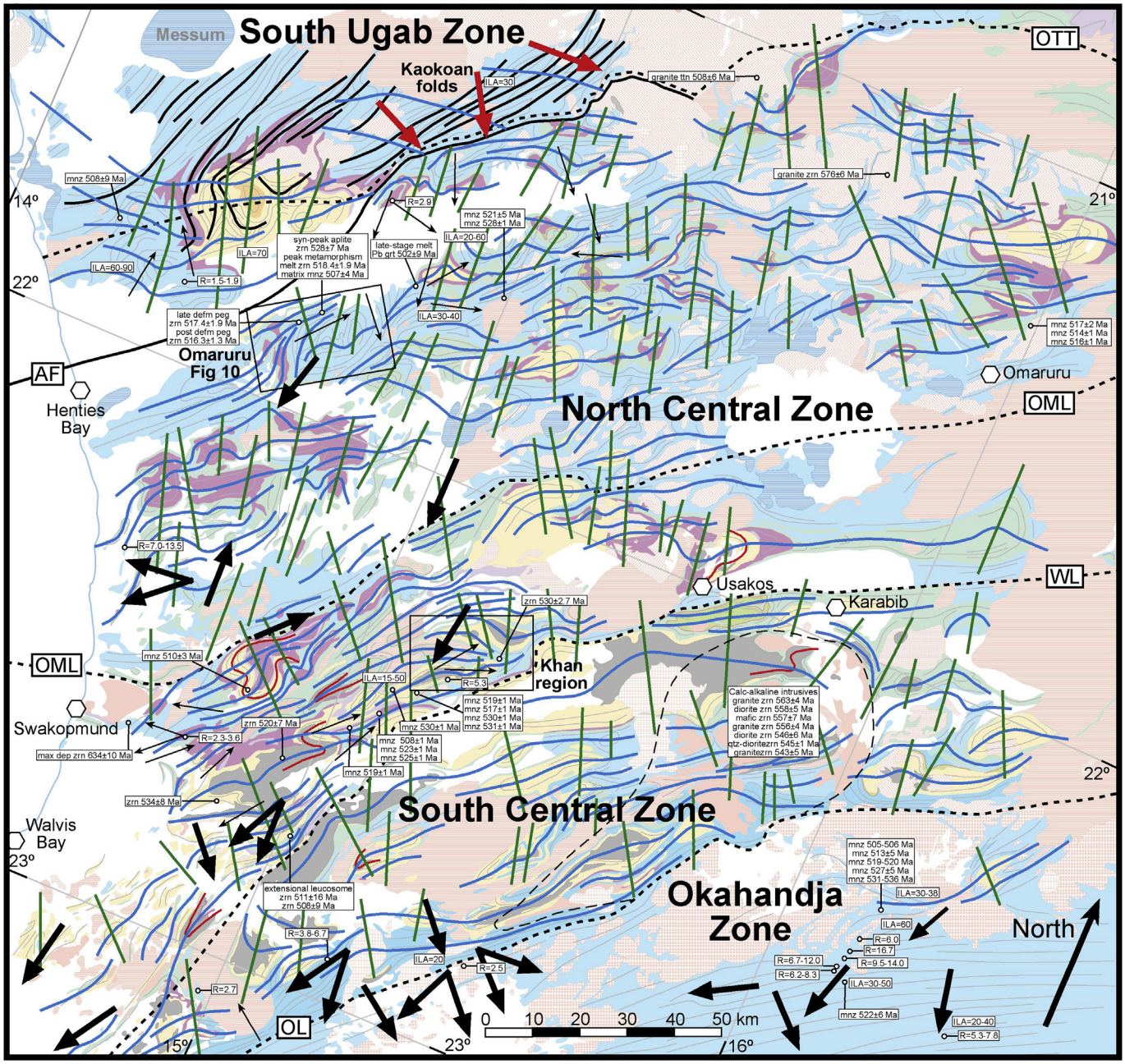

Figure 12. Structural map of the Central Zone plotted on a geological map base after Miller and Grote (1988) (see Fig. 3 for legend). A select number of interpretive map-scale fold axial trace of different periods of Damaran folding are indicated: early formed D1cz tight to isoclinal folds (red), undifferentiated main phase D2cz–D5cz tight to isoclinal inclined folds (blue), and late-stage D7cz upright to steeply inclined, close to open cross-folds (green). Main phase stretching lineations are indicated: where upper-plate transport direction is known (thick black arrows) and plunge of stretching lineations (thin black arrows). Kaokoan structures occur in the South Ugab Zone: main phase chevron fold axial trace (black) and transport direction along stretching lineations (red arrows). Robust peak metamorphic U-Pb monazite or zircon age determinations are annotated (Appendix 1). A select number of U-Pb magmatic age determinations and maximum deposition ages crucial to constraining the deformation and metamorphic history are also indicated (Appendix 1). Semi-quantitative strain ratio determinations and typical inter-limb angles are indicated (Appendix 4). Crustal-scale shear zone abbreviations are as listed in Fig. 3; also with WL – Welwitchia Lineament and OL – Okahandja Lineament.

4.2.5.2. D8nz brittle E–W shortening. Brittle reverse faults and enechelon quartz gash veins indicate weak, late-stage E–W shortening in the central Ugab Zone (D8nz). Reverse faults have steep dips and only form at small scales up to 25 cm wide. Displacements are very small and show W over E transport, whereas buckling of lithons within the faults indicate shortening across these zones. Some faults have alteration haloes containing fractures with chlorite and silica fill. Reverse faults in the west Ugab Zone offset granite sills, and are thus younger than ~516 Ma. Their late-stage of formation and E–W principle compressive stress in common, suggest that earlier E–W shortening and D7nz folding, eventually progressed into the brittle field.

4.2.6. South Ugab Zone transition into Central Zone

South Ugab Zone consists of Zerrissene Group turbidite sequences, isolated granite plutons, upper greenschist conditions and deformation history in common with the Ugab Zone to the north (Figs. 4 and 5). Southwest part of this zone transitions across a steep Damaran metamorphic gradient to grades and deformation structures more typical of the Central Zone, though still within

recognisable Zerrissene Group rocks. At highest grades immediately north of the Autseib Fault (AF), metapelites are recrystallized to biotite-sillimanite-quartz-plagioclase-K-feldspar foliated gneiss with quartz-feldspar segregations. Plutonic granite bodies are evident though regional metamorphic grade obscures contact metamorphic effects. Damaran folding is also recognisable with similarly ENE–WSW to E–W trends, steep axial surfaces, S over N vergence and inter-limb angles ranging of ~070°–120°. Kaokoan folding is also evident as large-scale chevrons and NE–SW trending sinistral-vergent folds typical of D3nz in the Ugab Zone. Main phase Kaokoan strain gauges such as flattened concretions, boudinage extension and rotated high-angle quartz veins, give strain ratios ranging 4.8–10.0, and Flynn ratios of 0.5–0.8 indicating oblate to plain strain regimes, in common with the Ugab Zone (Appendix 4). The Autseib fault boundary between the South Ugab Zone and Central Zone to the south is obscured and interpreted to be an eroded brittle structure. Nevertheless, structural grain and style, metamorphic grade and stratigraphy, all appear transitional and South Ugab and Central Zones are interpreted to be essentially contiguous. Primary differences being transition from deep-sea turbidites to passive margin sequences and increase in metamorphic grade southwards. Geometry and shortening direction of Damaran D4nz, D5nz and D7nz folds documented in the Ugab Zone can be correlated with fold events in the Central Zone; these giving elongate and inclined dome-basin fold interference (Section 4.3.4.3). Given widespread Kaokoan folding in the South Ugab Zone, it is probable that Kaokoan folds have counterpart fold structures in the North Central Zone. Though large-scale early folds may be preserved, Kaokoan fabrics would most likely have been lost during granulite grade Damara metamorphism.

4.3. High-grade orogen core: Central Zone and North Okahandja Zone

4.3.1. Overview

The Central Zone and northern Okahandja Zone constitute the upper-plate of the Damara Belt, with relatively thin Damara stratigraphy on attenuated Proterozoic crust of the Congo Craton passive margin. The Central Zone contrasts to all other parts of the belt and is dominated by high-T/low-P granulite metamorphism (Fig. 5); with large volumes of syn-kinematic S-type granitic melts of 546–515 Ma age (e.g. DeKock and Armstrong, 2014) and minor younger A-type granites (e.g. McDermott et al., 2000). The high-grade orogen core experienced protracted high heat flow conditions from 540 to 505 Ma, in a relatively stable tectonic setting associated with thinned lithosphere and highly radiogenic crust, and eventually terminated by extensional collapse at ~505 Ma (Goscombe et al., 2017a). N–S shortening across the orogen core was accommodated by large-scale upright to inclined folding, and later cross-folds produced dome and basin interference (Figs. 11 and 12). In contrast to the southern margin, the Central Zone is characterized by only moderate foliation intensity and bulk strains, with strongly transposed foliations and grain refinement fabrics being entirely absent. Despite widespread large-scale folding, most folds are upright to inclined with tight to moderate inter-limb angles, and bulk strain gauges such as boudinage extension, C-S fabrics and stretched clasts giving low to moderate strain ratios <10 (Appendix 4). At the leading edge of attenuated Congo Craton basement are 568–545 Ma I-type granitoids with some magmatic arc affinities (e.g. McDermott et al., 1996; Jung et al., 2001, 2015) and transition across the Okahandja Zone to Barrovian condition in the southern margin. The Okahandja Zone is a tightly folded upright synform of upper Damara stratigraphy at lower to upper amphibolite conditions, with metamorphic events shared in common with the Central Zone and intruded by post-kinematic Donkerhoek batholith of ~508–504 Ma age (Kukla et al., 1991; DeKock and Armstrong, 2014).

Similarities in stratigraphy, sedimentary provenance and basement indicate the Central Zone was contiguous with the Kaoko Belt and the Northern Zone throughout the passive margin history of the SW Congo craton (e.g. Foster et al., 2015). The Central Zone was also contiguous with the southern orogenic margin after collision with the Kalahari margin at the Uis-Pass Suture (UPS) at ~555–550 Ma. However, little is preserved in the Central Zone rock record from the period prior to Congo-Kalahari collision, either because stress propagating from the Kaoko Belt (between 590 and 555 Ma), and from subduction-accretion in the Southern Zone (prior to 555 Ma), was minor, or effects were later obscured by main phase Damaran events. Cryptic pre-collisional expressions are restricted to rare pre-kinematic granites of 580–570 Ma age (Allsopp et al., 1983; Armstrong et al., 1987; Bergemann et al., 2014; Milani et al., 2014) and discordant metamorphic zircon ages ranging 585–570 Ma (Armstrong et al., 1987; Foster et al., 2015). Despite being contiguous, the Central Zone experienced higher metamorphic grades, pervasive partial melting and voluminous magmatism resulting in distinctly different deformation style during Damaran orogenesis compared to the lower-grade marginal belts (Fig. 3). The lower metamorphic grade and largely coaxial deformation in the marginal provinces, along with well-constrained timing and stress field relationships, inform interpretation of the harder to decipher Central Zone.

4.3.2. Prograde Damaran events (D1cz)

Post-collision contraction across the Damara Belt gave rise to burial and prograde metamorphism producing earliest parageneses, partial melting, folds, penetrative fabrics and 546–534 Ma syn-kinematic S-type granites. Oldest metamorphic age determinations in the Central and Okahandja Zones cluster between 542 and 534 Ma, and are interpreted as prograde mineral parageneses (Jung et al., 2000b; Jung and Mezger, 2003a; Table 2). Detrital metamorphic zircons from molasse in the Fish River Subgroup mostly range 530–540 Ma (Newstead, 2010; Foster et al., 2015), over-lapping with prograde age determinations within the Central Zone, consistent with the greater component of shortening, crustal thickening and topographic development during prograde orogenesis. Peak metamorphic parageneses formed between 530 and 516 Ma in all parts of the Central Zone (e.g. Jung and Mezger, 2003a; Longridge et al., 2017), constraining the minimum age of ~530 Ma for prograde orogenesis. Earliest fabrics preserved are penetrative bedding-parallel D1cz gneissic layering on mm- to cm-scale, pervasively developed by mineral differentiation in most rock types. Gneissic banding is accentuated by development of thin mm-scale laterally continuous stringers of partial melt. In contrast to later peak metamorphic partial melt segregations, these melt stringers always parallel gneissic banding, have polygonal granoblastic micro-granite textures, and paratectic garnet and biotite-garnet melanosomes are rare. Melt stringers and gneissic layering were first folded by rare intrafolial isoclinal folds (late-D1cz) without axial planar foliation being developed. The relationship with large-scale early isoclines in the Central Zone map pattern is unknown, though both are correlated with prograde orogenesis (Fig. 12). Early formed large-scale SE over NW vergent folds have been reported from the northeast Central Zone and interpreted to have resulted in prograde burial (Longridge et al., 2011, 2014, 2017).

4.3.3. Peak Damaran events (D2cz–D5cz)

Deformation events accompanying peak metamorphism formed under moderate strains during N–S convergence, producing coarse-grained polygonal granoblastic granulite parageneses and

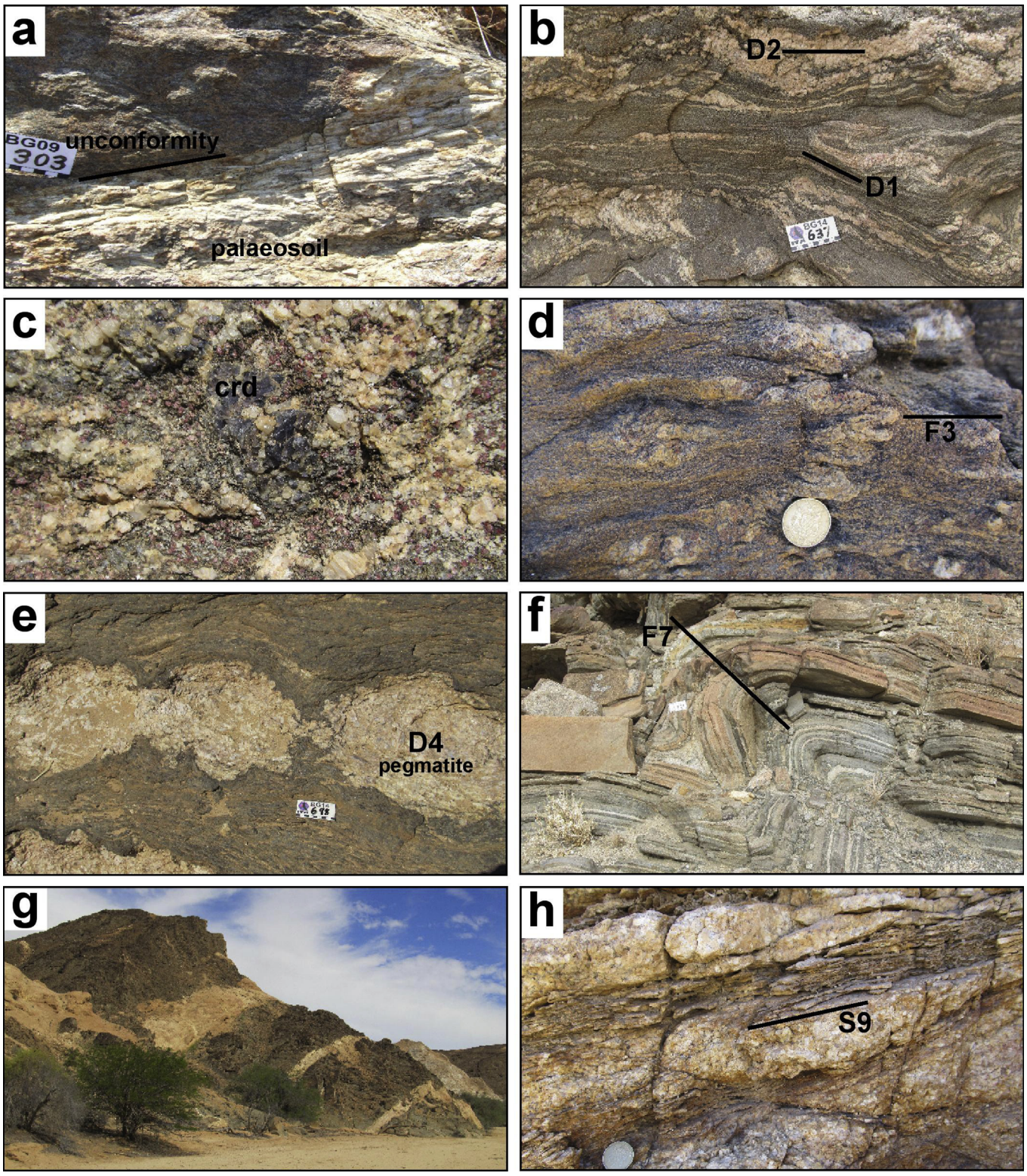

Figure 13. Representative deformation structures from the Central Zone. (a) Quartz-sillimanite aluminous meta-palaeosoil developed in the top 20 cm of basement at the unstrained unconformity immediately below Etusis Formation Damara Sequence. (b) Thin D1cz and thick, coarse D2cz stromatic partial melt segregations in metapelite granulite. (c) Coarse D3cz partial melt pool with paratectic cordierite, in metapelite granulite. (d) D2cz partial melt segregation folded by D3cz with axial planar biotite foliation. (e) D4cz biotite pegmatite with pseudo-boudinage collapse structures. (f) Asymmetric D7cz folds with east over west vergence. (g) Early-D6cz biotite-alkali feldspar dykes in the Omaruru river valley. (h) D9cz brittle crush zone within pegmatite in the Khan River region.

melt that were later over-printed by main phase folding with moderate S-L axial planar foliations. Peak parageneses, folds and fabrics were followed by further partial melting and granite pooling, ongoing flattening and at least two further fold generations, all near peak metamorphic conditions. Peak metamorphic conditions in the Central Zone were protracted and attained between 530 and 516 Ma (Armstrong et al., 1987; Jung et al., 2000a,b; Jung and Mezger, 2003a; Longridge et al., 2014, 2017; Table 2), and 528–519 Ma in the Okahandja Zone (Kukla et al., 1991; Jung and Mezger, 2001).

4.3.3.1. D2cz peak metamorphism between ~530 and 526 Ma. D2cz is defined by the main generation of partial melting, producing the predominant coarse-grained partial melt segregations with paratectic cordierite and or garnet porphyroblasts and biotite-garnet ± sillimanite melanosomes. Segregations are typically cm- to dm-scale and volumetrically the dominant partial melt generation, typically 5–20% and up to 35–50% in metapelite Kuiseb Formation (Fig. 13b and c). Segregations are sub-parallel to gneissic layering, though unlike first generation melts, are less planar and laterally continuous, forming; stromatic bands, lenses, irregular pools, inter-boudin pooling and pressure shadows around paratectic phases. Discordances are rare, and with no indication for injection, are interpreted as in situ melting with local pooling. Earliest generation leucogranite sills with paratectic garnet formed at this time and are interpreted as larger scale stromatic pooling of partial melt. Significant volumes of melt pooled as large-scale (0.3–20 m wide) aplitic to leucogranite sills with poikiloblastic paratectic garnet. These are typically sub-parallel to gneissic layering and main phase foliations and also show local discordance. Leucogranite sills in the North Central Zone give a U-Pb zircon age of 528.1 ± 6.9 Ma and 530.0 ± 2.7 Ma from the South Central Zone (Table 2). Melt pooling also formed irregular granite bodies in regions with high degrees of partial melting, indicating formation near the peak of metamorphism (Fig. 11). Kuiseb Formation shows transitional gradients of increasing partial melt proportion continuous into granite bodies, indicating large-scale melt pooling. Where aplite intrudes into marble units, they form lobate forms due to neutral buoyancy and local ballooning. Leucogranite sills are folded and boudinaged during main phase deformations and ongoing flattening and recycling of the biotite foliation. Domino boudinage of sills indicate top to the SW shear sense, similar to indicators from the main foliation.

Coarse-grained polygonal granoblastic matrix parageneses developed during D2cz and constitute the peak metamorphic assemblage. Predominant matrix assemblage in Kuiseb Formation metapelite is cordierite-garnet-biotite-quartz-plagioclase-K-feldspar-melt, throughout most of the Central Zone. Garnet and cordierite porphyroblasts were stretched by ongoing flattening that produced the main biotite foliation. Garnet is earliest formed and experienced greater flattening, whereas cordierite continued to grow as coronas on garnet porphyroblasts. Average peak metamorphic conditions based on THERMOCALC average PT calculations, from north to south across the orogen core are: 649 °C/4.5 kbar in the southwest South Ugab Zone, 738 °C/5.2 kbar in the North Central Zone, 700 °C/4.8 kbar in the South Central Zone and 678 °C/4.8 kbar in the north Okahandja Zone (Goscombe et al., 2017a). Higher grade conditions of 835 °C/4.9 kbar have been determined by pseudosection modelling of a garnet-cordierite-orthopyroxene granulite in the South Central Zone (Longridge et al., 2017). All regions experienced high-T/low-P thermal regimes ranging 41–44 °C and low ΔP/ΔT clockwise P-T paths with decompression through the peak and post-peak isobaric cooling, indicating relatively stable high heat flow setting without significant crustal over-thickening (Goscombe et al., 2017a).

4.3.3.2. D3cz main phase deformation at ~525–518 Ma. Tight to isoclinal D3cz folds with shallow NE-plunges and axial planar biotite foliation refold gneissic layering, leucogranite sills and melt segregations at outcrop- to map-scale (Figs. 11 and 13d). These constitute main phase folding that post-dates peak metamorphic matrix parageneses and leucogranite sills of ~530–528 Ma age and overlap in age with larger syn-kinematic granite bodies of 525–520 Ma age (Jung et al., 2001; Jung and Mezger, 2003a). Folding over-laps in age with ongoing peak metamorphic conditions and secondary partial melt pools that give a U-Pb zircon age determination of 518.4 ± 1.9 Ma in the North Central Zone (Table 2) and 520.3 ± 4.6 Ma in the South Central Zone (Longridge et al., 2017). Minimum age for peak metamorphism, main phase folding and fabric formation in the North Central Zone is constrained by late-kinematic biotite pegmatite veins with U-Pb zircon age of 517.4 ± 1.3 Ma and 516.3 ± 1.3 Ma post-kinematic biotite-alkali feldspar dykes (Table 2). Minimum age for main phase deformation and peak of metamorphism in the South Central Zone is constrained by widespread ~515 Ma post-kinematic granites that crosscut matrix parageneses and partial melt segregations (Longridge et al., 2011, 2014; Paul et al., 2014; Appendix 1).

D3cz deformation formed the regionally pervasive main foliation parallel to layering, gneissic banding and melt segregations, and was the dominant strain event in the Central Zone. The foliation is a moderate to strong biotite schistosity that flattens garnet and cordierite porphyroblasts in metapelite and pelo-psammite, and has a moderate grain shape fabric in calcsilicate, calc-psammite and psammite. At lower grades in the north Okahandja Zone, biotite foliation ranges from continuous to spaced schistosity, and calcsilicate lenses are flattened and stretched parallel to the S-L fabric. Once formed, this penetrative main foliation was recycled by ongoing flattening during different stages of boudinage of progressively younger granite-pegmatite-melting events (D3cz-D4cz). A weak stretching lineation defined by feldspar and quartz aggregate streaks, aligned biotite and stretched garnet and cordierite, is developed in the Central Zone and aligned quartz aggregate, biotite and sillimanite in the north Okahandja Zone. Stretching lineations and boudin extension directions show a wide range due to refolding, though most trend N–S to NE–SW. Nevertheless, obliquity between stretching lineation and main foliation trace is 60°–90° in most parts of the Central Zone, consistent with N–S directions predominating, and as low as 30° only in the region south of the basement domes, indicating NE–SW stretching direction in this region.

Most significant boudinage in the Central Zone occurred during D3cz shortening, with ongoing boudinage continuing into D4cz. Almost all involved only moderate stretch, producing predominately torn, necked and drawn boudins. Drawn boudins remain connected by a thin neck zone, and boudin separation was minor, indicating strain was not high during main phase deformation. Grain refinement fabrics such as mylonite and ultramylonite are absent from the Central Zone, including the basal unconformity (Section 4.3.6), confirming bulk strain was not high. Carbonate units are devoid of disrupted, highly stretched interbeds, rollup structures, flanking folds or mineral alignments that would otherwise preserve evidence for high-strains prior to annealing. Strain gauges using boudinage extension, rotation of high-angle veins and C-S fabrics in the Central Zone and north Okahandja Zone, give moderate strain ratios ranging 3.0–9.5 and flattened conglomerate clasts give 6.0–16.7 (Appendix 4). All subsequent deformation periods in the Central Zone are of lower strain. Shear sense determinations using boudinage, sigma shear-lenses and flanking folds, indicate predominantly north over south transport throughout the Central Zone. Most boudinage is symmetric, asymmetric lateral shear structures in general are uncommon, and

the main foliation is recycled by ongoing flattening. Aspect ratio of stretched clasts give Flynn ratios of 0.1–1.1 in the Central and Okahandja Zones, indicating oblate to plain strain regimes. All these features indicate pure shear dominated and absence of grain-refinement in the Central Zone indicate simple shear and layer-parallel slip were not important deformation mechanisms.

4.3.3.3. D4cz NNW–SSE shortening folds and biotite pegmatite at ~518–516 Ma. Large-scale D4cz folds with 20°–80° inter-limb angles and SW–NE to WSW–ENE trending axial surfaces, define the long-axis of basement domes and are the second major fold event (Fig. 11). These fold the main biotite foliation and develop weak axial planar biotite or biotite-sillimanite foliation seams and shearbands with NNW over SSE shear sense. Axial surfaces are inclined NNW and fold vergence is NNW over SSE in the Central Zone, steepening southward, and SE over NW vergence in the north Okahandja Zone. This period of ongoing shortening produced further boudinage and recycling of the main biotite foliation as the enveloping surface of boudinaged segregations and granite sills. Biotite pegmatite veins in the North Central Zone show low-angle discordances up to 10°–30°, over-print aplitic sills and partial melt, and in places are approximately axial planar to the large-scale folds (Fig. 11). Pegmatite veins were injected and show no evidence for in situ partial melting. Margins are irregular with protruding phenocrysts and collapse features that mimic boudinage (Fig. 13e). These pegmatites give a U-Pb zircon age of 517.4 ± 1.3 Ma (Table 2), interpreted as the probable age of the large-scale folds. This age constraint is consistent with folding and boudinage of earlier leucogranite sills and melt segregations of ~528–518 Ma age (Table 2), and cross cutting post-kinematic alkali-feldspar pegmatite dykes of 516.3 ± 1.3 Ma age in the North Central Zone (Table 2). This minimum age constraint is consistent with late- to post-kinematic granites of 515–507 Ma age throughout the Central Zone (Appendix 1) and extensional granitic veins of 511–508 Ma age in the South Central Zone (Longridge et al., 2011, 2014).

4.3.3.4. D5cz N–S shortening folds at ~516 Ma. D5cz folds have sub-horizontal E–W trending axes, are tight to close with 30°–70° inter-limb angles and S over N fold vergence. These fold the main biotite foliation and developed a weak axial planar biotite foliation. Axial surfaces have shallow south inclinations in the North Central Zone, ranging to steeper inclinations in the south, and upright chevron folding with weak axial planar crenulations and biotite foliation in the north Okahandja Zone. This phase of folding is tentatively correlated with N–S shortening in the Ugab Zone, constrained by the West Ugab granite to ~516 Ma.

4.3.4. Along orogen shortening events (D6cz–D7cz)

Peak metamorphic and main phase deformation associated with NNW–SSE to N–S convergence, were over-printed by a complex D6cz transitional phase involving ENE–WSW oblate shortening, magmatism, thermal anomaly and incipient extension followed by D7cz along-orogen shortening. Structural expressions of late-stage E–W shortening are of lower strain than main phase fold and fabric events, resulting in upright to inclined cross folding that gave rise to the dome and basin fold interference pattern characteristic of the Central Zone (Fig. 12).

4.3.4.1. Early-D6cz oblate shortening and magmatism between ~516 and 513 Ma. Oblate shortening produced a conjugate set of post-kinematic alkali-feldspar pegmatite dykes in the North Central Zone. This magmatic event constitutes discordant 1–20 m thick coarse-grained, biotite, quartz, alkali-feldspar (plagioclase-free) pegmatite and granite dykes (Fig. 13g). These pegmatites form a conjugate set of E–W to ENE–WSW striking dykes that dip ~40°–50° to both the north and south, indicating horizontal maximum compression stress and oblate strain regime with $\sigma_2 = \sigma_3$. Pegmatite dykes are planar and range from laterally continuous to short dyke lengths confined to specific rheological rock units (Fig. 11). In contrast to the widespread older magmatic events, alkali feldspar pegmatites are restricted to a small region of Arandis Formation calc-psammites, conducive to forming brittle dilation zones. The resulting box-work of short discontinuous dykes constitute up to 15–30% of the rock volume in a restricted region (Fig. 11). Schistose rock units such as Kuiseb Formation metapelite are devoid of these dykes, which otherwise pool against massive Karibib carbonates (Fig. 11). Partitioning of strain response between stratigraphic units, was accommodated by foliation recycling in metapelite schists and bedding-parallel slip on thin mylonites within carbonate units. Post-kinematic alkali-feldspar pegmatites in the North Central Zone give a U-Pb zircon age of 516.3 ± 1.3 Ma (Table 2), indicating ENE–WSW shortening as early as 516 Ma.

4.3.4.2. Late-D6cz extension and secondary thermal pulse between ~513 and 508 Ma. Late-D6cz is defined by late-stage biotite pegmatite and granite veins injected into extensional shear zones of the South Central Zone with ages of 511 ± 6 and 508 ± 2 Ma (Longridge et al., 2011, 2014). Late-kinematic granites from elsewhere in the Central Zone have similar ages ranging 512–507 Ma (Allsopp et al., 1983; Jung et al., 2001; DeKock and Armstrong 2014). A late-stage thermal anomaly in the Okahandja and Central Zones produced secondary partial melt and metamorphic age determinations ranging 515–505 Ma (Briqueu et al., 1980; Jung et al., 2000b; Jung and Mezger, 2003b; Longridge et al., 2011; Goscombe et al., 2017a), over-lapping in age with the extensional shear zones and late-kinematic granite and pegmatite. Late-stage extension is also documented in the north Okahandja Zone where asymmetric folds show top down to the north vergence, and dextral-normal shear zones and shearband boudinaged pegmatite veins.

4.3.4.3. D7cz E–W shortening cross-folds at ~512–508 Ma. D7cz is defined by late-stage, asymmetric tight to close cross-folds with ~30°–100° inter-limb angles, developed on both outcrop and map scales (Fig. 11). Folds have steep N- to NNE-trending axial surfaces and E over W vergence (Figs. 11 and 13f). These folds typically do not develop axial planar foliations. Cross-folds dominate the large-scale map pattern and refold main phase D3cz–D5cz folds resulting in the inclined, elongate dome and basin interference pattern of the Central Zone. Complex map patterns suggest more than one late-stage cross-fold event. Late-stage shearbands in the north Okahandja Zone have E over W shear sense in common. The timing of late-stage cross-folding is younger than 511–508 Ma granite and pegmatite veins intruded into extensional shear zones, and has been interpreted at ~508 Ma (Longridge et al., 2011, 2014). The Ugab Zone develops similar steep N–S crenulation cleavages and asymmetric D7nz folds with E over W vergence in common with the Central Zone.

4.3.5. Extensional exhumation events (D8cz–D9cz)

Deformation accompanying exhumation involved a stress switch to vertical flattening and significant N–S extension, resulting in flattening folds and metamorphic core complex-style extensional exhumation in the Central Zone and tilting of marginal zones to the north and south (Goscombe et al., 2017a). Youngest fold event recognised in the North Central Zone are D8cz asymmetric warps with monoclinic form, inter-limb angles of ~120°–160°, and shallow to flat-lying axial surfaces indicating vertical flattening. Deeper level ductile expressions of vertical flattening are over-printed by shallow level brittle crush zones

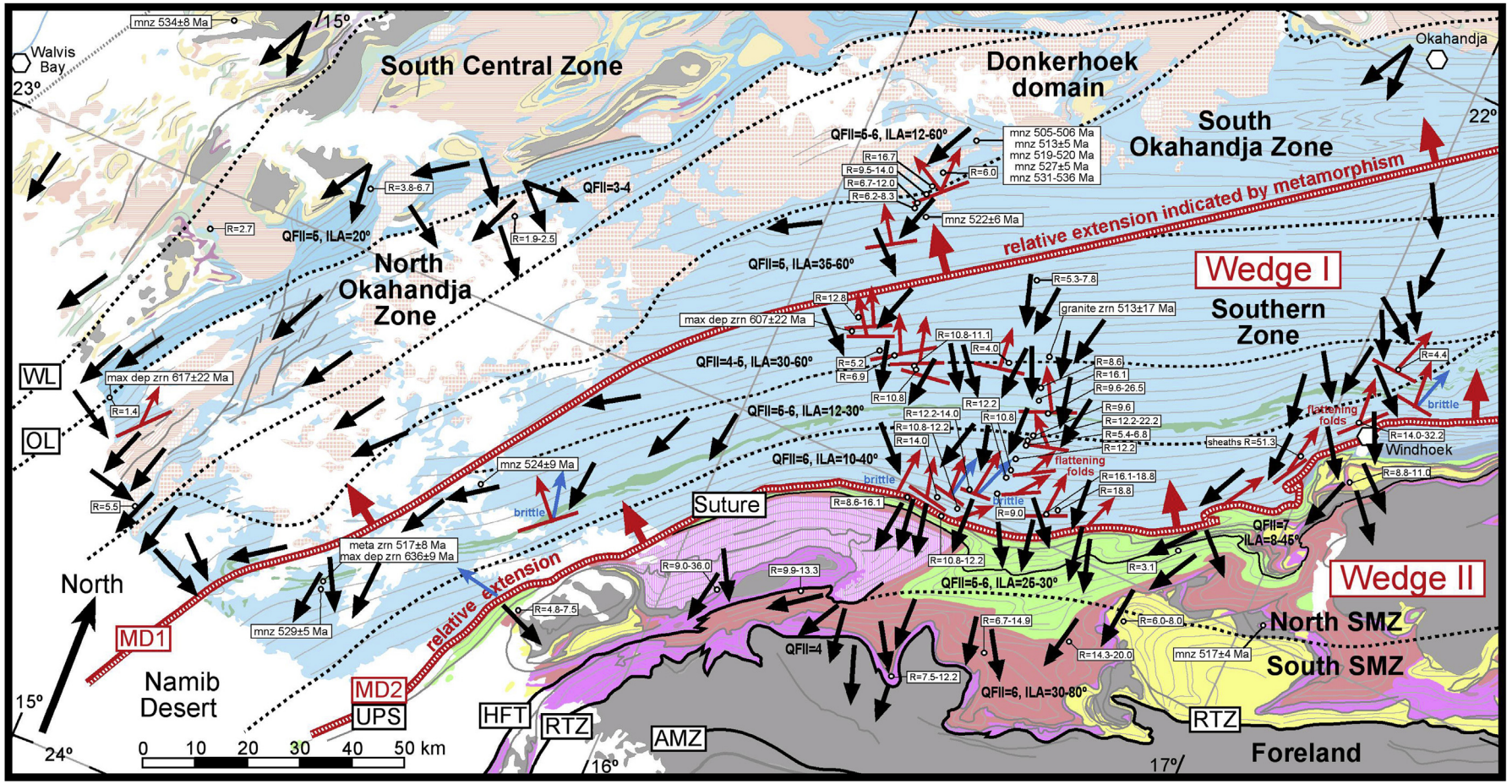

Figure 14. Simplified structural map of the southern margin indicating the major chronostratigraphic rock units, crustal structures and metamorphic discontinuities (Goscombe et al., 2017a). Geology based on Miller and Grote (1988) and legend contained in Fig. 3. Main phase D2sz-D4sz stretching direction and top to the south transport of the upper-plate is indicated by thick black arrow. Post-peak metamorphic D6sz-D7sz, ductile vertical flattening and extensional structures are indicated by red symbols. Strikes indicate extensional shearbands and axial trace of shallow dipping flattening folds. Arrows indicate top down to the north extensional transport directions based on boudinage, shear zones, shearbands and fold vergence. Upper-plate transport direction in significant late-stage brittle extensional faults (D8sz), are indicated by blue arrows. Robust peak metamorphic U-Pb age determinations are annotated (Appendix 1). A select number of U-Pb magmatic age determinations and maximum deposition ages crucial to constraining the deformation and metamorphic history are also indicated (Appendix 1). Semi-quantitative strain ratio determinations (Appendix 4), typical inter-limb angles and qualitative foliation intensity domains (Goscombe and Gray, 2008) are indicated. UPS – Uis-Pass Suture is a major crustal thrust corresponding to the suture between stratigraphy deposited on either the Kalahari or Congo cratons, and containing dismembered serpentinites (Barnes, 1983; Kasch, 1983; Kukla and Stanistreet, 1991); and later reactivated by extension during exhumation. Other crustal-scale shear zones, thrust or faults are indicated by the abbreviations: WL – Welwitchia Lineament, OL – Okahandja Lineament, AMZ – Areb Mylonite Zone, HFT – Hakos Frontal Thrust, RTZ – Rehoboth Thrust Zone. MD1 and MD2 are metamorphic discontinuities inferred from metamorphic field gradients (Goscombe et al., 2017a).

(D9cz), typically developed at high stratigraphic levels within the Kuiseb Formation. Brittle crush zones in the Omaruru River and Khan River areas are sub-horizontal to shallow north-dipping (~10°–20°) zones of 5–20 m width, containing disjunctive cleavages, fractures, gouge zones with slickenlines and brecciation (Fig. 13h). Crush zones are associated with fluid flow, retrogression and distinctive precipitation of iron oxides. Within these broad zones, expressions of brittle flattening are organised into packets of anastomosing fractures on dm-scale that are spaced on m-scale. Brittle breccia zones have sharp basal surfaces, below which is devoid of fracturing, retrogression and oxidation. Breccia zones show S-C asymmetric geometries, typically with sub-horizontal S-plane fractures and shallow NW- to NE-dipping extensional C-planes, indicating on average top down to the north extensional shear (Fig. 13h). Shallow dipping brittle breccia zones are interlinked by sub-vertical fracture zones of at least 20 m width, typically trending NNE–SSW and forming prominent valleys. Steep fracture zones post-date the sub-horizontal breccia zones, offsetting them by top down to the NW dextral-normal slip along shallow NNE-plunging slickenlines. All brittle features are best expressed in coarse-grained feldspathic rock types such as granite and pegmatite and can be mapped in regions pervaded with granites. Extension and exhumation of the Central Zone metamorphic core complex had wider deformational effects into the marginal regions to the north and south. Peak metamorphic isograd patterns were back-tilted and compressed producing steep metamorphic field gradients in these marginal zones (Fig. 5; Goscombe et al., 2017a). South of the Central Zone, the north Okahandja Zone is marked by a steep, tight synform of Tinkas Formation at highest stratigraphic levels. Late-stage tightening of this synform produced sinistral shearbands, brittle reverse faults, quartz-muscovite tension gash veins and kinkbands all showing N–NW over S–SE transport.

4.3.6. Basal unconformity

Basal units of the Damara Sequence in the Central Zone are Etusis and Khan Formations within the Nosib Group. These rock units have low-strain grainshape and weakly aligned gneissose fabrics throughout, with no strain gradient into the basal unconformity, or within the basement gneisses. This weak grainshape fabric is nowhere later reworked, and shows no grain refinement fabrics such as mylonite or ultramylonite, anywhere in numerous sections across the basal unconformity. In the Khan River region, the basal unconformity is a 10–30 cm wide unstrained aluminous sillimanite-quartz horizon, interpreted to be meta-palaeosoil (Fig. 13a). Basement gneisses at this locality are paragneiss with altered bulk compositions rich in Al and Fe and metamict zircons, consistent with being a palaeosoil profile. Altered Fe-Al-rich bulk compositions are evident in outcrop by high modal proportions of sillimanite, Fe-Ti oxides and biotite. This horizon continues to ~10 m depth below the unconformity, indicating a contiguous palaeosoil profile that has not been significantly disrupted. Absence of evidence for grain-refinement fabrics at this and other basal unconformity localities, or any other structural level in the Central Zone, and preservation of a palaeosoil horizon at the basement unconformity, is incompatible with Central Zone models that require a high-strain basal detachment (e.g. Oliver, 1994).

4.4. Southern orogenic Margin: South Okahandja, southern and Southern Margin Zones

4.4.1. Overview

The southern orogenic margin is a highly strained fold-thrust belt with half-flower geometry that experienced south-directed transport, deep burial and inverted Barrovian metamorphic response almost void of granitic melt generation or emplacement (Fig. 14). At highest structural levels, the south Okahandja Zone is a steep wedge of deeply buried Damara Sequence, juxtaposed against high-grade low-P metamorphics of the orogen core. Southern Zone is a homoclinal, intensely transposed sequence of deep marine turbidites with Congo Craton provenance, forming a thick accretionary prism (Kukla and Stanistreet, 1991; Foster and Goscombe, 2013; Foster et al., 2015). The Southern Margin Zone consists of sequences deposited on the Kalahari Craton margin, and highly strained in a fold-thrust belt with basement-cored nappes transported onto the Southern Foreland (Porada and Wittig, 1983). Uis-Pass Suture between these two zones is a crustal-scale shear zone with two-stage history; main phase N over S reverse shear and retrograde extensional reactivation during extensional telescoping of the southern margin (Goscombe et al., 2017a). This suture contains sheared Alpine serpentinites accreted during continent-continent collision (Barnes, 1983; Kasch, 1983), and marks the boundary between sequences with Kalahari or Congo Craton provenance (Foster et al., 2015). High-P, blueschist-eclogite subduction parageneses associated with subduction of Kalahari lithosphere are not preserved in the rock record. Nevertheless, ocean basin closure is indicated by: (1) contrasting sediment provenance on opposing margins (Foster et al., 2015), (2) inter-thrust oceanic lithosphere in the suture and Matchless Belt, at higher structural levels (Barnes, 1983; Killick, 2000), and (3) palaeo-magnetic poles, homoclinal accretionary wedge and gross structural asymmetry of the orogen (Meert et al., 1995; Meert and Torsvik, 2003; Gray et al., 2008; Foster and Goscombe, 2013).

The greater part of shortening across the Damara Belt was accommodated within the southern orogenic margin where main phase foliation intensity and bulk strain was highest, burial was deepest and significantly greater topography was likely developed. In response to deep burial, isostatic instability led to rapid lateral exhumation of crustal wedges resulting in extensional telescoping of the southern margin while still under contraction (Goscombe et al., 2017a). Main phase burial foliations, deformation structures and peak metamorphic parageneses, are over-printed by various extensional structures progressing from ductile to brittle, indicating vertical flattening accompanying exhumation of these crustal wedges. Top down to the north extensional structures are partitioned into broad zones that overlap with metamorphic discontinuities showing large pressure differentials. The most significant controlling structure was Uis-Pass Suture, reactivated by top down to the north extension, juxtaposing 11.0 kbar rocks in the footwall with 8.0–9.0 kbar rocks in the hanging wall Southern Zone. Extensional reactivation progressed from shallow N-vergent flattening folds, to chlorite-muscovite retrogressive shear zones and finally brittle faulting and pseudo-tachylite.

4.4.2. Prograde Damaran events (D1sz–D3sz)

Main phase penetrative foliations, thrusts, folds and nappes in the southern margin were developed during prograde burial phase of orogenesis and prior to the thermal peak of metamorphism. Best age estimates for closure of the Khomas Ocean and collision of Kalahari and Congo cratons come from the low-grade foreland margins, away from resetting by later deformation events in the internal parts of the orogen. Ar-Ar muscovite age of 555 Ma from phyllonite at the base of the Naukluft Nappe complex gives a minimum age for the very earliest phase of orogenesis (Gray et al., 2008). Collision at this time is confirmed by initiation of Fish River Subgroup molasse in the Nama Basin at ~552 Ma (Grotzinger et al., 1995; Newstead, 2010; Foster et al., 2015), and oldest K-Ar deformation ages of 556–550 Ma from phyllites in the Northern Platform (Clauer and Kroner, 1979). Detrital metamorphic zircons from molasse in the Fish River Subgroup range 540–530 Ma (Newstead,

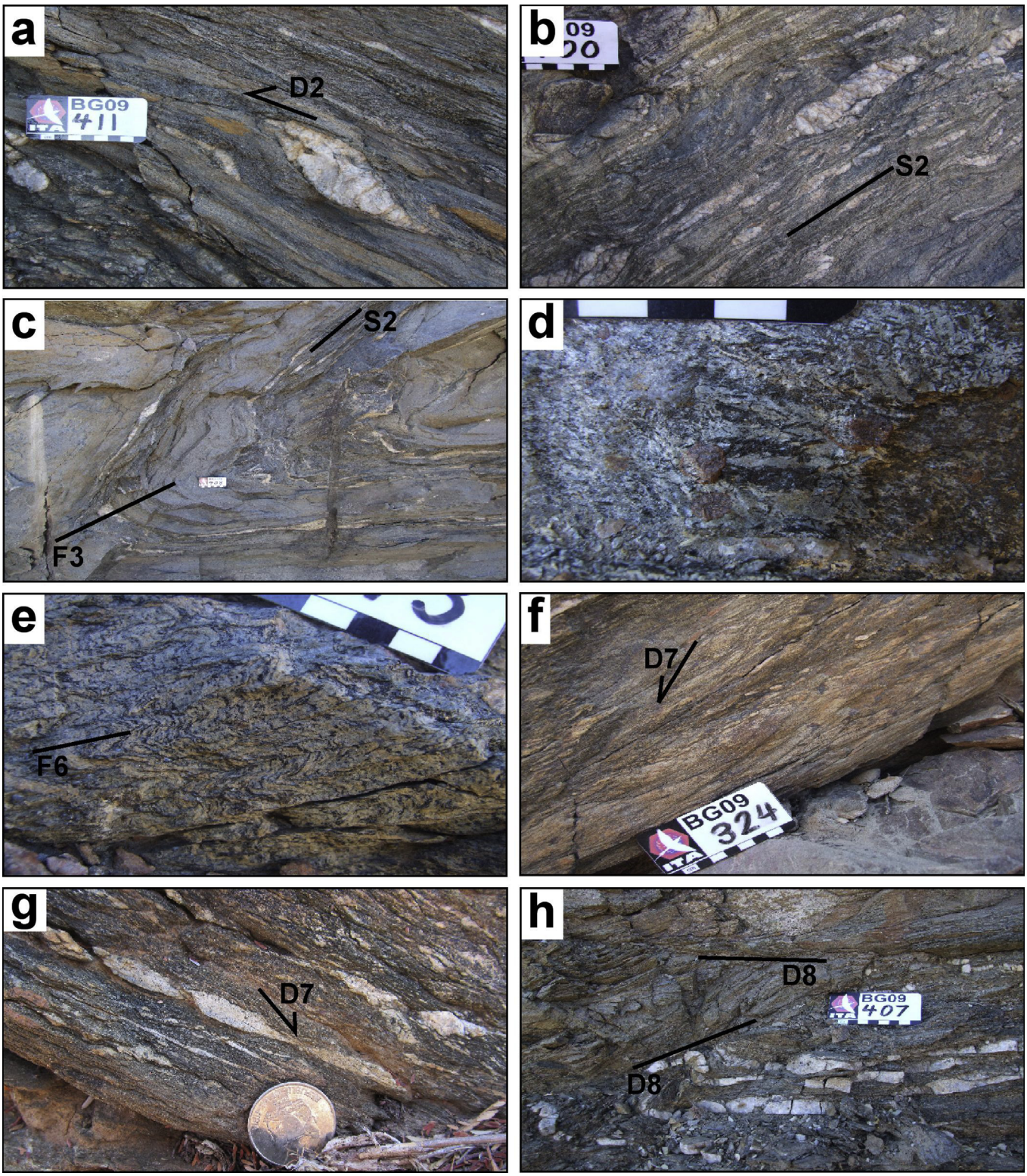

Figure 15. Representative deformation structures from the southern orogenic margin, including south Okahandja, Southern and Southern Margin Zones. (a) North over south main phase D2sz shear sense indicated by shearbands propogating off sigma clasts. (b) Strong D2sz foliation intensity with extreme stretch of early layer-parallel quartz veins. (c) Main phase D3sz folding of psammite-pelite bedding and main phase D2sz foliation. (d) Peak metamorphic random biotite laths and idioblastic garnet over-growing main foliation. (e) Shallow dipping D6sz flattening folds with spaced axial planar crenulation cleavage. (f) Top down to the north D7sz extensional shear band. (g) Top down to the north D7sz extensional shear zone in Matchless amphibolite. (h) D8sz brittle extensional fault zone.

2010), indicating this was the main period of convergent orogenesis with topography development. This age range for prograde deformation is consistent with bracketing between collision at 555–550 Ma and the onset of peak metamorphism in the southern margin at ~529 Ma (Goscombe et al., 2017a).

4.4.2.1. D1sz early foliations. Earliest formed structures are D1sz bedding-parallel foliations with no associated folding. Also early formed are large volumes of bedding-parallel quartz veins formed due to dewatering and dehydration reactions during burial and prograde metamorphism. These foliations are fine-grained mica schistosity and phyllonite, typically only preserved as relicts within low-strain shear lenses in the Southern and Southern Margin Zones. Elsewhere, early bedding-parallel foliations are well preserved in the Naukluft Nappes that are sufficiently distal from ongoing orogenesis and fabric recycling in the internal parts of the belt. The basal shear surface of the Naukluft Nappe has a strongly foliated phyllonite with C-S fabrics indicating NW over SE transport (Gray et al., 2006). At higher structural levels upright folds of E–W trend have steep axial planar crenulation cleavages. Main phase transport directions range from NNE over SSW along most of the southern margin, to NW over SE in the west; resulting in converging tectonic transports at the cratonic corner and the large 60–80 km transport of the Naukluft Nappes. Early bedding-parallel foliations are interpreted to overlap in age with Congo-Kalahari collision and Naukluft Nappe emplacement at ~555 Ma. These early foliations and veining probably also started to develop before this time, both within the Southern Zone accretionary wedge, and the subducting Kalahari passive margin (Southern Margin Zone), after termination of deposition at ~580 Ma and prior to collision by ~555 Ma.

4.4.2.2. D2sz main phase N over S foliations. The early schistosity was over-printed by meso- to macro-scale tight to isoclinal folding, producing the main phase D2sz axial planar penetrative foliation and down-dip stretching lineation. Folding is typically tight to isoclinal rootless folds with asymmetric geometries showing N over S vergence (Fig. 14). Main foliation is strongly transposed, bedding-parallel, fine-grained muscovite-biotite schistosity in the southern zones (Fig. 15b), whereas the Okahandja Zone shows refraction and ranges from spaced foliations in psammite to continuous schistosity in pelite interbeds. At highest strain intensity, main foliations have C-S and S-C′ geometries showing N over S shear sense. Main foliation is north-dipping throughout, and dip varies from 70° to 90° near the Okahandja Lineament to 20°–40° in north Southern Zone, 40°–70° in the south Southern Zone and decreases to 10°–40° in the vicinity of the Uis-Pass Suture and into the Southern Margin Zone (Fig. 14). At larger scale, crustal-scale thrusts in the southern margin and foreland such as the Uis-Pass Suture operated at this time and accommodated under-thrusting of the Kalahari margin. Stretching direction defined by aligned fine-grained biotite and quartz aggregate lineations are developed in the main foliation and margins of early quartz veins. Stretching lineations have down-dip plunges showing high-angle obliquity of 60°–90° with respect to strike, in most parts of the southern margin, except for lower obliquity of 20°–50° in north Southern Zone, Uis-Pass Suture and north Southern Margin Zone (Fig. 14). Shear sense indicated by boudinage, shearbands, S-C foliations and porphyroclasts, is consistently reverse, with N–NW over S–SE transport in the Southern Zone and N over S transport in the Southern Margin Zone (Fig. 15a). Early quartz veins are characteristically drawn and shearband boudinaged into widely separated sigma-shaped lenses with highly stretch tails (Fig. 15b).

Main foliation strain intensity is highest in the Southern Margin Zone and decreases semi-systematically northward and is lowest in

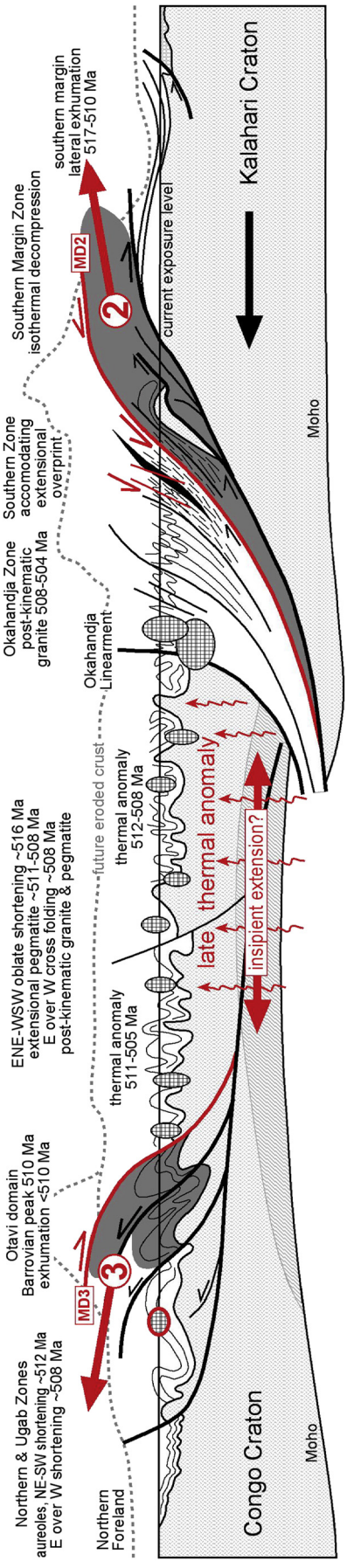

Figure 16. Diagrammatic summary of the crustal architecture in the Damara Belt during post-peak (<517 Ma), late-stage episodes in the orogenic cycle (modified after Goscombe et al., 2017a). In particular, illustrating relationship between deformation and metamorphic processes and sequence of lateral exhumation of Barrovian crustal wedges and vertical exhumation of the Central Zone as a metamorphic core complex. Lateral exhumation of the Southern Zone occurred slightly earlier at >517 Ma. Extensional telescoping events and thermal features are indicated by red.

the Okahandja Zone. Semi-quantitative strain gauges based on C-S fabrics, sheath folds, boudin trains, aspect ratios, pressure fringes and rotated gash veins with flanking folds (Goscombe and Gray, 2008), confirm this strain gradient (Appendix 4). Background strain from outside of the major shear zones is moderate, with strain ratios of 4.0–14.0 gauged from C-S fabrics, 1.4–9.0 from boudinage extension and 5.0–12.5 from stretched clasts. From north to south background strain averages; 4.6 ± 2.7 in the Okahandja zone, 4.8 ± 3.0 to 6.1 ± 3.7 across the Southern Zone and 7.7 ± 3.5 to 8.2 ± 3.3 across the Southern Marginal Zone. Stretched conglomerate clasts constrain variation in strain regime across the southern margin; with Flynn ratios of 0.14–0.75 indicating oblate strain in the Okahandja Zone, 0.80–1.1 indicating plain strain in the north Southern Margin Zone, and 1.24–2.75 indicating prolate strain further south (Appendix 4). Superimposed on the regional strain gradient are high strain shear zones, also showing an increase in strain towards the south. High strain zones within the Okahandja Zone have strain ratios ranging 9.5–17.0 and within the Southern Zone 13.0–16.0. The Uis-Pass Suture has highest strain ratios of 16.0–32.0, and pressure fringes and sheath fold gauges giving strain ratios as high as 36.0–51.0. Thrusts within the Southern Margin Zone have similar strain ratios of 13.0–30.0, and within the Southern Foreland; the Rehoboth Thrust Zone has strain ratios up to 13.0, Areb Mylonite Zone ranges 12.0–22.0, and basal thrust of the Naukluft Nappes range 9.0–16.0.

4.4.2.3. D3sz main phase N over S folding. Penetrative main foliations were folded around sub-horizontal axes, at all scales from crenulations to basement-cored nappes, during ongoing N–S convergence. These second-generation D3sz folds are typically asymmetric over-turned folds ranging from tight to close, and invariably verge southward (Fig. 15c). Progressive deformation strongly transposed units in the Southern and Southern Margin Zones and folding of the main foliation is generally uncommon. Inter-limb angles vary systematically across the southern margin; from 60°–90° to 20°–40° across the Okahandja Zone, 10°–30° in the Southern Zone, 10°–40° in the north Southern Margin Zone and increasing to 50°–80° into the Southern Foreland. Main phase folds develop spaced, axial planar crenulation cleavages, which progress to spaced mica schistosity and sheared out limbs in the Southern Margin Zone. Reverse shearbands indicating N over S transport are very common and associated with the axial planar cleavage.

4.4.3. Peak Damaran events (D4sz–D5sz)

Deformation near the thermal peak of metamorphism produced relatively low-strain minor D4sz folds and crenulations with ongoing N-S convergence. Peak metamorphic parageneses are indicated by the growth of post-kinematic idioblastic garnet, staurolite and biotite porphyroblasts across the main foliation in all parts of the southern margin (Fig. 15d). Blocky biotite porphyroblasts are weakly aligned and define bi-modal lineations plunging both N–NNW and E–ENE. These peak metamorphic mineral lineation directions are correlated with two crenulation events. Peak metamorphic folds are asymmetric with N–NW over S–SE vergence, and develop shallow dipping axial planar biotite differentiation cleavages with sub-horizontal lineations. Flanking folds developed on rotated quartz veins also indicate NW over SE, dextral-reverse shear. Biotite growth within crenulations is moderately well aligned, medium- to coarse-grained and interpreted to have formed near the peak of metamorphism. Multiple biotite differentiation crenulations developed and steeper generations are typically earliest formed. Youngest generation (D5sz) is a fine biotite differentiation crenulation with down-dip lineations, W over E vergence and post-date most porphyroblast growth.

Average peak metamorphic conditions from north to south across the southern margin are: 648 °C/7.2 kbar in the south Okahandja Zone, 628 °C/7.9 kbar in the north Southern Zone, 601 °C/7.9 kbar in the south Southern Zone and 568 °C and 9.4 kbar in the Southern Margin Zone (Goscombe et al., 2017a). All panels experienced medium-T/high-P thermal regimes ranging 17–26 °C/km and steep clockwise P-T paths with isothermal decompression, indicating deep burial, crustal over-thickening giving rapid isostatic response and decompression (Goscombe et al., 2017a). Thermal maxima and growth of peak metamorphic mineral parageneses are diachronous across the southern margin, younging southward towards the foreland. U-Pb age determinations from monazite in matrix assemblages constrain peak metamorphism to 522 ± 6 Ma in the south Okahandja Zone, 529 ± 5 Ma to 524 ± 9 Ma in the Southern Zone and 517 ± 4 Ma in the Southern Margin Zone (Goscombe et al., 2017a; Table 2). Peak metamorphism in the foreland is constrained to >510 ± 9 Ma, on the basis of the oldest Ar-Ar muscovite cooling age (Gray et al., 2006). Post-kinematic granites in the southern margin have ages of 513 ± 17 Ma and 514 ± 6 Ma (Table 2; Allsopp et al., 1979), and offer a minimum age constraint for peak metamorphism.

4.4.4. Extensional telescoping events (D6sz–D8sz)

The southern margin is over-printed by broad zones containing a characteristic suite of extensional top down to the north structures formed during exhumation (Fig. 14). Main phase foliations and peak metamorphic parageneses are over-printed by various extensional structures progressing from ductile to brittle, all formed in vertical flattening stress fields. These zones overlap with metamorphic discontinuities at; mid-Okahandja Zone, central Southern Zone near the Matchless Belt and centred on the Uis-Pass Suture, and are otherwise absent from elsewhere in the Damara Belt. Large pressure differences across these metamorphic discontinuities indicate lateral exhumation of crustal wedges, with sequential foreland propagation of out-wedging resulting in extensional telescoping of the southern margin while still under contraction (Fig. 16; Goscombe et al., 2017a). In all parts of the southern margin, peak metamorphism was attained at maximum pressure conditions and terminated by isothermal decompression. Consequently, peak metamorphic age determinations (Table 2) constrain maximum age for initiation of exhumation and development of structures formed under vertical principle compressive stress. Exhumation of the south Okahandja-Southern Zone crustal wedge was initiated after ~522 Ma, and before ~513 Ma post-kinematic granites. Extensional reactivation of the Uis-Pass Suture and exhumation of the Southern Margin Zone was initiated after ~517 Ma. Ar-Ar cooling ages of 510 ± 9 Ma in muscovite and 505 ± 4 Ma in hornblende indicate exhumation was well under way by this time (Gray et al., 2006).

4.4.4.1. D6sz vertical flattening folds. D6sz is a distinct episode of mesoscopic folds and crenulations with shallow north-dipping axial surfaces and top down to the NW to NE vergence, indicating vertical flattening and normal transport (Fig. 14). These folds develop axial planar crenulation cleavages, alignment of fine-grained biotite and spaced biotite differentiation crenulations without formation of a continuous schistosity (Fig. 15e). Vergence varies from top down to the N–NW in the Okahandja and north Southern Zones to top down to the N–NE in the southern zones. Vergence contrasts with all earlier deformations, which show N over S vergence associated with convergence. Flattening folds are most common immediately north of the Uis-Pass Suture, and progressive flattening produces pervasive crenulation development in short-limbs and extensional shearbands in long-limbs. Folds are typically asymmetric, tight to open with inter-limb

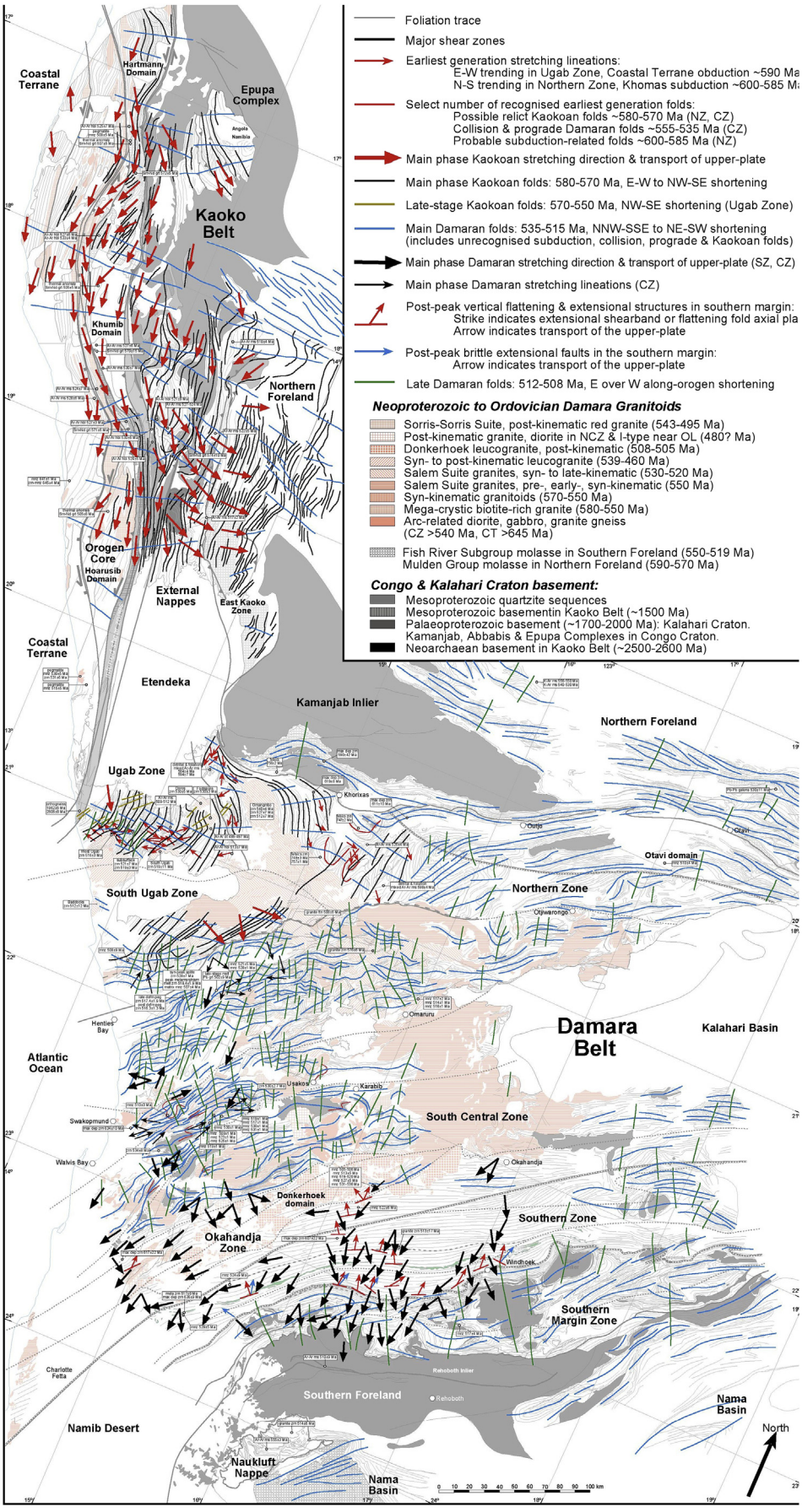
Foliation trace
Major shear zones
Earliest generation stretching lineations:
E-W trending in Ugab Zone, Coastal Terrane obduction ~590 Ma
N-S trending in Northern Zone, Khomas subduction ~600-585 Ma
Select number of recognised earliest generation folds:
Possible relict Kaokoan folds ~580-570 Ma (NZ, CZ)
Collision & prograde Damaran folds ~555-535 Ma (CZ)
Probable subduction-related folds ~600-585 Ma (NZ)
Main phase Kaokoan stretching direction & transport of upper-plate
Main phase Kaokoan folds: 580-570 Ma, E-W to NW-SE shortening
Late-stage Kaokoan folds: 570-550 Ma, NW-SE shortening (Ugab Zone)
Main Damaran folds: 535-515 Ma, NNW-SSE to NE-SW shortening
(includes unrecognised subduction, collision, prograde & Kaokoan folds)
Main phase Damaran stretching direction & transport of upper-plate (SZ, CZ)
Main phase Damaran stretching lineations (CZ)
Post-peak vertical flattening & extensional structures in southern margin:
Strike indicates extensional shearband or flattening fold axial pla
Arrow indicates transport of the upper-plate
Post-peak brittle extensional faults in the southern margin:
Arrow indicates transport of the upper-plate
Late Damaran folds: 512-508 Ma, E over W along-orogen shortening
Neoproterozoic to Ordovician Damara Granitoids
Sorris-Sorris Suite, post-kinematic red granite (543-495 Ma)
Post-kinematic granite, diorite in NCZ & I-type near OL (480? Ma)
Donkerhoek leucogranite, post-kinematic (508-505 Ma)
Syn- to post-kinematic leucogranite (539-460 Ma)
Salem Suite granites, syn- to late-kinematic (530-520 Ma)
Salem Suite granites, pre-, early-, syn-kinematic (550 Ma)
Syn-kinematic granitoids (570-550 Ma)
Mega-crystic biotite-rich granite (580-550 Ma)
Arc-related diorite, gabbro, granite gneiss
(CZ >540 Ma, CT >645 Ma)
Fish River Subgroup molasse in Southern Foreland (550-519 Ma)
Mulden Group molasse in Northern Foreland (590-570 Ma)
Congo & Kalahari Craton basement:
Mesoproterozoic quartzite sequences
Mesoproterozoic basementin Kaoko Belt (~1500 Ma)
Palaeoproterozoic basement (~1700-2000 Ma): Kalahari Craton.
Kamanjab, Abbabis & Epupa Complexes in Congo Craton.
Neoarchaean basement in Kaoko Belt (~2500-2600 Ma)
Coastal Terrane
Hartmann Domain
Epupa Complex
Kaoko Belt
Khumib Domain
Northern Foreland
Orogen Core
Hoarusib Domain
External Nappes
East Kaoko Zone
Coastal Terrane
Etendeka
Kamanjab Inlier
Northern Foreland
Ugab Zone
Khorixas
Outjo
Otavi domain
South Ugab Zone
Northern Zone
Otjiwarongo
Omaruru
Damara Belt
Kalahari Basin
Henties Bay
Atlantic Ocean
Usakos
Karibib
South Central Zone
Swakopmund
Walvis Bay
Okahandja
Donkerhoek domain
Southern Zone
Okahandja Zone
Windhoek
Southern Margin Zone
Charlotte Fella
Rehoboth Inlier
Southern Foreland
Rehoboth
Nama Basin
Namib Desert
North
Naukluft Nappe
Nama Basin
0 10 20 30 40 50 60 70 80 90 100 km

angles ranging 50°–100°. Axial surfaces are inclined north and dips are consistently shallower than the main foliation, ranging from 70° to 20° across the Okahandja Zone to 10°–60° in the southern zones. Flattening folds in the southern zones also develop as more angular structures ranging from asymmetric kinkbands to chevron folds of 1.5 m wavelength. Axial planar crenulations are variably over-printed by post-kinematic, idioblastic garnet over-growths, indicating that early stages of vertical flattening accompanied the thermal peak of metamorphism. Porphyroblastic biotites show similar relationships and both pre-date and post-date flattening folds and crenulations, and are mostly random indicating relatively low-strain conditions. Where weak alignments are evident, biotite plates are vertical and aligned at high-angles to the flattening fold hinges. Discordant granite sills in the Southern Zone have weak, shallow north-dipping quartz grainshape fabrics that possibly developed during this vertical flattening event.

4.4.4.2. D7sz retrogressive extensional shear zones. D7sz is defined by extensional shearbands (mm-scale), shear zones (cm- to m-scale) and shearband boudinage that overprint the main foliation and all fold episodes including flattening folds (Fig. 15f). Shearband geometries all show top down to the NE to NW shear sense, and formed with vertical principle compressive stress similar to flattening folds. Lower-grade retrogressive foliations include chlorite-muscovite, chlorite-biotite and muscovite-biotite growth. Retrograde shear zones in the Okahandja Zone are chlorite-muscovite schists and ultramylonite, with S-C geometries showing sinistral-normal shear sense, and over-printed by Donkerhoek granite and contact metamorphic muscovite growth. Extensional shearbands have steeper dips than flattening fold axial surfaces, and show decrease in dip southward from 70°–85° to 45°–65° across the Okahandja Zone, increasing from 20°–50° to 50°–80° across the Southern Zone, and 20°–80° in the Uis-Pass Suture and Southern Margin Zone. Larger-scale extensional shear zones with strong schistosity and S-C fabrics are developed in the south; 3–10 cm wide in the south Southern Zone and 30–100 cm wide in the north Southern Margin Zone. At largest scale, the Uis-Pass Suture was reactivated by top down to the NE dextral-normal shear, producing chlorite-muscovite retrogressive schists, and coincides with a major metamorphic discontinuity. Matchless Belt contains a 7 m wide extensional shear zone with retrograde chlorite-actinolite mafic schist with plagioclase aggregate ribbons (Fig. 15g), and transposed quartz veins showing shearband boudinage with top down to the north extensional shear. Bulk strain is high in these extensional shear zones; boudin extension and C-S fabric gauges give strain ratios ranging 9.6–26.5 in the Southern Zone and 7.7–22.0 in reactivated fabrics of the Uis-Pass Suture.

4.4.4.3. D8sz brittle extensional faults. D8sz constitutes the lowest temperature expressions of vertical flattening and extension in the southern margin, characterized by brittle top down to the N to NE dextral-normal faults. These range from discrete fault planes, fracture zones with rotated blocks, zones of brecciation, 0.1–4.5 cm wide pseudotachylite horizons, cm-scale gouge zones and 1–7 m wide laterally continuous major fault zones. All major fault zones contain; pseudotachylite, gouge, brittle fracturing, breccia, intense flattening folds, retrograde foliations, extensional shearbands and extreme boudinage stretching (Fig. 15h). Laterally continuous pseudotachylite horizons have cores of massive glass with angular 0.1–1 mm clasts and margins of laminated glass. Top surfaces are flat and basal contacts are undulating with wedge-shaped apophyses into highly disrupted zones pervaded with random networks of brittle faultlets. All major faults have shallow dips, down-dip slickenlines and discordances showing top down to the N–NE extensional shear sense (Fig. 14). Zones of significant extensional faulting are concentrated in the southern Okahandja Zone, within graphite horizons and Matchless Belt of central Southern Zone and immediately north of the Uis-Pass Suture (Fig. 14). 1–3 m wide graphitic horizons in the Southern Zone partition significant amounts of extensional strain and develop intense, chaotic and scaly foliations with down-dip slickenlines indicating extensional slip. These are pervaded by 1–2 cm wide quartz veining with irregular oxidized surfaces indicating hydraulic fluid pumping of meteoric water down into the extensional fault system. Major fault zones are over-printed by steep, discrete N–S trending conjugate faults with normal displacements indicating vertical σ_1. This late-stage normal faulting is sub-parallel to still active N–S grabens in the Windhoek region and fault lineaments in the landscape (Fig. 14).

4.4.5. Late-stage Damaran events (D9sz)

Main phase N–S convergence and later exhumation was followed by very low-strain brittle deformation features, which are associated with a greater degree of along orogen shortening (D9sz). Developed structures are sinistral-reverse kinkbands, steep planar quartz veins with flanking folds and sigmoidal quartz veins, both indicating sinistral rotation and NE over SW shortening.

5. Discussion and conclusions

5.1. Deformation correlations and stress field switches

Detailed age calibrated deformation histories for the four tectono-metamorphic provinces, are correlated with each other to establish an internally consistent deformation framework for the Damara Orogenic System, excluding the Gariep Belt (Fig. 2). Correlations are made on the basis of principle compressive stress directions, strain regimes, tectonic transports and age constraints shared in common (Figs. 17–19). This simple approach has been surprisingly fruitful because sufficient age data is now available to accurately narrow probable age ranges for most recognised deformation events, resulting in a complete understanding of stress field evolution from ~590 to 500 Ma. These correlations allow the identification of stress field rotation between the different deformation events where progressive, and stress field switches where large and rapid (Fig. 19). Horizontal principle compressive stress rotated clockwise ~180° in total during evolution of the Kaoko Belt starting from ~590 Ma, and ~135° during evolution of the Damara Belt starting from collision at ~555 Ma. Progressive rotation was punctuated by rapid stress switches at ~530–525 Ma, ~508 Ma and ~505–500 Ma. At most stages, changes in the stress field recorded within the Damara Orogenic System, can be rationalized

Figure 17. Distribution of Kaokoan Phase and Damaran Phase deformation effects throughout the whole Damara Orogenic System, based on a synthesis of deformation structures. Deformation structures for the Damara Belt are sourced from Figs. 6, 12 and 14, and Kaoko Belt is sourced from Goscombe et al. (2003a,b) and Goscombe and Gray (2008). Symbology is outlined in the legend and details are outlined in Figs. 6, 12 and 14. In general: main phase kaokoan folds (black), late-Kaokoan folds (gold), main phase Damaran folds (blue) and late-stage along orogen shortening (green). Main phase Kaokoan transport are indicated by thick red arrows and main phase Damaran transport by thick black arrows. Relict early-formed structures formed in different settings in the Ugab, Central and Northern Zones are indicated by thin red lines and arrows. Late-stage extensional and vertical flattening structures in the southern margin are indicated by red (ductile) and blue symbols (brittle). Robust peak metamorphic U-Pb age determinations are annotated (Appendix 1). A select number of U-Pb magmatic age determinations and maximum deposition ages crucial to constraining the deformation and metamorphic history are also indicated (Appendix 1).

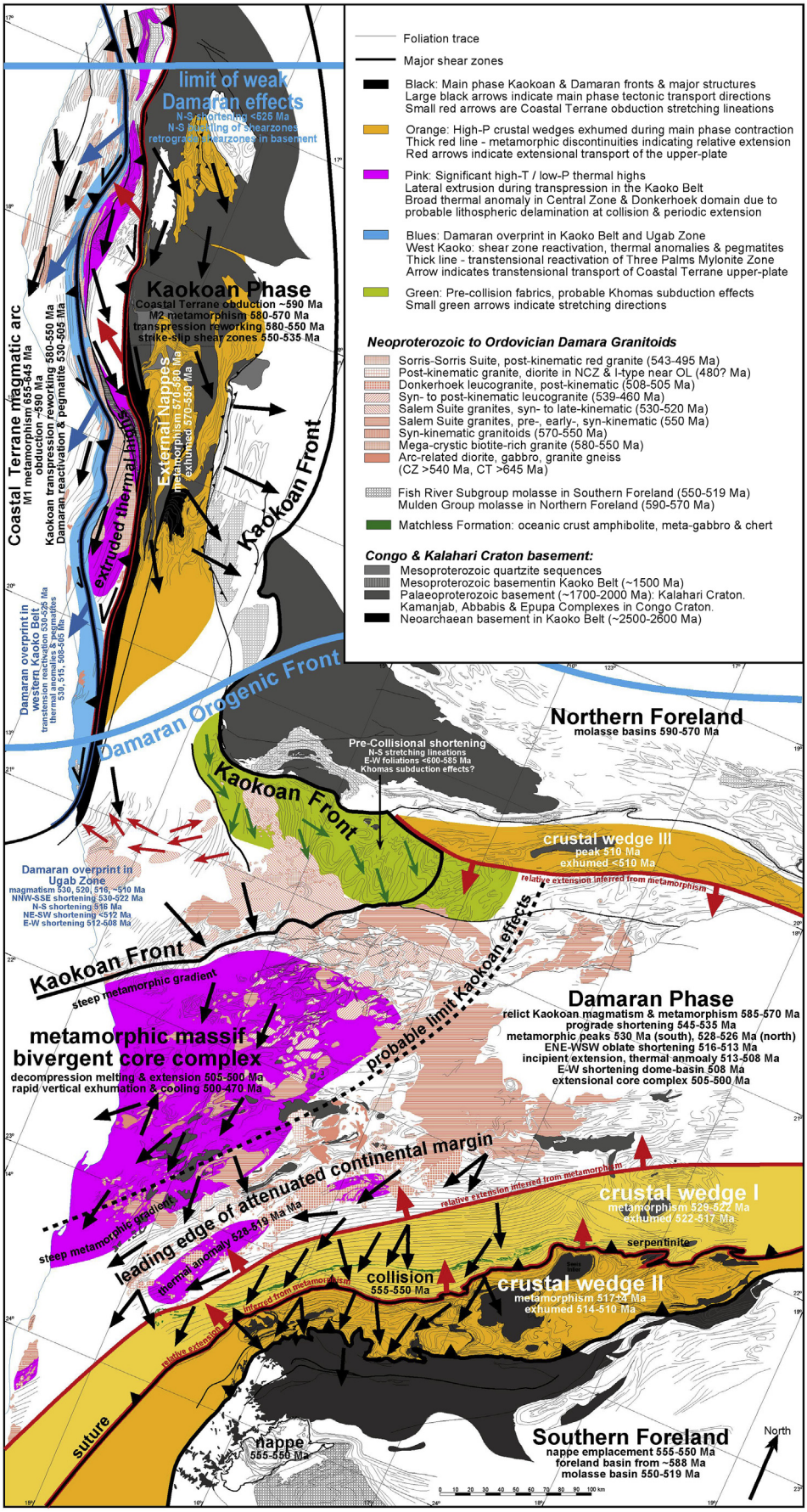

Figure 18. Chrono-spatial interpretation of the orogenic history of the whole Damara Orogenic System, based on the distribution of Kaokoan Phase and Damaran Phase deformation effects (Fig. 16; Goscombe et al., 2003a,b, 2004, 2005a,b; Goscombe and Gray, 2008).

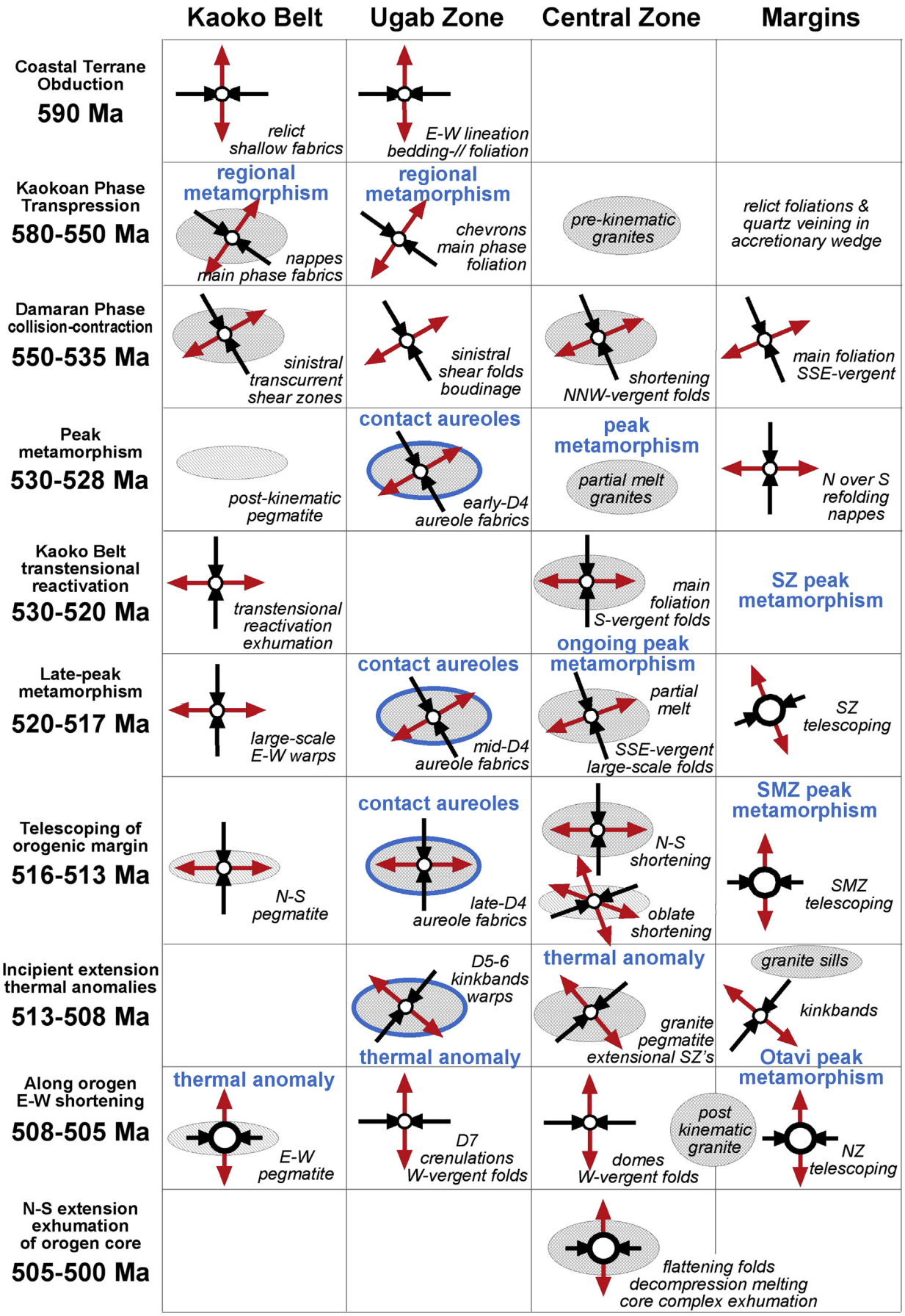

Figure 19. Time-space diagram summarizing stress-field evolution and correlations between different provinces of the Damara Orogenic System (see text). Black arrows or large black circles indicate maximum compressive stress (σ_1) and red arrows indicate maximum extension direction (σ_3). σ_2 is typically sub-vertical throughout the entire orogenic history, except during lateral exhumation of the Barrovian margins and vertical exhumation of the Central Zone core complex. Metamorphic peaks in the different provinces are indicated in blue.

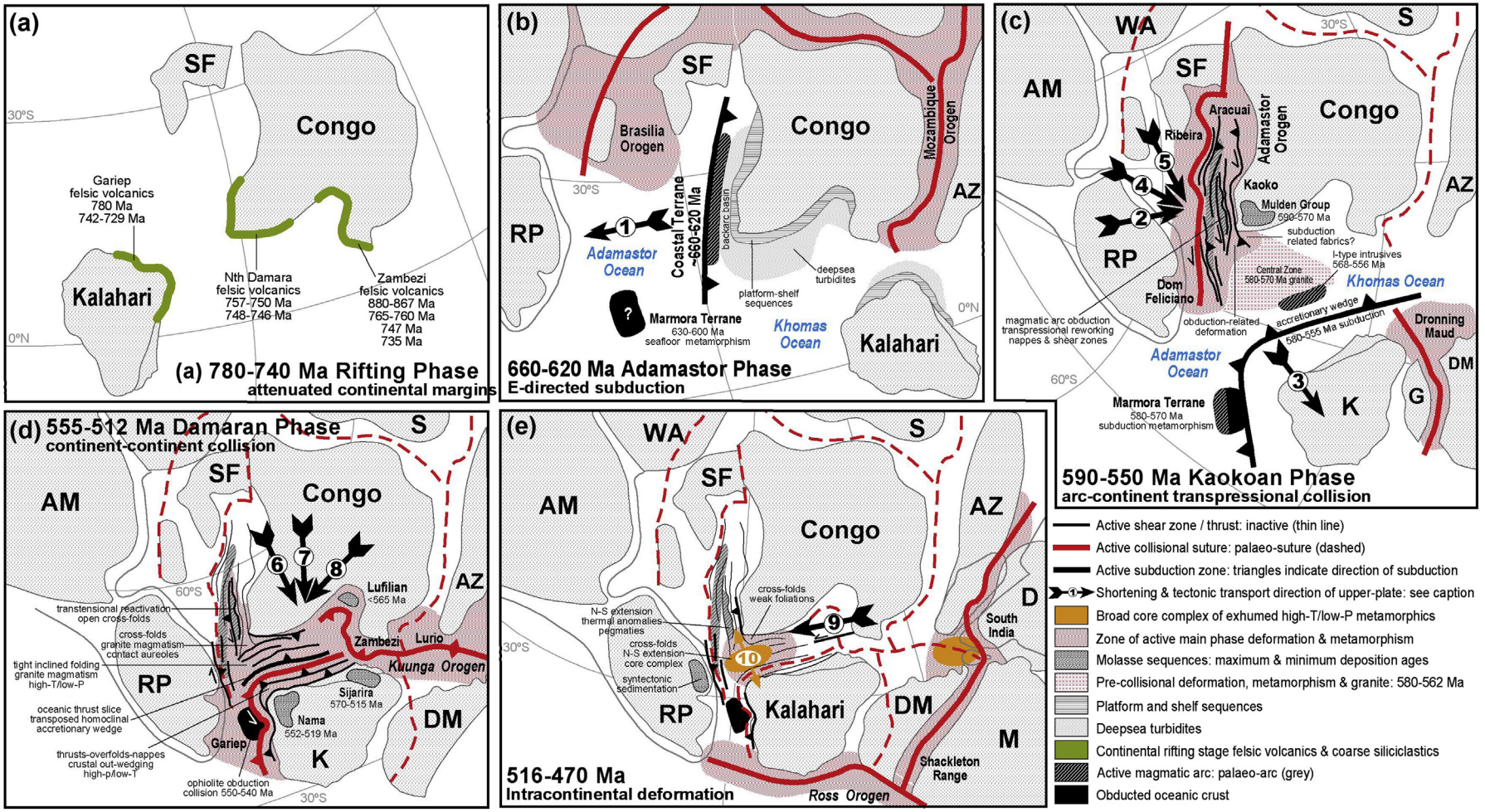

Figure 20. Time sequence reconstruction of continents at key periods in the evolution of the Damara Orogenic System, modified after Gray et al. (2008). All figures arranged relative to affixed Congo Craton in the current orientation with respect to north. (a) Rifting of continental margins stage at ~780–740 Ma. (b) Coastal Terrane magmatic arc stage ~660–620 Ma. (c) Kaoko Belt transpressional collision stage ~590–550 Ma. (d) Damara Belt continent-continent collision stage ~555–512 Ma. (e) Reactivation, exhumation and cooling stage in an intracontinental setting ~516–470 Ma. Deformation episodes during evolution of the Damara Orogenic System are numbered along with the interpreted tectonic transport direction of the upper-plate: (1) East-directed subduction and formation of the Coastal Terrane continental margin magmatic arc ~660–620 Ma. (2) East-directed obduction of the Coastal Terrane ~590 Ma. (3) North-directed subduction in the Khomas Ocean ~600–555 Ma. (4) Main phase transpressional orogenesis in the Kaoko Belt ~580–550 Ma. (5) Progressive strike-slip shear in the Kaoko Belt ~550–535 Ma. (6) Congo-Kalahari collision at the Uis-Pass Suture, NNW–SSE contraction and main phase orogenesis at ~555–520 Ma. (7) N–S contraction across the Damara Belt and outwedging of the Southern Margin between ~ 518 and 516 Ma. (8) NE–SW shortening and out-wedging of the Southern Margin Zone between ~516 and 512 Ma. (9) E–W shortening, cross folding and reactivation of the Damara Belt between ~510 and 508 Ma. (10) N–S extension, vertical shortening and core complex in the high-grade core of the Damara Belt from ~505 to 500 Ma.

by internal causes resulting from evolving interactions between the Rio De La Plata, Congo and Kalahari Cratons (Fig. 20).

5.1.1. Kaokoan phase progressive stress field rotation: 590–550 Ma

5.1.1.1. Obduction and E–W shortening: ~590–580 Ma. The Kaoko Belt, Ugab Zone and west Northern Zone were contiguous from inception of orogenesis. These regions preserve early flat-lying bedding-parallel L–S mylonitic fabrics with mineral aggregate lineations in unfolded original orientations trending E–W. These fabrics are partitioned into the footwall of the Thee Palms Mylonite Zone and are preserved in chert and carbonate bands in many parts of the Ugab Zone. Early boudins trains formed prior to main phase chevron folding in the Ugab Zone are correlated with this event. These structures are interpreted to have formed at the earliest stages of orogenesis during collision and W over E obduction of the Coastal Terrane onto the Congo Craton margin (Goscombe et al., 2003a; Konopásek et al., 2005).

5.1.1.2. Transpression and stress field switch to NW–SE shortening: 580–550 Ma. Main phase S-L foliations and peak metamorphic parageneses in the Kaoko Belt formed under ESE- to SE-directed transport at 580–570 Ma. Progressive sinistral transpression was partitioned into fold and nappe shortening across the belt and oblique-slip in crustal-scale shear zones (Fig. 17; Goscombe et al., 2003a,b; Goscombe and Gray, 2008). Kaokoan sinistral transpressive deformation was more distributed in the shallow crustal Ugab Zone, forming map-scale chevron folding with axial planar schistosity. Second generation folds and boudinage showing sinistral-reverse vergence, occurred in both regions and formed under shortening directions closer to NW–SE, indicating ~45° stress field switch from E–W obduction through main phase transpression (Fig. 17). These fold structures are over-printed by 530 Ma granites in the Ugab Zone, the minimum age limit for sinistral transpression. Main phase transpressional events in the Kaoko Belt are coeval with syn-kinematic granites ranging in age 580–550 Ma, with late-kinematic 550 Ma pegmatites being cross-cut by crustal-scale shears zones that became dominant from this time. Central Zone of the Damara Belt preserves cryptic indications of Kaokoan effects in the hinterland, such as rare granite and metamorphic age determinations ranging 580–570 Ma. Kaokoan fold generations have not been documented in the Central Zone, either because strain was low and structures did not develop, or early structures were obscured by subsequent high-grade metamorphism, deformation and magmatism (Fig. 18).

5.1.2. Pre-Damaran collision stress fields: >555 Ma

Apart from the Ugab Zone, little of the deformation history is preserved in the rock record of the Damara Belt prior to Congo-Kalahari collision at ~555 Ma. It is anticipated that the northern margin and Central Zone experienced deformational strain associated with obduction and transpression in the Kaoko Belt from ~590 Ma, as well as shortening strain associated with subduction and accretion in the Southern Zone accretionary wedge prior to 555 Ma. Central Zone preserves evidence for pre-collisional events in the form of; pre-kinematic granites of 580–570 Ma age (Allsopp et al., 1983; Armstrong et al., 1987; Bergemann et al., 2014; Milani et al., 2014) and rare metamorphic zircon age determinations ranging 585–570 Ma (Armstrong et al., 1987; Newstead, 2010; Foster et al., 2015). These may be indicating a broad dispersed magmatic arc related to subduction of Khomas ocean crust. In the southern margin, earliest formed fine-grained bedding-parallel schistosity and quartz veining, probably started to develop prior to collision at ≥555 Ma in both the Southern Zone accretionary wedge, and also the subducting passive margin sequences of the Southern Margin Zone. Earliest formed fabrics in the northern margin such as in the Goantagab Shear Zone and west Northern Zone, when unfolded, were flat-lying E–W foliations and N–S to NNW–SSE trending stretching lineations (Goscombe et al., 2004; Lehmann et al., 2015; Passchier et al., 2016). These have been correlated with the stress field associated with subduction-accretion in the Southern Zone, and Ar-Ar muscovite ages of 598–584 Ma from early bedding-parallel foliations in the west Northern Zone, are consistent with this interpretation (Lehmann et al., 2015).

5.1.3. Damaran Phase progressive stress field rotation: 555–508 Ma

5.1.3.1. Progressive NW–SE shortening: 550–530 Ma. Transpressional strain in the Kaoko Belt was progressively partitioned into oblique-slip to strike-slip shear zones, and shortening structures such as folds and nappes ceased to operate and were eventually over-printed by the steepening shear zones. This progression reflects rotation of principle compressive stress to lower angles with the grain of the belt and consequent smaller shortening component. Once established, these large-scale shear zones continued to operate and reactivate until ~525 Ma. Predominantly transcurrent slip was established at ~550 Ma, constrained by late-kinematic granites and pegmatites of 559–549 Ma age that over-print regional main phase foliations and are cut by the crust-scale shear zones. Ongoing transcurrent slip continued to at least 539 Ma inter-boudin melt infill, and was terminated before 531–530 Ma cross-cutting pegmatite dykes. This 550–530 Ma period coincides with collision and early orogenesis in the Damara Belt, indicating a Damaran imprint imposed on the Kaoko Belt stress field. Collision between the Congo and Kalahari Cratons is narrowed to 555–550 Ma by earliest deformation ages from low-T phyllonites in the northern and southern forelands (Clauer and Kroner, 1979; Gray et al., 2008) and initiation of molasse in the Nama Basin (Grotzinger et al., 1995; Foster et al., 2015). Prograde orogenesis forming significant topography in the Damara Belt is constrained by detrital metamorphic zircons shed into molasse, earliest metamorphic age determinations and widespread S-type granitoids, all between 546 and 534 Ma (e.g. Jung et al., 2000b; Jung and Mezger, 2003a; Foster et al., 2015). Both Kaoko and Damara Belts shared similar NW–SE shortening directions at this time, and Naukluft Nappe transport was to the SE (e.g. Gray et al., 2008; Longridge et al., 2011, 2014, 2017). Earliest phase of prograde shortening in the southern margin is less well constrained and largely obliterated by penetrative fabric development during N over S transport during later main phase orogenesis. These correlations indicate both Kaoko and Damara orogenic fronts were operating at the same time, and all three cratons were convergent during the 550–530 Ma period; Rio De La Plata SE-directed against the Congo Craton margin, which was SE-directed over the Kalahari Craton margin (Fig. 19).

5.1.3.2. Stress switch to NNW–SSE shortening: 530–525 Ma. Progressive rotation of principle compressive stress to more acute angles with the Kaoko orogenic grain, led to sinistral transtensional reactivation of crustal-scale shear zones in the west Kaoko Belt. Three Palms, Village and Khumib Mylonite Zones were reactivated under NNW–SSE directed shortening, resulting in top down to the SW oblique transport of the Coastal Terrane, transtension and exhumation of the core of the Kaoko Belt. Stress field switch of only ~25° therefore led to a marked change in tectonics in the Kaoko Belt and terminated waning transpressional orogenesis. This stress switch is accurately constrained by post-transpression pegmatites of 531–530 Ma age (Goscombe et al., 2005b), and thermochronology indicating rapid cooling through >600 °C to <300 °C at 533–525 Ma (Foster et al., 2009). From this time, convergence across the Kaoko Belt ceased and the stress field was dominated by convergence across the Damara Belt. Earliest Damaran over-print in

the Ugab Zone was also under NNW–SSE shortening in this same period, forming folds and fabrics in contact aureoles of 530 Ma granites and widespread ENE-trending folds and crenulations (Goscombe et al., 2004). Peak metamorphism, main phase partial melting, early leucogranite sills and main phase folding around ~E–W axes, all occurred between 530 and 518 Ma in the Central and Okahandja Zones (Table 2; Armstrong et al., 1987; Kukla et al., 1991; Jung et al., 2000a,b; Jung and Mezger, 2001, 2003a). Minimum age for the Central Zone thermal peak is constrained by cross cutting syn-kinematic granites of 525–515 Ma age (e.g. Jung et al., 2001; Jung and Mezger, 2003a; Longridge et al., 2014; Paul et al., 2014). Peak Barrovian metamorphism in the southern orogenic margin was attained immediately after main phase N over S folding events, and at 529–522 Ma in common with the high-grade orogen core (Goscombe et al., 2017a). Peak metamorphic conditions were attained at much the same time in most of the Damara Belt, including thermal induced biotite growth in the Ugab Zone that persisted from 530 to 516 Ma. This widespread thermal peak marks the culmination of main phase orogenesis, shortening, crustal thickening and burial in the Damara Belt, and all subsequent thermal and deformation events were superimposed during waning stages of orogenesis.

5.1.3.3. Progressive NNW–SSE shortening: 525–517 Ma. NNW–SSE directed shortening persisted in both the Ugab and Central Zones until at least 517 Ma. ENE-trending fabrics formed in the contact aureoles of ~520 Ma granites of the southwest Ugab Zone (Fig. 10). Peak metamorphic parageneses, melts and structures in the Central Zone experienced second generation re-folding that produced large-scale NNW over SSE inclined folds that form the long axes of basement domes. Main phase foliation development and flattening accompanied this generation of folding and oblate strain regimes generated along-axis extension (Longridge et al., 2017). Folding was approximately coeval with 520–515 Ma pegmatite and granite that overprints peak parageneses (Table 2; Longridge et al., 2017), indicating NNW–SSE shortening coeval with the Ugab Zone. At this time there is no known structural expression in the Kaoko Belt, indicating low strains, with almost all Congo-Kalahari convergence being accommodated within the Damara Belt. In contrast, transports in the southern orogenic margin were large, with out-wedging of the south Okahandja-Southern Zone crustal wedge being initiated at ~522–513 Ma. Out-wedging occurred while the belt was under contraction, by up thrusting to the south, and this rapid exhumation being accommodated by top down to the north shear at the upper boundary, indicated by a metamorphic discontinuity and extensional structures (Fig. 16; Goscombe et al., 2017a). This first stage of out-wedging in the southern margin, further buried the Southern Margin Zone, which then attained peak metamorphism and maximum depths of burial at 517 ± 4 Ma (Goscombe et al., 2017a). Major out-wedging events in the southern margin indicate contraction across the Damara Belt persisted to at least 517 Ma and possibly to ~510 Ma with out-wedging of the Otavi domain in the northern margin.

5.1.3.4. Progressive N–S shortening: 518–515 Ma. Widespread N–S shortening at ~518–515 Ma was experienced in both the Kaoko Belt and all parts of the Damara Belt (Fig. 17). NNE–SSW trending pegmatite dykes of 515 Ma age in the south Coastal Terrane are consistent with N-S shortening and correlated with late-stage kink-bands and large-scale E–W warping of the orogenic grain and shear zones of the Kaoko Belt (Goscombe and Gray, 2008). Folding post-dates transtensional reactivation of these shear zones, constraining E–W warps to younger than 525 Ma. Further south in the Ugab Zone, widespread E–W trending biotite foliations, crenulations and folds are coeval with fabrics and parageneses developed in the contact aureole of the 516 ± 3 Ma West Ugab granite (Fig. 10). E–W foliations and folds are cross cut by younger granites of ~513–511 Ma age, narrowing N-S shortening to between 518 and 513 Ma. Youngest Central Zone deformation associated with the orogenic grain of the belt are E–W trending folds ranging from inclined S over N asymmetric folds in the north to upright tight chevron folding in the Okahandja Zone. These are correlated with the waning stages of syn-kinematic S-type granite magmatism of 516–513 Ma age, and pre-date the post-kinematic Donkerhoek granite of 508–505 Ma age. South-directed upthrusting and out-wedging of the Southern Margin Zone occurred immediately after the peak of metamorphism at 517 ± 4 Ma, which was terminated by isothermal decompression (Goscombe et al., 2017a). Out-wedging was accommodated by extensional reactivation of the Uis-Pass Suture into the brittle field, and indicated by a major metamorphic discontinuity (Goscombe et al., 2017a). Initiation of lateral exhumation of this footwall crustal wedge is constrained to between 517 and 513 Ma, by post-kinematic granites of 514–513 Ma age that probably formed by decompression melting (Goscombe et al., 2017a). This second stage of out-wedging in the southern margin, thus coincides with N–S directed shortening in the waning stages of contraction and probable initiation of extensional events in the Central Zone from ~516 Ma, as discussed in Section 5.1.6 (Table 1).

5.1.3.5. Progressive NE-SW shortening: 512–508 Ma. A final phase of contraction across the Damara Belt is constrained by low-strain, low-grade relationships in the Ugab Zone. Map-scale upright open folds with WNW–ESE to NNW–SSE trends are tightened against pre-existing 516 Ma and 513–511 Ma granite bodies (Fig. 10). Kinkbands formed by NE–SW shortening are developed in low-grade domains distal from granites, and are correlated with this deformation period. Both kinks and open folds are devoid of axial planar foliations and mineral growth, and interpreted to have formed at sub-biotite grades <450 °C. Ar-Ar muscovite closure and regional cooling through 350 °C far from granites, was at 512–508 Ma indicating NE–SW shortening at ~512–508 Ma, consistent with the granite age constraints. These structures bracket the end of contraction across the Damara Belt and indicate progressive clockwise rotation of the stress field through 70° and possibly as much as 90°, from collision at 555 Ma to ~512–508 Ma. No deformation feature of this age is identified in the Kaoko Belt. Barrovian metamorphism in the east Northern Zone occurred at 510 ± 3 Ma (Table 2), with peak conditions terminated by isothermal decompression, indicating rapid exhumation at <510 Ma (Goscombe et al., 2017a). Stress fields in this region are unknown, particularly during this significant exhumation event; though over-lap in age with NE–SW shortening further west in the Ugab Zone.

5.1.4. Transitional events in the orogen core: 516–508 Ma

Coinciding with waning contraction across the Damara Belt, the Okahandja and Central Zones experienced a complex transitional phase between 516 and 508 Ma. Conjugate post-kinematic alkali feldspar dykes in the North Central Zone indicate ENE–WSW directed oblate shortening as early as ~516 Ma (Table 2). These were followed by a widespread thermal anomaly between ~515 and 505 Ma indicated by metamorphic age determinations throughout the Central Zone (Briqueu et al., 1980; Jung et al., 2000b; Jung and Mezger, 2003b; Longridge et al., 2011; Goscombe et al., 2017a). This anomaly was associated with late-kinematic granites between 512 and 507 Ma (Allsopp et al., 1983; Jung et al., 2001; DeKock and Armstrong 2014) and granite veins intruded into extensional shearzones between 511 and 508 Ma (Longridge et al., 2011, 2014). Regional stress fields in the Central

Zone at this time are not confidently known, though a secondary thermal peak accompanying extensional magmatic features and only minor deformation, is indicative of a conductive thermal anomaly, either without stress or accompanying incipient extension localized to the Central Zone.

5.1.5. Stress switch to along orogen E–W shortening: 508 Ma

Waning contraction across the Damara Belt at 512–508 Ma, was followed by rapid stress switch of 45° to E-W directed shortening along the length of the belt between 508 and 505 Ma (Fig. 19). Youngest deformation recognised in the west Ugab Zone are steep asymmetric folds with E over W vergence, and steep N-S trending crenulation cleavages with axial planar biotite growth. These post-date 516 Ma and 513–511 Ma granites, as well as NW–SE trending open folds that formed at sub-biotite grades (Fig. 10). Consequently, renewed biotite growth in these N–S crenulations indicate an increase in west Ugab Zone temperatures to >450 °C following earlier cooling to sub-biotite conditions. Central Ugab Zone cooled below 350 °C at 512–508 Ma, indicating the west Ugab Zone thermal anomaly post-dates regional cooling preserved in cooler parts of the Ugab Zone. Late-stage secondary thermal anomalies accompanying E–W shortening are also recognised in the Kaoko Belt. 508 Ma pegmatite dyke swarms in the Kaoko Belt have trends ranging E–W to ESE–WNW, consistent with an imposed E–W shortening direction. These swarms are associated with a local thermal anomaly of 507–505 Ma age that reset Sm-Nd isotopic systems in garnet (Goscombe et al., 2005b). Late-stage upright cross folds in the Central Zone produced dome-basin fold interference, and have E over W fold vergence in common with the west Ugab Zone. Dome-basin folding in the Central Zone post-dates 511–508 Ma granite veins and have been constrained to ~508 Ma by Longridge et al. (2011, 2014). Widespread evidence for E–W directed shortening along the Damara Belt at ~508 Ma, is significant because it indicates essentially instantaneous re-arrangement of the stress field by ~45°. Such a rapid stress switch implies an internal cause is unlikely and far-field effects at the margin of Gondwana most probable, such as arc collision in the Tasman-Ross Orogen (Foster et al., 2005). Furthermore, along orogen shortening also implies termination of convergence across the Damara Belt, and that the Congo and Kalahari Cratons were welded together and underwent renewed convergence against the Rio De La Plata.

5.1.6. Stress switch to vertical flattening and orogen collapse: 505–500 Ma

Along orogen shortening of the Damara Belt between 508 and 505 Ma, was followed by ~505 Ma switch from horizontal to vertical principle compressive stress, while still under N–S extension (Fig. 19). This stress switch was restricted to the Central Zone where vertical flattening and N–S extension led to rapid vertical exhumation as a broad bivergent metamorphic core complex (Fig. 18; Goscombe et al., 2017a). Vertical flattening evolved from ductile sub-horizontal flattening folds to shallow north-dipping brittle crush zones with top down to the north transport. Core complex exhumation is evident in the metamorphic record, with differential exhumation of 3.5–7.7 km relative to the Ugab Zone to the north, and 2.8–4.6 km relative to the Okahandja Zone in the south (Goscombe et al., 2017a). Initiation of decompression is bracketed by youngest late-kinematic granite and granulite facies parageneses ranging 512–507 Ma (Jung et al., 1998, 2000a,b; Longridge et al., 2011, 2014; Goscombe et al., 2017a), and oldest decompression melts in the footwall of 502 ± 9 Ma age (Jung and Mezger, 2003a). Immediately pre-dating exhumation, leucogranite and pegmatite possibly associated with incipient N–S extension occur between 516 and 508 Ma in the Central Zone (Table 2; Allsopp et al., 1983; Jung et al., 2001; Longridge et al., 2011, 2014), and 508–504 Ma in the Kaoko Belt, Ugab Zone and Okahandja Zone (Kukla et al., 1991; Goscombe et al., 2005b; DeKock and Armstrong, 2014). Rapid exhumation and cooling of the Central Zone from high-grade conditions followed the 505 Ma stress switch. Thermochronometers spanning monazite closure at ~700 °C to biotite closure at ~300 °C, give cooling ages ranging 500–470 Ma and defining an average cooling rate of ~11 °C/Ma (Hawkesworth et al., 1983; Jacob et al., 2000; Jung et al., 2000a,b; Jung and Mezger, 2003a; Singletary et al., 2003; Foster unpublished data). Elsewhere, slower cooling through 350–300 °C occurred between 499 and 481 Ma in all other parts of the Kaoko and Damara Belts. The stress switch to E–W shortening at 508 Ma, followed by vertical flattening and exhumation of the hot orogen core from ~505 Ma, are most plausibly causally connected. Sudden switch to E–W directed shortening is interpreted as a far-field effect imposed on the Damara Orogenic System. This imposed stress field established a N–S extension direction exploited by decompression melts, and is interpreted to have triggered gravitational collapse and extension of the thermally weakened hot orogen core between 505 and 500 Ma, producing the broad Central Zone core complex.

5.2. Implications for Gondwana assembly

The structural style and sequence of deformation that results from this study and the summary of previous work has important implications for the tectonic cycle of the Congo and Kalahari cratons from Rodinia rifting to accretion of Gondwana. This is summarized in the section below and shown in Figs. 16, 19 and 20.

5.2.1. Rifted cratonic margins

The Khomas basin was traditionally interpreted as either (1) an intra-continental rift between the Congo and Kalahari cratons with sedimentation on attenuated continental lithosphere (Kroner, 1977; Porada, 1979, 1983, 1989; Hawkesworth et al., 1983; Hanson et al., 1998; Hanson, 2003), or (2) a small ocean basin with minor spreading at ~700 Ma, formed after intra-continental rifting between the Congo and Kalahari cratons (e.g. Barnes and Sawyer, 1980; Miller, 1983; Kasch, 1983; DeKock, 1992). Neoproterozoic rifting of once contiguous Congo and Kalahari cratons was inferred from the basis of rift-related volcanism on both margins that was thought to be the same age. It is now known that Neoproterozoic bimodal volcanic rocks on the margins of Congo and Kalahari are not the same age (Gray et al., 2008; Appendix 1), which implies that these cratons rifted from different parts of Rodinia (Foster et al., 2015).

Like many fragments of Rodinia, continental breakup and formation of passive margins was under way by ~750 Ma on both Kalahari and Congo cratonic margins (Fig. 20; Frimmel et al., 1996; Hoffman et al., 1996). Rift related mafic-felsic volcanism on the Congo Craton margin occurred at: 880–876, 867, 765–760 and 747–735 Ma in the Lufilian-Zambezi Belt (Key et al., 2001; Master et al., 2005; Johnson et al., 2005, 2007; Goscombe et al., 2017a,c) and ~840–805, 764, 759–756, 757–752, 750, 748–746, ~714–705 Ma in the Kaoko and Damara Belts (Hoffmann, 1994; Hoffman et al., 1996; DeKock et al., 2000; Halverson et al., 2002; Konopásek et al., 2007; DeKock and Armstrong, 2014; Nascimento et al., 2016). Rift volcanism on the northern Kalahari margin was more continuous and includes episodes not recorded in Congo: 870–869, 858–849, 808–804, 797–794, 764 and 750–737 Ma in the Lufilian-Zambezi Belt (Dirks et al., 1998, 1999; Hanson et al., 1998; Vinyu et al., 1999) and 820, 780 and 742–729 Ma in the Damara Belt (Frimmel et al., 1996; Kampunzu et al., 2000; Gray et al., 2008). εNd values of metapelites and detrital zircon populations from meta-psammites of the Damara Supergroup show distinctly different provenance for the sequences deposited on Congo and

Kalahari margins. Sequences north of the Uis-Pass suture have ε_{Nd} values of pelites that ranges from −3.0 to −5.0 and sandstones with detrital zircons with Congo provenance, whereas those in the Southern Margin Zone have ε_{Nd} of −8.0 and detrital zircons with Kalahari provenance (Foster et al., 2015). Overall the Neoproterozoic sequences show no evidence for a direct connection between the Congo, Kalahari and Rio De La Plata Cratons prior to the Cambrian, which indicates that they must have been separated by wide ocean basins consistent with existing palaeomagnetic data (Kröner and Cordani, 2003; Meert, 2003; Meert and Torsvik, 2003; Pesonen et al., 2003; Tohver et al., 2006; Gray et al., 2008). Intra-continental rifting models lacks a plausible mechanism for contraction in the absence of subduction slab pull, and require far-field collision on the margin of Gondwana as early as 555 Ma.

5.2.2. Khomas Ocean setting

Sedimentation within the Adamastor and Khomas Ocean basins continued until ~580 Ma when the passive margin sequence was terminated by arc-collision in the Kaoko Belt (Miller, 1983; Hoffman et al., 1994, 1998; Prave, 1996; Hoffmann et al., 2004; Foster et al., 2015). Prior to 580 Ma deposition in the northern Khomas ocean basin occurred on highly attenuated Congo Craton crust, whereas south (present coordinated) of the continental leading edge at the Okahandja Zone, deposition occurred in thick turbidite fans shed into an deep ocean basin (now exposed in the Southern Zone) (Martin and Porada, 1977; Barnes and Sawyer, 1980; Kasch, 1983; Miller, 1983; Hoffmann, 1989; Kukla et al., 1991; Kukla and Stanistreet, 1991; DeKock 1992; Gray et al., 2006, 2008; Foster et al., 2015). The Southern Zone sequence contains the MORB-affinity rocks of the fault-bounded Matchless Suite, with sheared tholeiitic gabbro, pillow basalt, serpentinite and meta-chert-Cu/Zn mineralization association, which is interpreted as inter-thrust relict oceanic lithosphere (Barnes, 1983; Schmidt and Wedepohl, 1983; Killick, 2000; Foster and Goscombe, 2013). Rocks in the Southern Zone are exposed as a homoclinal, intensely transposed wedge of deep marine turbidites with Congo Craton and Coastal Terrane provenance, entirely consistent with formation as an accretionary prism (Kukla and Stanistreet, 1991; Gray et al., 2006, 2008; Foster et al., 2015). Uis-Pass Suture between the Southern and Southern Margin Zones is a crustal-scale shear zone containing sheared Alpine serpentinites accreted during continent-continent collision (Barnes, 1983; Kasch, 1983), and marks the suture between Kalahari and Congo sequences (Foster and Goscombe, 2013; Foster et al., 2015). Closure of the Khomas Ocean did not produce a voluminous Andean-type magmatic arc with margin-parallel linear batholiths (Barnes and Sawyer, 1980; Kasch, 1983; Miller, 1983; DeKock, 1992). However, I-type granitoids with magmatic arc affinities of 568–556 Ma age, and pre-collisional granites and metamorphic ages ranging ~570–580 Ma in the Central Zone (Barnes and Sawyer, 1980; Hawkesworth et al., 1981; Haack et al., 1982; Kasch, 1983; McDermott et al., 1996; Maloof, 2000; Jung et al., 2001), are consistent with subduction of Khomas Ocean lithosphere beneath attenuated Congo Craton if the evolved isotopic signatures are interpreted as being the result of mixing (contamination) between juvenile and evolved sources (Gray et al., 2008; Foster and Goscombe, 2013). High-P/low-T blueschist-eclogite subduction parageneses commonly associated with subduction of oceanic lithosphere are not preserved in the Damara Belt. This is typical of collisional orogenic belts because these assemblages need to be accreted into the hanging wall, and are typically recrystallized and obliterated during collisional orogenesis and metamorphism (Yardley, 1982; Mortimer, 2000). Along strike the Lufilian-Zambezi Belt contains ~575 Ma, MORB-type eclogite and whiteschist buried to 90 km depth during subduction, inferring a closed ocean basin (John et al., 2003, 2004; Goscombe et al., 2017c).

5.2.3. North Adamastor Ocean

Closure of the North Adamastor Ocean occurred when the Coastal Terrane magmatic arc was obducted onto the Congo Craton margin at ~590–580 Ma (Goscombe et al., 2005b; Goscombe and Gray, 2007) (Fig. 20). Prior to closure the Coastal Terrane formed as a 661–620 Ma calc-alkaline magmatic arc intercalated with juvenile meta-arenites with maximum deposition ages of 674 Ma (Seth et al., 1998; Kröner et al., 2004; Masberg et al., 2005; Goscombe et al., 2005b; Goscombe and Gray, 2007; Foster et al., 2015). The lithostratigraphy, provenance, magmatism and metamorphism in the Coastal Terrane are different from deep basin turbidite and slope facies deposited on Congo Craton passive margin that form the remainder of the Kaoko Belt (Goscombe et al., 2003b, 2005a,b; Goscombe and Gray, 2007). Coastal Terrane magmatism developed above an outboard east-directed subduction zone, with the Kaoko Belt occupying a back-arc position floored by thinned continental crust (Fig. 20; Basei et al., 2000, 2005; Goscombe et al., 2005a,b; Goscombe and Gray, 2007, 2008). Magmatic arcs of similar 680–580 Ma age are strung along the core of West Gondwana Orogen (Fig. 20; Trompette and Carozzi, 1994; Trompette, 1997; Basei et al., 2000; Heilbron and Machado, 2003; Saalmann et al., 2005). Like the Kaoko Belt, the arcs on the Rio De La Plata Craton (Basei et al., 2000), and those in the Dom Feliciano Belt and Aracaui Orogen formed above an east-directed subduction zone (Pedrosa-Soares et al., 1998, 2001; Basei et al., 2000).

The West Gondwana Orogen formed when the Northern Adamastor Ocean closed by a highly oblique convergence followed by transpression. Different sectors of the orogen between the Rio De La Plata-Sao Francisco and Congo Cratons share similar histories of deformation including strain that was progressively partitioned into steep crustal-scale transcurrent shear zones that remained active to ~530 Ma (Pedrosa-Soares et al., 1998, 2001; Brueckner et al., 2000; Schmitt et al., 2004; Heilbron et al., 2004; Basei et al., 2005; Goscombe et al., 2005b; Goscombe and Gray, 2008; Foster et al., 2009). The resulting crustal architecture of the West Gondwana Orogen has a symmetric bivergent form, dominated by crustal-scale shear zones of opposing listric inclination, dipping east in South America and west in Africa (Trompette and Carozzi, 1994; Trompette, 1997; Basei et al., 2005; Goscombe and Gray, 2007). Oblique collision and transpressional orogenesis occurred at much the same time in the Dom Feliciano and Ribeira Belts flanking the Rio de la Plata Craton and Kaoko Belt flanking the Congo Craton (Frantz and Botelho, 2000; Heilbron and Machado, 2003; Heilbron et al., 2004; Goscombe et al., 2005b). Along both continents closure propagated southward in concert with the younging direction of magmatic arcs (Stanistreet et al., 1991; Gresse and Germs 1993; Germs 1995; Frimmel and Frank 1998; Maloof, 2000; Gray et al., 2008). For example, on the Congo craton side, obduction of the Coastal Terrane was initially E-directed along a shallow W-dipping Three Palms Mylonite Zone, and progressed to ESE- and SE-directed transport as sinistral transpression progressed (Goscombe et al., 2003a, 2005b; Goscombe and Gray, 2008; Gray et al., 2008; Foster et al., 2015). Oblique collision of the Rio Negro arc in the Ribeira Orogen was at ~595–590 Ma and dextral transpressional orogenesis progressed to steep transcurrent shear zones between 590 and 560 Ma (Machado et al., 1996; Heilbron and Machado, 2003; Heilbron et al., 2004). Collision in the Dom Felicianao Belt was at ~580 Ma (Basei et al., 2000), and both sinistral and dextral transcurrent shear zones developed (Basei et al., 2000; Frantz and Botelho, 2000; Saalmann et al., 2005).

5.2.4. South Adamastor Ocean

Magmatic arcs are absent from southern Adamastor Ocean, but oceanic lithosphere of the Marmora Terrane was obducted obliquely onto the Kalahari Craton margin in the Gariep Belt at 550 and 540 Ma (Frimmel, 1995; Frimmel and Frank, 1998), and eroded into the Nama

Basin by 540 Ma (Gresse and Germs, 1993; Gresse, 1995; Frimmel, 2000). Ensimatic, subduction-related origin of the Marmora Terrane is indicated by deep-sea turbidites, meta-volcanics and mélange containing mafic and ultramafic blocks with near blueschist facies parageneses (Frimmel and Hartnady, 1992; Frimmel, 2000). Detrital zircon populations are similar in Dom Feliciano and Gariep Belt strata, indicating that they formed within the same ocean basin (Basei et al., 2005). Consequently, this basin was closed by W-directed subduction beneath the Rio De La Plata Craton followed by obduction of the Marmora terrane along west-dipping decollements (Frimmel et al., 1996). Tectonic transport and the age of collision in the Gariep Belt is identical to closure of the Khomas Ocean at the Uis-Pass Suture in the Damara Belt, as recorded by SE-directed transport of the Naukluft Nappe Complex onto the foreland at ~555 Ma (Gray et al., 2006). Collision at this time on both the northern and western margins of Kalahari (present coordinates) is confirmed by maximum deposition age of ~552 Ma for Fish River Subgroup molasse in the Nama Basin (Grotzinger et al., 1995; Foster et al., 2015). This establishes a continuous, arcuate NW-directed subduction system that closed the southern Adamastor and Khomas Oceans at the same time, and the resultant Gariep-Damara Belt constitutes the western-most sector of the greater Kuunga Orogen (Fig. 20; Meert, 2003). The belts developed after the earlier collision and amalgamation of the Congo and Rio De La Plata Cratons that is defined by main phase orogenesis, metamorphism and magmatism in the Kaoko Belt between 580 and 550 Ma and summarized above (Seth et al., 1998; Franz et al., 1999; Kröner et al., 2004; Goscombe et al., 2005b). After Congo-Kalahari collision all parts of the Damara Orogenic System shared the same deformation history, with maximum compressive stress direction varying systematically from NW–SE at 555 Ma to E–W at ~508 Ma. Palaeomagnetic poles also indicate all components of West Gondwana had amalgamated by 550 Ma and shared a single apparent polar wander path (Rapalini, 2006; Tohver et al., 2006).

5.2.5. Damaran collisional orogenic cycle

Closure of the Khomas Ocean was complete by 555–550 Ma; culmination of orogenesis and peak metamorphism was between 530 and 520 Ma in the Damara and Lufilian-Zambezi Belts, 530–510 Ma in the Ribeira Belt and similar timing along the length of Kuunga Orogen (Goscombe et al., 1998; Meert, 2003; John et al., 2003, 2004; Schmitt et al., 2004; Boger and Miller, 2004; Gray et al., 2008). Collisional orogenesis in the Kuunga Orogen was responsible for stitching north and south Gondwana in the final phase of Gondwana assembly. Subsequent events in the Damara Orogenic System therefore occurred in an intra-plate setting driven by orogenesis on the margins of Gondwana. Subduction under the margins of Gondwana began at ~560 Ma off Antarctica, and was established by ~530 Ma in Australia and South America, producing major accretionary orogens. Major arc collisions and magmatism in the Ross-Delamerian Orogen took place by 520–510 Ma, followed by extension along the margins of Gondwana and within older mobile belts (e.g., Goodge et al., 1993; Goodge, 1997; Meert, 2003; Boger and Miller, 2004; Foster et al., 2005; Foden et al., 2006), significantly effecting late-stage evolution of the Damara Orogenic System.

Contraction, crustal thickening and prograde metamorphism in the Damara Belt between 555 and 530 Ma accompanied NW-directed trajectory of convergence of the Kalahari Craton into the already contiguous Congo-Rio De La Plata Cratons (Fig. 20). The Kaoko Belt and Damara Belt both underwent NW–SE shortening at this time; expressed as waning transpression in Kaoko Belt and high-angle collisional orogenesis in the Damara Belt (Gray et al., 2008). This event produced the earliest structures in the Damara Belt, which were NW-vergent in the Central Zone (Kisters et al., 2004; Longridge et al., 2011, 2014, 2017) and SE-vergent in the southern margin (Section 4.4.2). Crustal thickening and burial resulted in significant topography development and molasse shed into the Nama Basin at this time (Gresse and Germs, 1993; Gresse, 1995; Foster et al., 2015).

A tectonic switch occurred at 530–520 Ma in response to change in Kalahari Craton trajectory to NNW-directed transport, giving higher-angle convergence in the Damara Belt (Section 5.1.3.2). Culmination of main phase orogenesis, crustal thickening, partial melting and peak metamorphism coincides with this period (Armstrong et al., 1987; Kukla et al., 1991; Jung et al., 2000a,b; Jung and Mezger 2001, 2003a; Jung et al., 2001; Longridge et al., 2014; Paul et al., 2014). Prolonged high heat flow in the orogen core was likely the result of anomalously high radiogenic heat production (Haack et al., 1983; Ballard et al., 1987), thinned lithospheric architecture of the Congo Craton passive margin (Ritter et al., 2003) and asthenospheric upwelling in response to break off of subducted Khomas Ocean lithosphere or Kalahari lithosphere and eclogized lower crust after collision (Goscombe et al., 2017a; Longridge et al., 2017). These initial conditions established at ~550 Ma generated high-heat flow from the mantle, resulting in peak metamorphism in the mid-crust after a conductive delay of ~25 Ma (e.g. Houseman and Molnar, 1997). Peak metamorphism at lower temperatures but higher pressures in the southern orogenic margin was attained at the same time, under relatively low-strain conditions immediately after main phase folding, penetrative foliations and burial (Goscombe et al., 2017a). Rearrangement of the stress field at this time must have been accommodated by transcurrent sinistral slip outboard to the west of the Kalahari Craton, and led to a major rearrangement of the Kaoko Belt, terminating transpression, and sinistral-normal reactivation of shear zones resulting in rapid exhumation and cooling (Foster et al., 2009).

Ongoing NNW–SSE shortening persisted to at least 517 Ma, resulting in large-scale SSE-vergent folds that form the long axes of basement domes in the Central Zone. In contrast, the deeply buried (~28–39 km) southern margin was being exhumed at this time by sequential, foreland propagating up-thrusting events that resulted in extensional elongation of the orogen margins (Fig. 16). The waning stages of contraction in the Damara Belt, saw ongoing rotation of the stress field to N–S shortening at ~517–515 Ma and NE–SW shortening at ~512–508 Ma, resulting in total ~90° clockwise variation of the stress field during the Damaran orogenic cycle. Mechanisms leading to variation in convergence trajectory of the Kalahari Craton are unknown. We speculate probable causes were irregular continental margins influencing trajectories as different parts of the Kuunga Orogen closed, and later far field effects from orogens on the margins of Gondwana (Fig. 20). A rapid stress switch of 45° at ~508 Ma, lead to E–W directed shortening along the length of the belt producing widespread cross folds (Fig. 20; Longridge et al., 2014; Sections 4.2.5 and 4.3.4.3). These structures indicate an essentially instantaneous and significant rearrangement of the stress field, inconsistent with any plausible trajectory between Rio De La Plata, Congo and Kalahari Cratons. Consequently, far-field effects at the margin of Gondwana are the probable cause, and over-lap in age with arc collisions in the Ross Orogen (Meert, 2003; Boger and Miller, 2004; Foster et al., 2005). These events drove extensional collapse of the orogen core, leading to another phase of magmatism. It is possible that some of the later changes in stress field were related to body forces within the orogen itself and loss of dense crust and lithosphere below.

Major out-wedging events in the southern margin indicate contraction across the Damara Belt persisted to at least 517 Ma (Section 5.1.3.4). Furthermore, out-wedging in the northern margin at ~510 Ma, E–W shortening along the belt at ~508 Ma and metamorphic chronology showing high-grade conditions persisted to ~505 Ma, all indicate that collapse of the orogen core was ongoing from this time. Gravitational collapse of the thermally

weakened orogen core may have been triggered by along-orogen shortening, which established a N–S extension direction, or by body forces within the orogenic pile. The stress switch from horizontal to vertical principle compressive stress occurred at ~505 Ma and was largely restricted to the Central Zone where vertical flattening and N-S extension led to rapid vertical exhumation as a broad bivergent metamorphic core complex. Coincident shortening via out wedging along the northern margin of the orogen and extension in the core of the orogen in the Central Zone (CZ) could have occurred in a similar way to the modern Himalayan-Tibet system (Dewey, 1988) and Eocene of Canadian Cordillera-northern Rocky Mountains system (Foster et al., 2001).

Acknowledgements

This research was a largely self-funded ITAR project that was also generously supported by ARC grants A00103456 and DP0210178 to Prof. David Gray and NSF grants EAR0440188 and EAR0738874 to Prof. David Foster, making the large-scale mapping programs possible. Namibian Geological Survey contributed towards fieldwork while BG was on staff 1997–1999. Richard Armstrong (ANU) contributed time and expertise to collaborate on metamorphic chronology. A detailed review by Prof. Ruben Diez Fernandez significantly improved the manuscript. Peter Weber, Jeanette Steiner, Ben Thompson, Mimi Dunaiski and Mr Blum assisted with vehicles and logistics in Namibia. We acknowledge discussions with Richard Blewett, Karol Czarnota, Martin Hand, Charlie Hoffmann, Paul Hoffman, Cees Passchier, Rudolph Trouw and Galen Halverson on a wide range of geology during this project. Mike and Rida Jacob, Mr Gift, Dorette Knobel, Mark and Norma Jeanne, Miranda and Angus Campbell, Margaret and Roddy MacAskill, Mrs Gunn, Finlay and Rachel McDonald, Ronnie MacPhee and Alex Urquhart are thanked for their kind hospitality at bonnie camps, farms and crofts during analysis and write up.

Appendix A. Supplementary data

Supplementary data related to this article can be found at http://dx.doi.org/10.1016/j.gsf.2017.05.001.

References

Allsopp, H.L., Kostlin, E.O., Welke, H.J., Burger, A.J., Kroner, A., Blignault, H.J., 1979. Rb-Sr and U-Pb geochronology of late Precambrian-early Palaeozoic Igneous Activity in the Richtersveld (South Africa) and southern South West Africa. *Unpublished manuscript lodged at Namibian Geological Survey.*

Allsopp, H.L., Barton, E.S., Kröner, A., Welke, H.J., Burger, A.J., 1983. Emplacement versus inherited isotopic age patterns: a Rb-Sr and U-Pb study of Salem-type granites in the central Damara Belt. In: Miller, R.McG. (Ed.), Evolution of the Damara Orogen, vol. 11. Special Publication of the Geological Society of South Africa, pp. 281–287.

Armstrong, et al., 1987. *Unpublished Australian National University Report.*

Ballard, S., Pollack, H.N., Skinner, N.J., 1987. Terrestrial heat flow in Botswana and Namibia. Journal of Geophysical Research 92, 6291–6300.

Barnes, S.J., Sawyer, E.W., 1980. An alternative model for the Damara Mobile Belt: ocean crust subduction and continental convergence. Precambrian Research 13, 297–336.

Barnes, S.J., 1983. Pan-African serpentinites in central south West Africa/Namibia and the chemical classification of serpentinites. Special Publication of the Geological Society of South Africa 11, 147–155.

Basei, M.A.S., Siga, O., Masquelin, H., Harara, O.M., Reis Neto, J.M., Preciozzi, F., 2000. The Dom Feliciano Belt of Brazil and Uruguay and its foreland domain. In: Cordani, U. (Ed.), Tectonic Evolution of South America, pp. 311–334, 31st International Geological Congress, Rio de Janiero, Brazil.

Basei, M.A.S., Frimmel, H.E., Nutman, A.P., Preciozzi, F., Jacob, J., 2005. A connection between the Neoproterozoic Dom Feliciano (Brazil/Uruguay) and Gariep (Namibia/South Africa) orogenic belts – evidence from a reconnaissance provenance study. Precambrian Research 139, 195–221.

Bergemann, C., Jung, S., Berndt, J., Stracke, A., Hauff, F., 2014. Generation of magnesian, high-K alkali-calcic granites and granodiorites from amphibolitic continental crust in the Damara Orogen, Namibia. Lithos 198–199, 217–233.

Blewett, R.S., Czarnota, K., 2007a. A new integrated tectonic framework of the Eastern Goldfields Superterrane. In: Bierlein, F.P., Knox-Robinson, C.M. (Eds.), Proceedings of Geoconferences (WA) Inc. Kalgoorlie 07' Conference. Geoscience Australia Record 2007/14, pp. 27–32.

Blewett, R.S., Czarnota, K., 2007b. The Y1-P763 project final report November 2005. Module 3 Terrane Structure: Tectonostratigraphic architecture and uplift history of the Eastern Yilgarn Craton. Geoscience Australia Record 2007/15.

Blewett, R.S., Czarnota, K., Henson, P.A., 2010. Structural-event framework for the eastern Yilgarn Craton, Western Australia, and its implications for orogenic gold. Precambrian Research 183, 203–229.

Boger, S.D., Miller, J.McL., 2004. Terminal suturing of Gondwana and the onset of the Ross-Delamerian Orogeny: the cause and effect of an Early Cambrian reconfiguration of plate motions. Earth and Planetary Science Letters 219, 35–48.

Briqueu, L., Lancelot, J.P., Valois, J.P., Walgenwitz, F., 1980. Géochronologie UPB et genése d'un type de minéralization uranifere: les alaskites de Goanikontes (Namibie) et leur encaissant. Bulletin des centres de recherches exploration-production Elf-Aquitaine 4, 759–811.

Brueckner, H.K., Cunningham, D., Alkmin, F.F., Marshak, S., 2000. Tectonic implications of Precambrian Sm-Nd dates from the southern São Francisco craton and adjacent Araçuaí and Ribeira belts, Brazil. Precambrian Research 99, 255–269.

Clauer, N., Kroner, A., 1979. Strontium and argon isotopic homogenization of pelitic sediments during low-grade regional metamorphism: the Pan-African Upper Damara Sequence of northern Namibia. Earth and Planetary Science Letters 43, 117–131.

Corner, B., 2000. Crustal framework of Namibia derived from magnetic and gravity data. Communications of the Geological Survey of Namibia 12, 13–19.

Corner, B., 2004. Total Magnetic Intensity Data of Southern Africa, 1:3,000,000 Map. Branko Corner Consulting.

Coward, M.P., 1981. The junction between Pan African Mobile belts in Namibia: its structural history. Tectonophysics 76, 59–73.

Coward, M.P., 1983. The tectonic history of the Damara belt. In: Miller, R.McG. (Ed.), Evolution of the Damara Orogen, vol. 11. Special Publication of the Geological Society of South Africa, pp. 409–421.

Czarnota, K., Champion, D.C., Goscombe, B., Blewett, R.S., Cassidy, K.F., Henson, P.A., Groenewald, P.B., 2010. Geodynamics of the eastern Yilgarn Craton. Precambrian Research 183, 175–202.

DeKock, G.S., 1992. Forearc basin evolution in the Pan-African Damara Belt, central Namibia: the Hureb Formation of the Khomas Zone. Precambrian Research 57, 169–194.

DeKock, G.S., Eglington, B., Armstrong, R.A., Harmer, R.E., Walraven, F., 2000. U-Pb and Pb-Pb ages of the Naauwpoort rhyolite, Kawakeup leptite and Okongava Diorite: implications for the onset of rifting and of orogenesis in the Damara belt, Namibia. Communications of the Geological Survey of Namibia 12, 81–88.

DeKock, G.S., Armstrong, R., 2014. SHRIMP dating on magmatic rocks from the Karabib-Otjimbingwe region, Namibia. In: Roy Miller Symposium, Namibia, 2014.

Dewey, J.F., 1988. Extensional collapse of orogens. Tectonics 7, 1123–1139.

Dingeldey, D.P., Dürr, S.B., Charlesworth, E.G., Franz, L., Okrusch, M., Stanistreet, I.G., 1994. A geotraverse through the northern coastal branch of the Damaran Orogen west of Sesfontein, Namibia. Journal of African Earth Science 19, 315–329.

Dingeldey, P., 1997. Tectono-metamorphic Evolution of the Pan-African Kaoko Belt, NW-Namibia. Ph. D. Thesis. Julius-Maximilians-Universitat Wurzburg, p. 246.

Dirks, P.H.G.M., Jelsma, H.A., Vinyu, M.L., Munyanyiwa, H., 1998. The structural history of the Zambezi belt in N E Zimbabwe: evidence for crustal extension during the early Pan African. South African Journal of Geology 101, 1–16.

Dirks, P.H.G.M., Kroner, A., Jelsma, H.A., Sithole, T.A., Vinyu, M.L., 1999. Pb-Pb zircon dates from the Makuti gneisses: evidence for a crustal-scale Pan African shear zone in the Zambezi Belt, NW Zimbabwe. Journal of African Earth Sciences 28, 427–442.

Dürr, S.B., Dingeldey, D.P., 1996. The Kaoko belt (Namibia): part of a late neoproterozoic continental-scale strike-slip system. Geology 24, 503–506.

Foden, J., Marlina, A.E., Dougherty-Page, J., Burtt, A., 2006. The timing and duration of the Delamarian orogeny: correlation with the Ross orogen and implications for Gondwana assembly. The Journal of Geology 114, 189–210.

Foster, D.A., Schafer, C., Fanning, C.M., Hyndman, D.W., 2001. Relationships between crustal partial melting, plutonism, orogeny, and exhumation: Idaho-Bitterroot batholith. Tectonophysics 342, 313–350.

Foster, D.A., Gray, D.R., Spaggiari, C.V., 2005. Timing of subduction and exhumation along the Cambrian East Gondwana margin, and the formation of Paleozoic backarc basins. Geological Society of America Bulletin 117, 105–116. http://dx.doi.org/10.1130/B25481.1.

Foster, D.A., Goscombe, B.D., Gray, D.R., 2009. Rapid exhumation of deep crust in an obliquely convergent orogen: the Kaoko Belt of the Damara Orogen. Tectonics 28, TC4002.

Foster, D.A., Goscombe, B.D., 2013. Continental growth and recycling in convergent orogens with large turbidite fans on oceanic crust. Geosciences 3, 354–388. http://dx.doi.org/10.3390/geosciences3030354.

Foster, D.A., Goscombe, B.D., Newstead, B., Mapani, B., Mueller, P.A., Gregory, L.C., Muvangua, E., 2015. U-Pb age and Lu-Hf isotopic data of detrital zircons from neoproterozoic Damara Sequence: implications for pre-Gondwana proximity of Congo and Kalahari. Gondwana Research 28, 179–190.

Frantz, J.C., Botelho, N.F., 2000. Neoproterozoic granitic magmatism and evolution of the eastern Dom Feliciano Belt in southernmost Brazil: a tectonic model. Gondwana Research 3, 7–19.

Franz, L., Romer, R.L., Dingeldey, D.P., 1999. Diachronous Pan-African granulite-facies metamorphism (650 Ma and 550 Ma) in the Kaoko belt, NW Namibia. European Journal of Mineralogy 11, 167–180.
Freyer, E.E., Halbich, I.W., 1994. Deformation history of the lower Ugab Belt. In: Niall, M., McManus, C. (Eds.), Proterozoic Crustal and Metallogenic Evolution. Abstracts of Geological Society and Geological Survey of Namibia 18, Windhoek.
Frimmel, H.E., Hartnady, C.J.H., 1992. Blue amphiboles and their significance for the metamorphic history of the Pan-African Gariep belt, Namibia. Journal of Metamorphic Geology 10, 651–669.
Frimmel, H.E., 1995. Metamorphic evolution of the Gariep Belt. South African Tydskr. Geology 98, 176–190.
Frimmel, H.E., Klotzli, U.S., Siegfried, P.R., 1996. New Pb-Pb single zircon age constraints on the timing of neoproterozoic glaciation and continental break-up in Namibia. The Journal of Geology 104, 459–469.
Frimmel, H.E., Frank, W., 1998. Neoproterozoic tectono-thermal evolution of the Gariep Belt and its basement, Namibia and South Africa. Precambrian Research 90, 1–28.
Frimmel, H.E., 2000. The Pan-African Gariep Belt in southwestern Namibia and western South Africa. In: Miller, R.McG. (Ed.), Henno Martin Commemorative Volume, vol. 12. Communications of the Geological Survey of Namibia, pp. 197–209.
Germs, G.J.B., 1995. The Neoproterozoic of southwestern Africa, with emphasis on platform stratigraphy and paleontology. Precambrian Research 73, 137–151.
Goodge, J.W., Hansen, V.L., Walker, N., 1993. Neoproterozoic-Cambrian basement-involved orogenesis within the Antarctic margin of Gondwana. Geology 21, 37–40.
Goodge, J.W., 1997. Latest neoproterozoic basin inversion of the Beardmore Group, central Transantarctic Mountains, Antarctica. Tectonics 16, 682–701. http://dx.doi.org/10.1029/97TC01417.
Goscombe, B.D., Trouw, R., 1998. The geometry of folded tectonic shear sense indicators. Journal of Structural Geology 21, 123–127.
Goscombe, B.D., Armstrong, R., Barton, J.M., 1998. Tectonometamorphic evolution of the Chewore Inliers: partial re-equilibration of high-grade basement during the Pan-African orogeny. Journal of Petrology 39, 1347–1384.
Goscombe, B.D., Passchier, C., 2003. Asymmetric boudins as shear sense indicators an assessment from field data. Journal of Structural Geology 25 (4), 575–589.
Goscombe, B.D., Hand, M., Gray, D., 2003a. Structure of the Kaoko Belt, Namibia: progressive evolution of a classic transpressional orogen. Journal Structural Geology 25, 1049–1081.
Goscombe, B.D., Hand, M., Gray, D., Mawby, J., 2003b. The metamorphic architecture of a transpressional orogen: the Kaoko Belt, Namibia. Journal of Petrology 44, 679–711.
Goscombe, B.D., Gray, D., Hand, M., 2004. Variation in metamorphic style along the northern margin of the Damara Orogen, Namibia. Journal of Petrology 45, 1261–1295.
Goscombe, B.D., Gray, D., Hand, M., 2005a. Extrusional tectonics in the core of a transpressional orogen, the Kaoko Belt, Namibia. Journal of Petrology 46, 1203–1241.
Goscombe, B., Gray, D.R., Armstrong, R.A., Foster, D.A., Vogl, J., 2005b. Event geochronology of the Pan-African Kaoko Belt, Namibia. Precambrian Research 140, e1–41.
Goscombe, B.D., Gray, D., 2007. The Coastal Terrane of the Kaoko Belt, Namibia: outboard arc-terrane and tectonic significance. Precambrian Research 155, 139–158.
Goscombe, B.D., Gray, D., 2008. Structure and strain variation at mid-crustal levels in a transpressional orogen: a review of Kaoko Belt structure and the character of West Gondwana amalgamation. Gondwana Research 13, 45–85.
Goscombe, B., Foster, D.A., Gray, D., Wade, B., 2017a. Metamorphic response and crustal architecture in a classic collisional orogen: The Damara Belt, Namibia. Gondwana Research Focus Paper (in press).
Goscombe, B., Gray, D., Foster, D.A., Wade, B., 2017b. Metamorphic evolution of Gondwana 2. The Damara Orogenic System: amalgamation of central Gondwana and evolution of orogen architecture. Geoscience Australia Record (in press).
Goscombe, B., Gray, D., Foster, D., 2017c. Metamorphic evolution of Gondwana 3. The Pan-African orogenic system: thermo-mechanical response to orogenesis during Gondwana assembly. Geoscience Australia Record (in press).
Gray, D.R., Foster, D.A., Goscombe, B., Passchier, C.W., Trouw, R.A.J., 2006. 40Ar/39Ar thermochronology of the Pan-African Damara Orogen, Namibia, with implications for tectonothermal and geodynamic evolution. Precambrian Research 150, 49–72.
Gray, D.R., Foster, D.A., Maas, R., Spaggiari, C.V., Gregory, R.T., Goscombe, B., Hoffmann, K.H., 2007. Continental growth and recycling by accretion ofdeformed turbidite fans and remnant ocean basins: Examples from Neoproterozoic and Phanerozoic orogens. In: Hatcher Jr, R.D., Carlson, M.P., McBride, J.H., Martínez Catalán, J.R. (Eds.), 4-D Framework of Continental Crust. Geological Society of America Memoir 200, pp. 63–92. http://dx.doi.org/10.1130/2007.1200(05).
Gray, D.R., Foster, D.A., Meert, J.G., Goscombe, B.D., Armstrong, R., Trouw, R.A.J., Passchier, C.W., 2008. A Damara Orogen perspective on the assembly of southwestern Gondwana. Geological Society of London Special Publications 294, 257–278.
Gresse, P.G., Germs, G.J.B., 1993. The Nama foreland basin: sedimentation, major unconformity and bounded sequences and multisided active margin advance. Precambrian Research 63, 247–272.
Grotzinger, J.P., Bowring, S.A., Saylor, B.Z., Kaufman, A.J., 1995. Biostratigraphic and Geochronologic contraints on early animal evolution. Science 270, 598.
Guj, P., 1970. The Damara mobile Belt in the South-western Kaokoveld, south West Africa. Ph.D. Thesis. University of Cape Town, p. 168.
Haack, U., Hoefs, J., Gohn, E., 1982. Constraints on the origin of Damaran granites by Rb/Sr and d18O data. Contributions to Mineralogy and Petrology 79, 279–289.
Haack, U., Hoefs, J., Gohn, E., 1983. Genesis of Damaran granites in the light of Rb/Sr and d18O data. In: Martin, H., Eder, F.W. (Eds.), Intracontinental Fold Belts. Springer-Verlag, Berlin, pp. 848–872.
Halverson, G.P., Hoffman, P.F., Schrag, D.P., 2002. A major perturbation of the carbon cycle before the Ghaub glaciation (Neoproterozoic) in Namibia: Prelude to snowball earth? Gechemistry, Geophysics, Geosystems 3, 24.
Hanson, R.E., Martin, M.W., Bowring, S.A., Munyanyiwa, H., 1998. U-Pb zircon age for the Umkondo dolerites, eastern Zimbabwe: 1.1 Ma large igneous province in southern Africa-East Antarctica and possible Rodinia correlations. Geology 26, 1143–1146.
Hanson, R.E., 2003. Proterozoic geochronology and tectonic evolution of southern Africa. Geological Society of London, Special Publications 206, 427–463.
Hartmann, O., Hoffer, E., Haack, U., 1983. Regional metamorphism in the Damara Orogen: interaction of crustal motion and heat transfer. Special Publication of the Geological Society of South Africa 11, 233–241.
Hawkesworth, C.J., Kramers, J.D., Miller, R.M.G., 1981. Old model Nd ages in Namibian Pan-African rocks. Nature 289, 278–282. http://dx.doi.org/10.1038/289278a0.
Hawkesworth, C.J., Gledhill, A.R., Roddick, J.C., Miller, R.McG., Kroner, A., 1983. RbSr and KAr studies bearing on models for the thermal evolution of the Damara belt, Namibia. In: Miller, R.McG. (Ed.), Evolution of the Damara Orogen, vol. 11. Special Publication of the Geological Society of South Africa, pp. 323–338.
Hedberg, R.M., 1979. Stratigraphy of the Ovamboland Basin, south West Africa. Bulletin of the Precambrian Research Unit, University of Cape Town 24, 325.
Heilbron, M., Machado, N., 2003. Timing of terrane accretion in the neoproterozoic-Eopaleozoic Ribeira orogen (SE Brasil). Precambrian Research 125, 87–112.
Heilbron, M., Pedrosa-Soares, A., Neto, M., da Silva, L., Trouw, R., Janasi, V., 2004. Brasiliano orogens in Southeast and south Brazil. In: Weinberg, R., Trouw, R., Fuck, R., Hackspacher, P. (Eds.), The 750–550 Ma Brasiliano Event of South America, Journal of the Virtual Explorer, Electronic Edition, vol. 17. ISSN 1441–8142, Paper 4.
Henry, G., Osborne, M.A., Schmerold, R.K., 1992/93. Note: Proposed lithostratigraphic subdivision of the Ugab Subgroup (Damara Sequence) in Kaokoland, Namibia. Communications of the Geological Survey Namibia 8, 143–145.
Hoffman, P.F., Swart, R., Eckhardt, E.F., Guowei, H., 1994. Damara Orogen of Northwest Namibia. Geological excursion guide of the Geological Survey of Namibia, Windhoek, p. 55.
Hoffman, P.F., Hawkins, D.P., Isachsen, C.E., Bowring, S.A., 1996. Precise U-Pb zircon ages for early Damaran magmatism in the Summas Mountains and Welwitschia Inlier, northern Damara belt, Namibia. Communications of the Geological Survey Namibia 11, 47–52.
Hoffman, P.F., Kaufman, A.J., Halverson, G.P., Schrag, D.P., 1998. A Neoproterozoic snowball earth. Science 281, 1342–1346.
Hoffmann, K.H., 1989. New aspects of lithostratigraphic subdivision and correlation of late proterozoic to early Cambrian rocks of the southern Damara Belt, and their correlation with central and northern Damara Belt and the Gariep Belt. Communications of the Geological Survey Namibia 5, 59–67.
Hoffmann, K.H., 1994. New constraints on the timing of continental breakup and collision in the Damara Belt. In: Niall, M., McManus, C. (Eds.), Proterozoic Crustal and Metallogenic Evolution. Abstracts of Geological Society and Geological Survey of Namibia Conference, Windhoek, p. 30.
Hoffmann, K.H., 1997. Stratigraphy of the Damara orogen. Unpublished figure, Namibian, Geological Survey.
Hoffmann, K.H., Condon, D.J., Bowring, S.A., Crowley, J.L., 2004. U-Pb zircon date from the neoproterozoic Ghaub Formation, Namibia: constraints on Marinoan glaciation. Geology 32, 817–820.
Houseman, G.A., Molnar, P., 1997. Gravitational (Rayleigh-Taylor) instability of a layer with non-linear viscosity and convective thinning of continental lithosphere. Geophysical Journal International 128, 125–150.
Jacob, R.E., Moore, J.M., Armstrong, R.A., 2000. Zircon and titanite age determinations from igneous rocks in the Karibib District, Namibia: implications for Navachab vein-style gold mineralization. Communications of the Geological Survey of Namibia 12, 157–166.
John, T., Schenk, V., Haase, K., Scherer, E., Tembo, F., 2003. Evidence for a Neoproterozoic ocean in south-central Africa from mid-oceanic-ridge-type geochemical signatures and pressure-temperature estimates of Zambian eclogites. Geology 31, 243–246.
John, T., Schenk, V., Mezger, K., Tembo, F., 2004. Timing and PT evolution of whiteschist metamorphismin the Lufilian Arc-Zambezi Belt orogen (Zambia): implications for the assembly of Gondwana. The Journal of Geology 112, 71–90.
Johnson, S.P., Rivers, T., De Waele, B., 2005. A review of the Mesoproterozoic to early Palaeozoic magmatic and tectonothermal history of south-central Africa: implications for Rodinia and Gondwana. Journal of the Geological Society of London 162, 433–450.
Johnson, S.P., De Waele, B., Evans, D., Banda, W., Tembo, F., Milton, J.A., Tani, K., 2007. Geochronology of the Zambezi supracrustal sequence, southern Zambia: a record of neoproterozoic divergent processes along the southern margin of the Congo Craton. Journal of Geology 115, 355–374.
Jung, S., Mezger, K., Masberg, P., Hoffer, E., Hoernes, S., 1998. Petrology of an intrusion-related high-grade migmatite: implications for partial melting of metasedimentary rocks and leucosome-forming processes. Journal of Metamorphic Geology 16, 425–445.

Jung, S., Hoernes, S., Mezger, K., 2000a. Geochronology and petrogenesis of Pan-African, syn-tectonic, S-type and post-tectonic A-type granite (Namibia): products of melting of crustal sources, fractional crystallization and wall rock entrainment. Lithos 50, 259–287.

Jung, S., Hoernes, S., Mezger, K., 2000b. Geochronology and petrology of migmatites from the proterozoic Damara Belt – importance of episodic fluid-present disequilibrium melting and consequences for granite petrology. Lithos 51, 153–179.

Jung, S., Mezger, K., 2001. Geochronology in migmatites – a Sm-Nd, U-Pb and Rb-Sr study from the proterozoic Damara Belt (Namibia: implications for polyphase development of migmatites in high-grade terranes. Journal of Metamorphic Geology 19, 77–97.

Jung, S., Mezger, K., Hoernes, S., 2001. Trace element and isotopic (Sr, Nd, Pd, O) arguments for a mid-crustal origin of Pan-African garnet-bearing S-type granites from the Damara Orogen (Namibia). Precambrian Research 110, 325–355.

Jung, S., Mezger, K., 2003a. U-Pb garnet chronometry in high-grade rocks; case studies from the central Damara Orogen (Namibia) and implications for the interpretation of Sm-Nd garnet ages and the role of high U-Th inclusions. Contributions to Mineralogy and Petrology 146, 382–396.

Jung, S., Mezger, K., 2003b. Petrology of basement-dominated terranes: I. regional metamorphic T-t path from U-Pb monazite and Sm-Nd garnet geochronology (central Damara orogen, Namibia). Chemical Geology 198, 223–247.

Jung, S., Kroner, A., Hauff, F., Masberg, P., 2015. Petrogenesis of Synorogenic diorite-granodiorite-granite complexes in the Damara Belt, Namibia: constraints from U-Pb zircon ages and Sr-Nd-Pb isotopes. Journal of African Earth Sciences 101, 253–265.

Kamona, A.F., Leveque, J., Friedrich, G., Haack, U., 1999. Lead isotopes of the carbonate-hosted Kabwe, Tsumeb, and Kipushi Pb-Zn-Cu sulphide deposits in relation to Pan African orogenesis in the Damaran-Lufilian fold belt of Central Africa. Mineralium Deposita 34, 273–283.

Kampunzu, A.B., Armstrong, R.A., Modis, M.P., Mapeo, R.B.M., 2000. Ion microprobe U-Pb ages on detrital zircon grains from the Ghanzi Group: implications for the identification of a Kibaran-age crust in northwest Botswana. Journal of African Earth Sciences 30, 579–587.

Kasch, K.W., 1983. Continental collision, suture propogation and thermal relaxation: a plate tectonic model for the Damara Orogen in central Namibia. In: Miller, R. McG. (Ed.), Evolution of the Damara Orogen of South West Africa/Namibia, vol. 11. Special Publication of Geological Society South Africa, pp. 423–429.

Key, R.M., Liyungu, A.K., Njamu, F.M., Somwe, V., Banda, J., Mosley, P.N., Armstrong, R.A., 2001. The western arm of the Lufilian Arc in NW Zambia and its potential for copper mineralization. African Earth Sciences 33, 503–528.

Killick, A.M., 2000. The matchless Belt and associated sulphide mineral deposits, Damara Orogen, Namibia. Communications of the Geological Survey of Namibia 12, 73–80.

Kisters, A.F.M., Jordaan, L.S., Neumaier, K., 2004. Thrust-related dome structures in the Karibib district and the origin of orthogonal fabric domains in the south Central Zone of the Pan-African Damara belt. Namibia. Precambrian Research 133, 283–303.

Konopásek, J., Kröner, S., Kitt, S.L., Passchier, C.W., Kröner, A., 2005. Oblique collision and evolution of large-scale transcurrent shear zones in the Kaoko belt, NW Namibia. Precambrian Research 136, 139–157.

Konopásek, J., Kosler, J., Tajcmanová, L., Ulrich, S., Kitt, S.L., 2008. Neoproterozoic igneous complex emplaced along major tectonic boundary in the Kaoko Belt (NW Namibia) – ion probe and laser ablation ICP-MS dating of magmatic and metamorphic zircons. Journal of the Geological Society 165, 153–165.

Kroner, A., 1977. Precambrian mobile belts of southern and eastern Africa – ancient sutures or sites of ensialic mobility? A case for crustal evolution towards plate tectonics. Tectonophysics 40, 101–135.

Kröner, A., Cordani, U., 2003. African, southern Indian and South American cratons were not part of the Rodinia supercontinent: evidence from field relationships and geochronology. Tectonophysics 375, 325–352.

Kröner, S., Konopásek, J., Kröner, A., Passchier, C.W., Poller, U., Wingate, M.T.D., Hofmann, K.H., 2004. U-Pb and Pb-Pb zircon ages for metamorphic rocks in the Kaoko Belt of Northwestern Namibia: a Palaeo- to Mesoproterozoic basement reworked during the Pan-African orogeny. South African Journal of Geology 107, 455–476.

Kukla, C., Kramm, U., Kukla, P.A., Okrusch, M., 1991. U-Pb monazite data relating to metamorphism and granite intrusion in the northwestern Khomas Trough, Damara Orogen, central Namibia. Communications of the Geological Survey of Namibia 7, 49–54.

Kukla, P.A., Stanistreet, I.G., 1991. Record of the Damaran Khomas Hochland accretionary prism in central Namibia: refutation of an "ensialic" origin of a late Proterozoic orogenic belt. Geology 19, 473–476.

Lehmann, J., Saalmann, K., Naydenov, K.V., Milani, L., Belyanin, G.A., Zwingmann, H., Charlesworth, G., Kinnaird, J.A., 2015. Structural and geochronological constraints on the Pan-African tectonic evolution of the northern Damara Belt, Namibia. Tectonics. http://dx.doi.org/10.1002/2015TC003899.

Lister, G.S., Snoke, A.W., 1984. S-C mylonites. Journal of Structural Geology 6, 617–638.

Lobo-Guerrero Sanz, A., 2005. Pre- and Post-Katangan Granitoids of the Greater Lufilian Arc: Geology, Geochemistry, Geochronology and Metallogenic Significance. Ph.D. Thesis. University of Witswatersrand.

Longridge, L., Gibson, R.L., Kinnaird, J.A., Armstrong, R.A., 2011. Constraining the timing of deformation in the southwestern Central Zone of the Damara Belt, Namibia. Geological Society of London Special Publications 357, 107–135.

Longridge, L., Kinnaird, J.A., Gibson, R.L., Armstrong, R.A., 2014. Amphibolites of the Central Zone: new SHRIMP U-Pb ages and implications for the evolution of the Damara orogen, Namibia. South African Journal of Geology 117, 67–86.

Longridge, L., Gibson, R.L., Kinnaird, J.A., Armstrong, R.A., 2017. New constraints on the age and conditions of LPHT metamorphism in the southwestern Central Zone of the Damara Belt, Namibia and implications for tectonic setting. Lithos 278–281, 361–382.

Machado, N., Valladres, C., Heilbron, M., Valeriano, C., 1996. U-Pb geochronology of the central Ribeira belt (Brazil) and implications for the Brazilian Orogeny. Precambrian Research 79, 347–361.

Maloof, A.C., 2000. Superposed folding at the junction of the inland and coastal belts, Damara Orogen, NW Namibia. Communications of the Geological Survey of Namibia 12, 89–98.

Martin, H., Porada, H., 1977. The intracratonic branch of the Damara orogen in south West Africa. II. Discussion of Relationships with the Pan-African mobile belt system. Precambrian Research 5, 339–357.

Masberg, P., 2000. Garnet growth in medium-pressure granulite facies metapelites from the central Damara Orogen: igneous versus metamorphic history. Communications of the Geological Society of Namibia 12, 115–124.

Masberg, P., Mihm, D., Jung, S., 2005. Major and trace element and isotopic (Sr, Nd, O) constraints for Pan-African crustally contaminated grey granite gneisses from the southern Kaoko belt, Namibia. Lithos 84, 25–50.

Master, S., Rainaud, C., Armstrong, R.A., Phillips, D., Robb, L.J., 2005. Provenance ages of the neoproterozoic Katanga Supergroup (Central African Copperbelt), with implications for basin evolution. Journal of African Earth Sciences 42, 41–60.

McDermott, F., Harris, N.B.W., Hawkesworth, C.J., 1996. Geochmical constraints on crustal anatexis: a case study from the Pan-African Damara granitoids of Namibia. Contributions to Mineralogy and Petrology 123, 406–423.

McDermott, F., Harris, N.B.W., Hawkesworth, C.J., 2000. Geochemical constraints on the petrogenesis of Pan-African A-type granites in the Damara Belt, Namibia. Communications of the Geological Survey of Namibia 12, 139–148.

Meert, J.G., 2003. A synopsis of events related to the assembly of eastern Gondwana. Tectonophysics 362, 1–40.

Meert, J.G., Torsvik, T.H., 2003. The making and unmaking of a supercontinent:Rodinia Revisited. Tectonophysics 375, 261–288.

Meert, J.G., Van Der Voo, R., Ayub, S., 1995. Palaeomagnetic investigation of the neoproterozoic Gagwe lavas and Mbozi Complex, Tanzania and the assembly of Gondwana. Precambrian Research 75, 225–244.

Milani, L., Kinnaird, J.A., Lehmann, J., Naydenv, K.V., Saalmann, K., Frei, D., Gerdes, A., 2014. Role of crustal onribution in the early stage of the Damara Orogen, Namibia: new constraints from combined U-Pb and Lu-Hf isotopes from the Goas Magmatic Complex. Gondwana Research 28, 961–986.

Miller, R.McG., 1980. Geology of a portion of central Damaraland, South West Africa/Namibia. Memoirs of the Geological Survey of South Africa, S.W.A. Series 6, 1–78.

Miller, R.McG., 1983. The Pan-African Damara orogen of Namibia. In: Miller, R. McG. (Ed.), Evolution of the Damara Orogen of South West Africa/Namibia, vol. 11. Special Publication, Geological Society South Africa, pp. 431–515.

Miller, R. McG., Grote, W., 1988. Geological map of the Damara orogen, Namibia (scale 1:500,000). Geological Survey of Namibia. Windhoek, 2 sheets.

Mortimer, N., 2000. Metamorphic discontinuities in orogenic belts: example of garnet–biotite–albite zone in the Otago Schist, New Zealand. International Journal of Earth Science 89, 295–306.

Nascimento, D.B., Ribeiro, A., Trouw, R.A.J., Schmitt, R.S., Passchier, C.W., 2016. Stratigraphy of the Neoproterozoic Damara Sequence in northwest Namibia: slope to basin sub-marine mass-transport deposits and olistolith fields. Precambrian Research 278, 108–125.

Newstead, B., 2010. Provenance of the Damara Sequence, Damara Orogen, Namibia. Masters Thesis. University of Florida.

Oliver, G.J.H., 1994. Mid-crustal detachment and domes in the central zone of the Damaran Orogen, Namibia. Journal of African Earth Sciences 19, 331–344.

Passchier, C.W., Simpson, C., 1986. Porphyroclast systems as kinematic indicators. Journal of Structural Geology 8, 831–843.

Passchier, C.W., 2001. Flanking structures. Journal of Structural Geology 23, 951–962.

Passchier, C.W., Trouw, R.A.J., Ribeiro, A., Paciullo, F.V.P., 2002. Tectonic evolution of the southern Kaoko Belt, Namibia. Journal of African Earth Sciences 35, 61–75.

Passchier, C.W., Trouw, R.A.J., 2005. Microtectonics, 2nd ed. Springer, p. 366.

Passchier, C.W., Trouw, R., Goscombe, B., Gray, D., Kroner, A., 2007. Intrusion mechanisms in a turbidite sequence: the Voetspoor and Doros plutons in NW Namibia. Journal of Structural Geology 29, 481–496.

Passchier, C.W., Trouw, R., Coelho, S., De Kemp, E., Schmitt, R., 2011. Key-ring structure gradients and sheath folds in the Goantagab Domain of NW Namibia. Journal of Structural Geology 33, 280–291.

Passchier, C.W., Trouw, R., Schmitt, R.S., 2016. How to make a transverse triple junction – new evidence for the assemblage of Gondwana along the Kaoko-Damara belts, Namibia. Geology 44, 843–846.

Paul, A., Jung, S., Romer, R.L., Stracke, A., Hauff, F., 2014. Petrogenesis of synorogenic high-temperature leucogranites (Damara orogen, Namibia): constraints from U-Pb monazite ages and Nd, Sr and Pb isotopes. Gondwana Research 25, 1614–1626.

Payne, J.L., Hand, M., Barovich, K.M., Wade, B.P., 2008. Temporal constraints on the timing of high-grade metamorphism in the northern Gawler Craton: implications for assembly of the Australian Proterozoic. Australian Journal of Earth Sciences 55, 623–640.

Pedrosa-Soares, A.C., Vidal, P., Leonardos, O.H., Brito-Neves, B.B., 1998. Neoproterozoic oceanic remnants in eastern Brazil: further evidence and refutation of an exclusively ensialic origin for the Araçuaí-West Congo craton. Geology 26, 519–522.
Pedrosa-Soares, A.C., Noce, A.C., Widemann, C.M., Pinto, C.P., 2001. The Araçuaí-West Congo Orogen in Brazil: an overview of a confined orogen formed during Gondwanaland assembly. Precambrian Research 110, 307–323.
Pesonen, L.J., Elming, S.-A., et al., 2003. Palaeomagnetic configuration of continents during the proterozoic. Tectonophysics 375, 289–324.
Porada, H., 1979. The Damara-Ribeira Orogen of the Pan-African-Brasiliano cycle in Namibia (Southwest Africa) and Brazil as interpreted in terms of continental collision. Tectonophysics 57, 237–265.
Porada, H., Ahrendt, H., Behr, H.J., Weber, K., 1983. The Join of the Coastal and Intracontinental Branches of the Damara Orogen, Namibia, South West Africa. Springer-Verlag, pp. 901–912.
Porada, H., Wittig, R., 1983. Turbidites and their significance for the geosynclinal evolution of the Damara orogen, south West Africa/Namibia. In: Miller, R.McG. (Ed.), Evolution of the Damara Orogen, vol. 11. Special Publication of the Geological Society of South Africa, pp. 21–36.
Porada, H., 1983. Geodynamic model for the geosynclinal development of the Damara orogen, Namibia, south West Africa. In: Martin, H., Eder, F.W. (Eds.), Intracontinental Fold Belts. Springer-Verlag, Berlin, pp. 502–538.
Porada, H., 1989. Pan-African rifting and orogenesis in southern to Equatorial Africa and Eastern Brazil. Precambrian Research 44, 103–136.
Prave, A.R., 1996. Tale of three cratons: Tectonostratigraphic anatomy of the Damara Orogen in northwestern Namibia and the assembly of Gondwana. Geology 24, 1115–1118.
Rapalini, A.E., 2006. New late proterozoic palaeomagnetic pole for the Rio de la Plata Craton: implications for Gondwana. Precambrian Research 147, 223–233.
Ritter, O., Weckmann, U., Vietor, T., Haak, V., 2003. A magnetotelluric study of the Damara Belt in Namibia 1. Regional scale conductivity anomalies. Physics of the Earth and Planetary Interiors 138, 71–90.
Saalmann, K., Hartmann, L.A., Remus, M.V.D., Koester, E., Conceiao, R.V., 2005. Sm-Nd isotope geochemistry of metamorphic volcano-sedimenatry successions in the Sao Gabriel Block, southernmost Brazil: evidence for the existence of juvenile Neoproterozoic crust to the east of the Rio de la Plata Craton. Precambrian Research 136, 159–175.
Schmidt, A., Wedepohl, K.H., 1983. Chemical composition and genetic relations of the matchless amphibolite (Damara orogenic belt). In: Miller, R.G. (Ed.), Evolution of the Damara Orogen of Southwest Africa/Namibia, vol. 11. Geological Society of South Africa, Special Publication, pp. 139–145.
Schmitt, R.S., Trouw, R.A.J., Van Schmus, W.R., Pimentel, M.M., 2004. Late amalgamation in the central part of West Gondwana: new geochronological data and the characterisation of a Cambrian collisional orogeny in the Ribeira Belt (SE Brazil). Precambrian Research 133, 29–61.
Schmitt, R.S., Trouw, R.A.J., Passchier, C.W., Medeiros, S.R., Armstrong, R., 2012. 530 Ma syntectonic syenites and granites in NW Namibia – their relation with sollision along the junction of the Damara and Kaoko belts. Gondwana Research 21, 362–377.
Seth, B., Kroner, A., Mezger, K., Nemchin, A.A., Pidgeon, R.T., Okrusch, M., 1998. Archaean to neoproterozoic magmatic events in the Kaoko belt of NW Namibia and their geodynamic significance. Precambrian Research 92, 341–363.
Seth, B., Okrusch, M., Wilde, M., Hoffmann, K.H., 2000. The Voetspoor Intrusion, Southern Kaoko Zone, Namibia: mineralogical, geochemical and isotopic constraints for the origin of a syenitic magma. Communications of the Geological Survey of Namibia 12, 125–137.
Simpson, C., 1984. Borrego Springs-Santa Rosa mylonite zone: a Late Cretaceous west-directed thrust in southern California. Geology 12, 8–11.
Singletary, S.J., Hanson, R.E., Martin, M.W., Crowley, J.L., Bowring, S.A., Key, R.M., Ramokate, L.V., Direng, B.B., Krol, M.A., 2003. Geochronology of basement rocks in the Kalahari Desert, Botswana, and implications for regional Proterozoic tectonics. Precambrian Research 121, 47–71.
Stanistreet, I.G., Kukla, P.A., Henry, G., 1991. Sedimentary basinal responses to a Late Precambrian Wilson Cycle: the Damara orogen and Nama Foreland, Namibia. Journal of African Earth Science 13 (1), 141–156.
Stanistreet, I.G., Charlesworth, E.G., 2001. Damaran basement-cored fold nappes incorporating pre-collisional basins, Kaoko Belt, Namibia, and controls on Mesozoic supercontinent breakup. South African Journal of Geology 104, 1–12.
Swart, R., 1992. The sedimentology of the Zerrissene turbidite system, Damara Orogen, Namibia. Memoir Geological Survey of Namibia 13, 54.
Tohver, E., D'Agrella-Filho, M.S.D., Trindade, R.I.F., 2006. Palaeomagnetic record of Africa and South America for the 1200–500 Ma interval, and evaluation of Rodinia and Gondwana assemblies. Precambrian Research 147, 193–222.
Trompette, R., Carozzi, A.V., 1994. Geology of Western Gondwana (2000–500 Ma). Pan-African-Brasiliano Aggregation of South America and Africa. A.A. Balkema, Rotterdam, Brookfield, p. 350.
Trompette, R., 1997. Neoproterozoic (~600 Ma) aggregation of westernGondwana: a tentative scenario. Precambrian Research 82, 101–112.
Van de Flierdt, T., Hoernes, S., Jung, S., Masberg, P., Hoffer, E., Schaltegger, U., Friedrichsen, H., 2003. Lower crustal melting and the role of open-system processes in the genesis of syn-orogenic quartz diotite-granite-leucogranite associations: constraints from Sr-Nd-O isotopes from the Bandombaai Complex, Namibia. Lithos 67, 205–226.
Vinyu, M.L., Hanson, R.E., Martin, M.W., Bowring, S.A., Jelsma, H.A., Krol, M.A., Dirks, P.H.G.M., 1999. U-Pb and 40Ar/39Ar geochronological constraints on the tectonic evolution of the easternmost part of the Zambezi orogenic belt, northeast Zimbabwe. Precambrian Research 98, 67–82.
Weber, K., Ahrendt, H., 1983. Structural Development of the Ugab Structural Domain of the Northern Zone of the Damara Orogen. Intracontinental Damara Orogen. Springer-Verlag, pp. 699–721.
Will, T.M., Okrusch, M., Gruner, B.B., 2004. Barrovian and Buchan type metamorphism in the Pan-African Kaoko belt, Namibia: implications for its geotectonic position within the framework of Western Gondwana. South African Journal of Geology 107, 431–454.
Yardley, B.W.D., 1982. The early metamorphic history of the Haast Schists and related rocks of New Zealand. Contributions to Mineralogy and Petrology 81, 317–327.

Dr Ben Goscombe is currently Courtesy Professor with Department of Geology at University of Florida. Research interests are structural and metamorphic processes in a range of orogenic systems and utilizing integrated structural-metamorphic-chronologic datasets towards orogen-scale problems. PhD at Melbourne University 1989; contracts with government geological surveys in Zimbabwe, Namibia, Tasmania, Western Australia and Northern Territory; Honorary Research Associate at Adelaide University 2000–2014; Research Associate at Melbourne University 2001–2003. Freelance researcher from 2006 and established Integrated Terrane Analysis Research (ITAR) to undertaking self-funded research in Namibia, Zimbabwe, Oman, Nepal, Australia and Scotland and collaborations with Geoscience Australia and University of Florida. Received the Phaup Award in 1998 and 2000 for contributions to Zimbabwe Geology and inaugural Gondwana Research best paper award in 2007.

David A. Foster is Professor and Chair of the Department of Geological Sciences, University of Florida. He studies the tectonic evolution of continents throughout earth history using high and low temperature thermochronology integrated with other geological and geophysical data. He is a Fellow of the Geological Society of America and was twice the recipient of the Stillwell award from the Geological Society of Australia

Prof. David Gray is University Associate at the University of Tasmania. Research interests are in structural geology and tectonics with particular focus on evolution of eastern Australia, Otago Schist belt in New Zealand, Damara Orogen in Namibia, and ophiolite obduction in Oman. Was an academic at University of New South Wales (1975–1977), Virginia Tech (1977–1983) Monash University (1983–2001), and Australian Professorial Fellow at the University of Melbourne (2002–2006). Structural geology consultant to the minerals industry through his company Geostructures Pty Ltd (2006–2016). Awarded the Geological Society of Australia Selwyn Medal for his contributions to Victorian Geology (1997), Carey Medal for contributions to Structural Geology and Tectonics (1998), and Stillwell Award (1997 and 2004).

Benjamin Wade is a senior microscopist at Adelaide Microscopy in the University of Adelaide. He received his PhD (2006) from the University of Adelaide for research on the Musgrave Provence, Arunta Provence and Gawler Craton. He has worked in industry and held undertaken postdoctoral research from 2006 to 2008, and since has been employed at Adelaide Microscopy. His primary interests and research include the application of micro-analytical techniques such as SEM, TEM, EPMA, and LA-ICP-MS to geological problems.

Antonios E. Marsellos is an Assistant Professor in the Department of Geology, Environment and Sustainability at Hofstra University. He studies tectonic and surface processes using thermochronology, GIS-GPS, and satellite and earth-based sensor data.

Jason Titus is a current Ph.D. student in the Geological Sciences at the University of Florida. He is studying the thermotectonic history of the Damara Orogen. He received his Bachelor of Science in Geological Sciences from the University of South Carolina in 2014 and is a United States Navy veteran.